D5.1 RELIABLE POSITIONING

REVISION: V.1.0

Work package	WP 5
Task	Task 5.1
Due date	30/12/2025
Submission date	27/02/2026
Deliverable lead	Mounia Belhabib (TAS-F), Karine Zidane (TAS-F)
Version	V1.0
Authors	Mounia Belhabib (TASF), ZIDANE Karine (TASF), CALMETTES Thibaud (TASF), Karthik Anantha Swamy (QCOM) , PANAITOPOL Dorin (TH-SIX)
Reviewers	Husnain Shahid (CTTC), Sebastian Euler (Ericsson), Eduardo medeiros (Ericsson), Chao Zhang C (Ericsson), Luca Feltrin (Ericcson), Yves Teganya (Ericsson), Luca Feltrin (Ericsson), Nicolas Chuberre (Thales Alenia Space France)
Abstract	The emergence of mega-constellations for telecommunications and the rapid evolution of 3GPP cellular standards to integrate NTN, paved the way for exploiting LEO satellites not only for telecommunications but also for positioning purposes. In this context, this document presents an extensive state of the art and an exhaustive feasibility study on using NTN signals for positioning in the future 6G standard. Ranging based positioning techniques are assessed in several frequency scenarios and several LEO satellite constellations. Positioning accuracies in the order of tens of meters are obtained and multiple ways forward to achieve cm-level positioning are

Grant Agreement No.: 101096479
Call: HORIZON-JU-SNS-2022

Topic: HORIZON-JU-SNS-2022-STREAM-B-01-03
Type of action: HORIZON-JU-RIA

	discussed. Moreover, Doppler based positioning techniques are assessed independently and showed around 40 meters of positioning accuracy. Furthermore, hybrid TN-NTN positioning is described, mainly for regulatory constraints where terminals need to verify their location using TNs when available. In conclusion, as satellite constellations expand, it is clear that integrated communication-navigation architectures and new signal designs will enable robust, seamless positioning services, especially in challenging or GNSS-denied environments.
Keywords	Positioning, accuracy, satellite

Document Revision History

Version	Date	Description of change	List of contributor(s)
V0.1	10/12/2025	1st version of the template for comments	Mounia Belhabib (TASF)
V0.2	23/12/2025	2nd version of the template for comments	Mounia Belhabib (TASF), Karthik Anantha Swamy (QCOM), PANAITOPOL Dorin (TH-SIX)
V0.3	17/02/2026	Consolidation of the results	ZIDANE Karine (TASF), CALMETTES Thibaud (TASF), CHUBERRE Nicolas (TASF)
V1.0	24/02/2026	Adding the abstract	ZIDANE Karine (TASF), CHUBERRE Nicolas (TASF)

DISCLAIMER

Co-funded by the European Union

Project funded by
Schweizerische Eidgenossenschaft
Confédération suisse
Confederazione Svizzera
Confederaziun svizra
Swiss Confederation
Federal Department of Economic Affairs, Education and Research EAER
State Secretariat for Education, Research and Innovation SERI

6G-NTN (*6G Non Terrestial Network*) project has received funding from the Smart Networks and Services Joint Undertaking (SNS JU) under the European Union's Horizon Europe research and innovation programme under Grant Agreement No 101096479. Views and opinions expressed are however those of the author(s) only and do not necessarily reflect those of the European Union. Neither the European Union nor the granting authority can be held responsible for them. This work has received funding from the Swiss State Secretariat for Education, Research and Innovation (SERI).

COPYRIGHT NOTICE

Project co-funded by the European Commission in the Horizon Europe Programme		
Nature of the deliverable:	**to specify R, DEM, DEC, DATA, DMP, ETHICS, SECURITY, OTHER***	
Dissemination Level		
PU	*Public, fully open, e.g. web (Deliverables flagged as public will be automatically published in CORDIS project's page)*	✓

SEN	*Sensitive, limited under the conditions of the Grant Agreement*	
Classified R-UE/ EU-R	*EU RESTRICTED under the Commission Decision No2015/ 444*	
Classified C-UE/ EU-C	*EU CONFIDENTIAL under the Commission Decision No2015/ 444*	
Classified S-UE/ EU-S	*EU SECRET under the Commission Decision No2015/ 444*	

* R: Document, report (excluding the periodic and final reports)

DEM: Demonstrator, pilot, prototype, plan designs

DEC: Websites, patents filing, press & media actions, videos, etc.

DATA: Data sets, microdata, etc.

DMP: Data management plan

ETHICS: Deliverables related to ethics issues.

SECURITY: Deliverables related to security issues

OTHER: Software, technical diagram, algorithms, models, etc.

EXECUTIVE SUMMARY

The emergence of mega-constellations for telecommunications and the rapid evolution of 3GPP cellular standards to integrate NTN, paved the way for exploiting LEO satellites not only for telecommunications but also for positioning purposes. In this context, this document presents an extensive state of the art and an exhaustive feasibility study on using NTN signals for positioning in the future 6G standard. Ranging based positioning techniques are assessed in several frequency scenarios and several LEO satellite constellations. Positioning accuracies in the order of tens of meters are obtained and multiple ways forward to achieve cm-level positioning are discussed. Moreover, Doppler based positioning techniques are assessed independently and showed around 40 meters of positioning accuracy. Furthermore, hybrid TN-NTN positioning is described, mainly for regulatory constraints where terminals need to verify their location using TNs when available. In conclusion, as satellite constellations expand, it is clear that integrated communication-navigation architectures and new signal designs will enable robust, seamless positioning services, especially in challenging or GNSS-denied environments.

Co-funded by the European Union

TABLE OF CONTENTS

LIST OF FIGURES

LIST OF TABLES

LIST OF ACRONYMS

AMF: access and mobility management function

AOA: Angle Of Arrival

CID: Cell ID

CN: core network

CP: cyclic Prefix

CU: centralized unit

DL: Downlink

DU: distributed unit

E-CID: Enhanced Cell ID

ESMLC: Enhanced Serving Mobile Location Centre

FCC: Federal Communications Commission

GMLC: gateway mobile location center

GPS: Global Positioning System

LBS: Location based services

LCS: Location Services

LEO: Low Earth Orbit

LMF: location management function

LPP: LTE Positioning Protocol

MCRB: Modified Cramer Rao Bound

MEO: Medium Earth Orbit

NG-eNB: next generation evolved Node B

NG-RAN: Next Generation RAN

NRPPa: New Radio Positioning Protocol Annex

NTN: Non Terrestrial Network

OFDM: orthogonal frequency division multiplexing

OMA: Open Mobile Alliance

OTDOA: Observed Time Difference Of Arrival

PPP: Precise Point Positioning

PRB: physical resource block

PRS: Positioning Reference Signal

QoS: Quality of Service

RAN: Radio Access Network

RAT: Radio Access technology

RFPM: RF pattern matching

RRC: radio resource control

SLP: SUPL Location Platform

SoOP: Signal of Opportunity

SRS: Sounding Reference Signal

SUPL: Secure User Plane Location

TA: timing advance

TDOA: Time Difference Of Arrival

TN: Terrestrial Network

TRP: Transmission Reception Point

UE: User Equipment

UL: Uplink

UL-TOA: Uplink Time of Arriva

UTDOA: Uplink Time Difference Of Arrival

1 CONTEXT AND OBJECTIVE OF THE STUDY

The rapid evolution of telecommunications technologies, coupled with the continuous growth in the number of connected devices over recent decades, has driven the need for NTNs. As the number of smartphones increases and data consumption is expected to quadruple, achieving high throughput becomes crucial. In WP2, a market analysis was conducted for the 6G NTN network, which considers a total of 5.2 billion mobile subscribers. According to some market research, it is projected that by 2030, at least 7.5% of users will have NTN-capable user equipment (UE) [1].

Moreover, sixth-generation (6G) wireless communication aims for full coverage of the Earth. Therefore, NTN present themselves as an effective solution for challenging 6G use cases that cannot be handled solely by TNs. One such use case is to provide reliable positioning and localization service to UE in the middle of an ocean or a desert. One of the enabling technologies of the 6G system is the provision of an accurate user position with low latency. Indeed, being able to locate a terminal can be of great value for contextual applications. Notably, as part of the 3GPP NR-NTN standard from Rel-17 on, it is assumed that the UE implements a global navigation satellite system (GNSS) receiver, which enables us to determine its location. Once in connected mode, the UE may be requested by the 5G Core network to report its GNSS position[1] as illustrated in Figure 1 below.

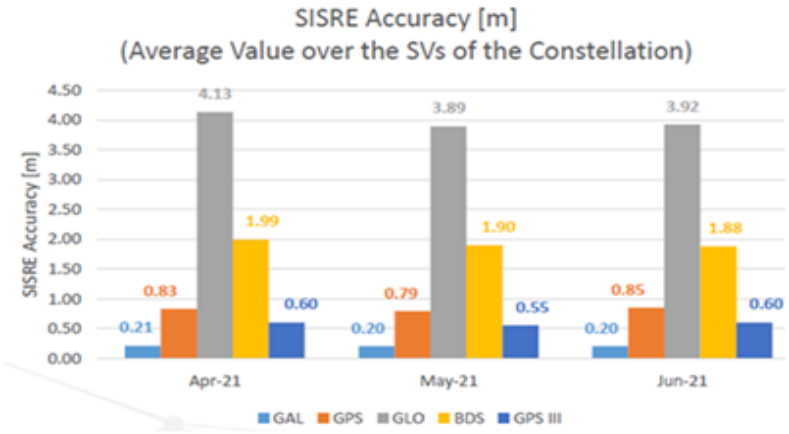

FIGURE 1: TYPICAL PERFORMANCE FOR ALL CONSTELLATION OBSERVED AT GRC

Furthermore, in Release 17 it has been identified that "To support regulated services and features 3GPP networks should have the capability to locate each UE in a reliable manner and determine the policy that applies to their operation depending on their location and/or context."

This means it is necessary to know the location of the UE in a reliable or trusted manner to ensure that the user is served with the service center of the country in which the UE is located.

However, in Release 18, it is noted that "any method which relies solely on UE-generated location information is unlikely to be considered reliable for network *selection purposes. Therefore, a method such as GNSS/Assisted GNSS (A-GNSS) cannot be considered reliable or trusted unless the information provided by the UE can be verified by the network*." The reason is twofold. On the one hand, a user could intentionally provide a fake location by tampering with his own phone in order to maliciously obtain a specific service that he wouldn't access otherwise.

On the other hand, there is a wide spread of jammers and spoofers that weaken GNSS service availability and require counter measures. For this reason, 3GPP has started a study on a network-verified UE location as part of the Rel-18 work.This scheme aims at providing the network with a way to cross check the reported UE location and, therefore, enable the location information to become reliable. Already, it is anticipated that the principle will be to allow the network to determine the UE with a rough positioning accuracy of typically few kms since the aims is simply to check the GNSS information. Overall, the state of the art in terrestrial 5G, will be to locate the UE reliably with an accuracy of typically a few meters. This is not considered sufficient by certain vertical stakeholders, like the car manufacturer, that consider that sub cm accuracy may be needed for autonomous driving. This sub-centimeter accuracy will be studied in this task, but reliability is even more important.

The integration of positioning capabilities into next-generation 6G satellite networks is expected to become a fundamental component for enabling both seamless network access and enhanced navigation services. Currently, the GNSS is the only solution for satellite-based outdoor positioning, widely adopted across user platforms.

The objective of this task is to define end-to-end Positioning and Timing solutions for 6G NTN able to meet the accuracy and reliability requirements based on integrity and. Trade-offs supported by simulations will be carried out on the functional architecture and apportionment of the performance across UE. A proof of concept (PoC) will be implemented based on a simulator using 4G/5G signals for positioning. The simulator is described in detail in this document and presents the complete simulation workflow. It includes the satellite constellation, specifically a 6G NTN constellation with detail of link budget, with emulation of the satellites in view according to the constellation defined in WP3. The study also considers UE receiver model, positioned in Toulouse.

To achieve this objective, this work focuses on extending cellular positioning capabilities to NTN. Since 3GPP standards primarily consider LEO satellites for NTN integration into cellular networks, our study concentrates specifically on LEO-based positioning. We identify LEO satellites as the next key enabler for advancing cellular positioning, for several compelling reasons:

- Growing commercial interest and investments in deploying NTN satellites for communication purposes.
- Availability of larger communication bandwidth, faster acquisition time, and improved accuracy.
- No additional UE implementation complexity.
- LEO satellites orbit at much lower altitudes compared to GNSS, offering significant advantages such as better link budget and evolving satellite geometry due to dynamic satellites movement.

However, LEO-based systems also face significant challenges due to their high mobility, including strong Doppler effects and frequent handovers between satellite clusters to ensure continuous coverage. Despite these issues, LEO-based positioning presents a promising alternative to GNSS, particularly in challenging environments such as dense urban areas or indoor settings, where GNSS signals are often degraded due to non-line-of-sight (NLOS) propagation.

In the following, we explore positioning technologies within the 6G NTN framework, specifically leveraging LEO satellites. A PRS simulator is proposed to support navigation and localization

tasks. The study builds upon an analysis of 6G RAT, examining positioning algorithms, identifying key factors affecting positioning performance, and evaluating performance through 6G NTN constellation. We propose a hybrid algorithmic approach aimed at achieving centimeter-level positioning accuracy, targeting ~10 cm level. As an alternative solution for NTN-based positioning, this work investigates the use of PRS signals and evaluates the influence of various parameters on positioning accuracy. To this end, the role of PRS in 5G/6G TNs is analyzed for adaptation to NTN environments under different configurations.

Furthermore, the study assesses the impact of satellite parameters, deployment scenarios, and satellite position uncertainties on overall positioning performance. A proof of concept is demonstrated using a MATLAB-based PRS simulator, developed to carry out the simulation and performance evaluation. While the foregoing focused on ranging-based techniques, we also study and assess the feasibility of Doppler-based approaches to LEO-satellite positioning. We present simulation studies in the challenging scenarios of one and two satellite visibility, which is the expectation of broadband communication satellites networks. While the foregoing focused on ranging-based techniques, we also study and assess the feasibility of Doppler-based approaches to LEO-satellite positioning. We present simulation studies in the challenging scenarios of one and two satellite visibility, which is the expectation of broadband communication satellites networks.

The structure of this deliverable is as follows:

- Chapter 1 introduces NTN and the positioning requirements for use cases in WP2.
- Chapters 2 and 3 review the state of the art in positioning techniques, covering both TN and NTN. A synthesis of the positioning methods found in the literature is provided at the end of the chapter. A dedicated section discusses recent developments in mega-constellations relevant to 6G NTN up to 2030, with a focus on their feasibility for supporting location-based services.
- Chapters 4and 5 explore the trade-offs of different positioning solutions for 6G NTN, based on various localization techniques, presents solution models, along with a PoC through simulation.
- In Chapter 6, a description of the hybrid TN-NTN solution model will be presented.
- Finally, Chapter 7 provides recommendations for the standardization of this work and outlines future research directions.
- Chapter 8 concludes the report, summarizing key findings.

1.1 NTN IN 6G OVERVIEW

This section begins with an overview of NTNs, followed by a classification of the different types of platforms utilized within these networks. The final part presents the overall NTN architecture, based on the 6G Next Generation Radio Access Network (NG-RAN) framework.

NTNs broadly encompass communication systems that rely on satellite technologies and aerial platforms like High-Altitude Platform Stations (HAPS). Satellite networks use space-based platforms to connect with terrestrial infrastructure, while HAPS leverages airborne unmanned systems, such as balloons and airships, to provide connectivity from the stratosphere.

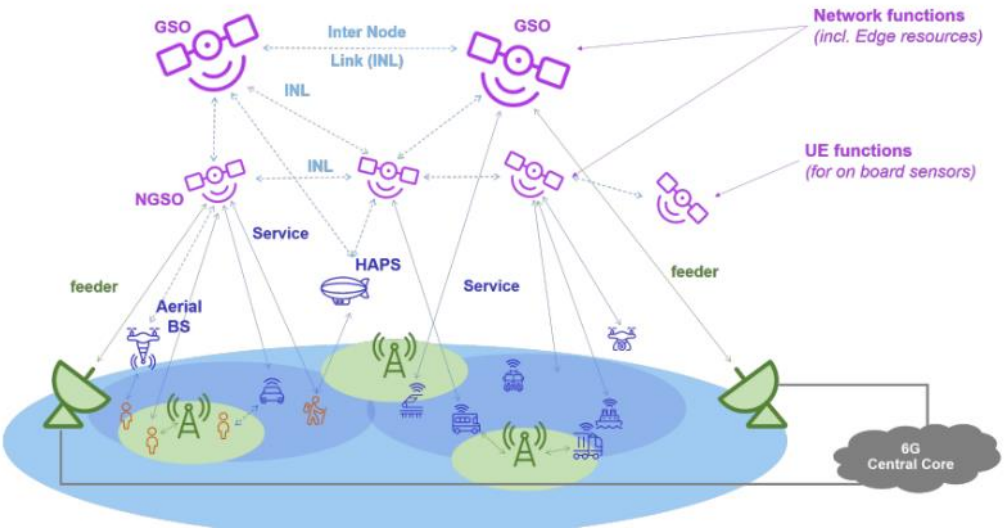

FIGURE 2: 6G NTN VISION FOR A3D FULLY INTGRATED NETWORK

As illustrated in Figure 2, a typical NTN comprises Unmanned Aircraft System (UAS) platforms and/or satellites, along with one or more satellite gateways (sat-gateways), feeder links, service links, inter-satellite links (ISLs), and UE.

The satellite or UAS platform can be equipped with either a transparent or a regenerative payload. In the case of a transparent payload, the waveform signal is frequency-filtered, frequency-converted, and amplified. In contrast, a regenerative payload performs additional processing, including demodulation/decoding, switching and/or routing, and re-encoding/modulation, alongside frequency filtering, conversion, and amplification.

The sat-gateway serves as the interface between the NTN and the core data network. The feeder link connects the sat-gateway to the satellite or UAS platform, while the service link connects the platform to the UE. ISLs enable communication between multiple satellites when deployed [2].

1.2 NTN ARCHITECTURE FOR POSITIONING

A NG-RAN can be adapted to support NTN in the case of using transparent or regenerative satellites. The transparent satellites act as RF repeaters. As shown in Figure 3. It repeats the New Radio air interface (NR-Uu) from the feeder link to the service link and vice versa. Moreover, The NTN gateway has all the needed functions to forward the signal of NR-Uu interface. Therefore, the NG-RAN architecture is suitable to support transparent satellite access without the need for any modification. However, NR- timers should be adapted to the long round trip times introduced in NTN [3].

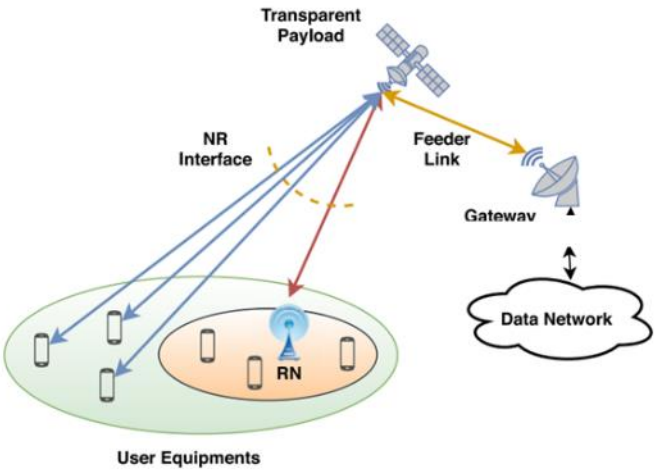

FIGURE 3: ARCHITECTURE WITH TRANSPARENT PAYLOAD [TR 38.863]

On the other hand, in case of a regenerative payload see Figure 4, the base station functionalities can be performed by the satellite. This option, even though it is more complex, would improve significantly the round trip time (RTT) of the communication. In addition, due to the regenerative payload, an ISL can be also established, which would be beneficial for hand-over procedures in the case of satellite constellation. Both architecture options can ensure direct or non-direct access to the UE on ground.

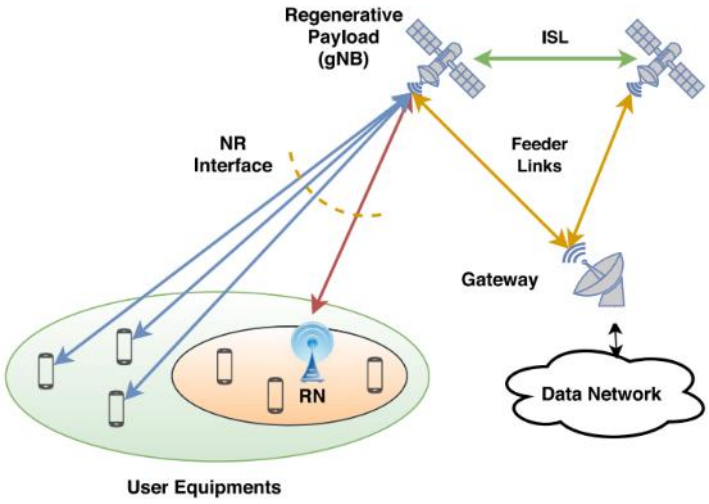

FIGURE 4: ARCHITECTURE WITH REGENRATIVE PAYLOAD

The Positioning architecture described in 3GPP standard for verification location is illustrated in Figure 5, the LCS signaling in the CN was also standardized. A dedicated LMF was introduced to interact with external clients (i.e. application, UE, or other CN nodes) and location request/response.

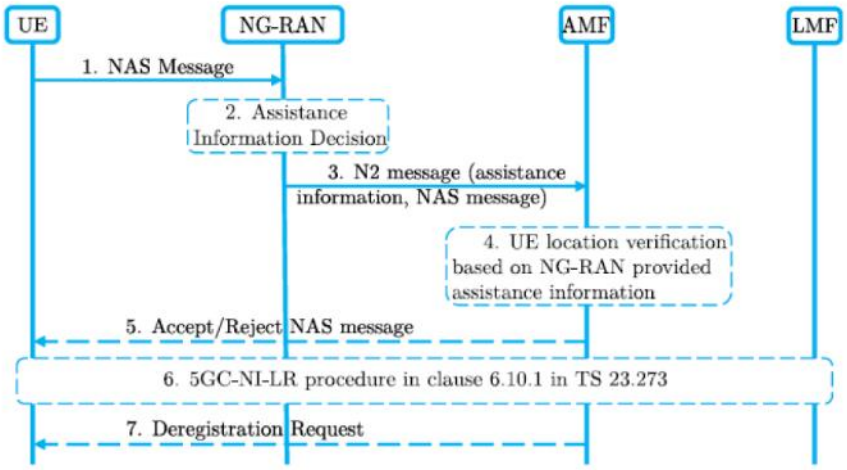

FIGURE 5: 5G TN POSITIONING ARCHITECTURE BASED ON LOCATION VERIFICATION SOLUTION DISCUSSED IN 3GPP (SA) [TR 28.877]

The LCS signaling and LMF continue to be the central theme of the 5G positioning architecture, which added further enhancements (see Figure 5). An LCS session may be initiated upon a location request from a UE or external client via the GMLC, or CN node e.g., AMF [3].

The LMF interacts with the UE using the LPP, and gNBs using NRPPa. The UE receives the required radio configuration from the NG-RAN over RRC via the NR-Interface. Leveraging the CU and DU split introduced in 5G NR, both LPP and NRPPa protocols are transported over the control plane of the NG interface (NG-C) via AMF. The architecture of the future extension including NTN positioning framework is illustrated in Figure 6.

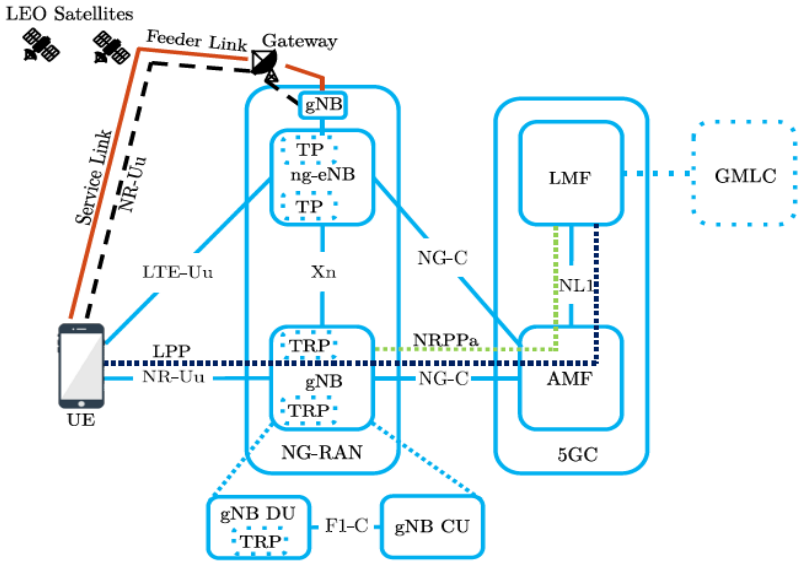

FIGURE 6: POSITIONING ARCHITECTURE WITH FUTURE EXTENSION TO NTN [4]

In NTN access, a satellite can either use a bent-pipe payload or a regenerative payload. The positioning framework shown in Figure 6 assumes the use of a bent-pipe payload. The core of the positioning process relies on measuring the time difference between transmission and reception at the TRP, which could be either an on-ground or onboard NTN gNB, or any

reference point defined by the network. Additionally, the network is able to closely track the satellites, which accounts for the feeder link delay. Therefore, the type of payload chosen does not have a significant effect on the overall accuracy of NTN-based positioning system.

1.3 POSITIONING REQUIREMENTS OF THE TARGET USES CASES

6G NTN positioning will play a crucial role in expanding the range of services that rely on precise, real-time positioning data, NTN will be instrumental in providing global coverage, ultra-reliable positioning, and high-accuracy measurements. In WP2 of the 6G NTN Project, particularly in D2.1, a variety of use cases across industries such as transportation, agriculture, public safety, and others are developed, as shown in Table 1.

TABLE 1: TARGETED VERTICALS AND SERVICE CATEGORY FOR THE PROPOSED USE CASES

		UC1	UC2	UC3	UC4	UC5	UC6	UC7
Targeted verticals								
1	Consumer					x		
2	Automotive			o		o	x	x
3	Public Safety & Defense	x		o	x	o		x
4	Utilities / Energy / IoT		x			o		x
5	Media and Entertainment				x			
6	Railways transportation		o	o				o
7	Maritime transportation	x				o		x
8	Aeronautic / drone sector		x	x				o
10	Road transportation / Smart cities			x		o	o	o
Service category								
1	Service Continuity	x	x	x		x	x	
2	Service Ubiquity	x		x	x	x		x
3	Service Scalability				x			

In WP2, multiple vertical use cases for 6G NTN networks are explored. The positioning work package will provide a detailed focus on specific use cases that are particularly relevant for further studies.

1.3.1 PUBLIC SAFETY AND EMERGENCY CALL USE CASES

For the Public Safety and Emergency Services use case, particularly in the context of 6G NTN. The requirements focus on ensuring that emergency responders, citizens, and infrastructure can rely on robust, high precision and resilient communication and positioning systems. This is crucial for improving the effectiveness of emergency responses, ensuring the safety of first responders, and enabling efficient rescue operations. The requirements on accurate positioning for emergency services in [5] are considered baseline, i.e., with tighter

requirements than for the previous application, where the positioning of UE in emergency call is provided to first responders. As defined in [5], a tight performance target is based on the FCC E911 emergency call requirements, which are 50 m horizontal accuracy and 3 m vertical accuracy on the 80% of calls.

1.3.2 REGULATORY AND LEGAL USE CASES

As defined in [5], a relaxed performance target is based on regulatory critical applications, such as call, digital tachograph, hazardous material tracking or livestock tracing, which requires below 5 m horizontal accuracy (here considered on the 90% of UEs) with a positioning availability of 99.5% and latency of 1 s. The vertical position accuracy is here assumed below 3 m on the 90% of UEs.

- **Lawful Interception (LI)**: The legal requirements for intercepting communications and ensuring that the UE's location can be accurately determined for this purpose.
- **Emergency Calls:** There are typically regulations that require accurate positioning for emergency response, so this should be addressed in sections related to safety, emergency services, and location accuracy
- **Public Warning Services**: Regulations often mandate that services such as mass notifications or alerts must work across different network types, including NTNs, which means the system should have the ability to accurately pinpoint the UE's location for notifications.

1.3.3 AUTOMOTIVE VEHICLES AND TRANSPORTATION USE CASE

The second family of users gathers all the users in deep urban areas. In these areas, connectivity to TNs is assured, but GNSS visibility may be difficult, as GNSS relies on MEO satellites. Consequently, 6G NTN LEO satellites will be considered complementary sources. The following benefits are expected.

In urban canyons, the number of visible GNSS satellites is often not sufficient to enable a positioning solution with acceptable performance for the most demanding applications (e.g., autonomous vehicles). The availability of at least one additional ranging source offered by 6G NTN LEO satellites may be sufficient to significantly increase positioning solution performance.

Depending on the frequency of band trade-off output, 6G NTN satellites will transmit wideband signals in the FR2 band. Associated ranging measurements will offer robustness to high noise, multipath, and interference, reducing measurement uncertainties to a few centimeters. With this accuracy, the applications can be:

- Cars, targeting autonomous vehicle applications
- Drones, targeting one of several applications (taxi drone, last mile delivery, critical infrastructure surveillance)

As defined in [6], the tight performance target is derived from automated driving use cases, representing safety-critical applications. It specifies a horizontal positioning accuracy below 10 cm, achieved in 90% of UEs. The positioning availability is set at 99.9%, with a latency requirement of 1 second.

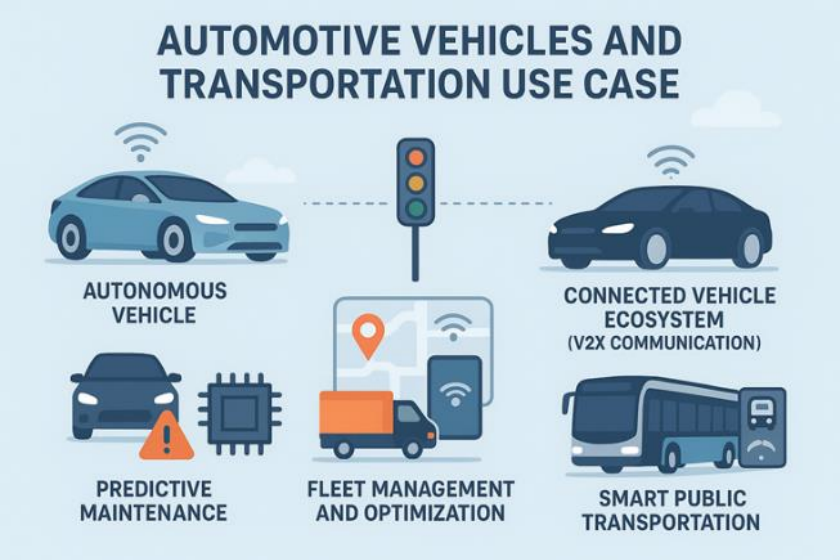

FIGURE 7: AUTOMOTIVE AND TRANSPORTATION ILLUSTRATION FOR POSITIONING

1.3.4 PRECISION AGRICULTURE USE CASE

With 6G NTN, precision agriculture can be conducted on a global scale, even in areas far from the reach of TNs, providing farmers with precise location data for every aspect of the crop lifecycle. Application: Automated crop management, smart irrigation, precision soil mapping, and livestock tracking. Agriculture using 6G NTN positioning refers to leveraging the advanced capabilities of NTN enabled by 6G technology to enhance agricultural practices. With NTN positioning, farmers can access precise, real-time data from remote sensors, drones, and IoT devices, even in rural or hard-to-reach areas. This enables more accurate monitoring of crop health, soil conditions, and weather patterns, leading to optimized resource management, improved yields, and sustainable farming practices. The integration of NTN with 6G allows for a seamless, global network that supports precision agriculture, making farming smarter and more efficient.

FIGURE 8: AGRICULTURE USING 6G NTN POSITIONING WHITH DRONES

1.3.5 MARITIME NAVIGATION USE CASE

Many vessels navigate using GNSS receivers. However, this solution presents two main drawbacks:

- It is vulnerable to Radio Frequency Interference (RFI) attacks, like any GNSS receiver in the world.
- To improve positioning performance, it is combined with very expensive high grade IMUs.

The use of 6G NTN signals to complement the current maritime navigation architecture may help improve the resilience of the solution and maybe reduce the cost of the navigation solution. Constellations are fully exploited based on native NTN positioning methods for high performance positioning applications, where TN-NTN is used as a complementary positioning technology under GNSS degraded conditions or alternative positioning technology under GNSS unavailability.

FIGURE 9: MARITIME EXAMPLE OF NTN POSITIONING

1.3.6 ASSET TRACKING USE CASE IN IOT NTN

Internet of things (IoT)-NTN satellite constellations are used with native NTN positioning methods, specifically tailored for low-power and coarse positioning.

The performance targets are set with tight and relaxed requirements, specifying horizontal accuracy of 10 m and 30 m (assumed for 80% of cases), respectively. The positioning availability is defined at 99%, with relaxed latency. These accuracy requirements align with TR 22.872 and the indicative values in [7] based on receiver conditions. For both target levels, the vertical position accuracy is considered to be below 3 m for 80% of UEs.

FIGURE 10: ASSET TRACKING USE CASE

1.3.7 SUMMARY OF POSITIONING REQUIREMENTS

Table 2 summarizes the positioning requirements derived from all the targeted use cases identified in previous sections. The summary aims to provide a unified view of the key

performance indicators—such as accuracy and position availability, to support diverse application domains.

In summary, positioning requirements across targeted use cases involve customizing the positioning system to meet specific needs, considering environmental, technological, regulatory, and user-related factors that vary for each scenario.

From the analysis of requirements in WP2, it is important to highlight that some of these requirements when taken alone are reachable with today's technologies (high precision, availability, etc.). But the combined need for high precision, and availability, and integrity throws the challenge, especially when further considering Hardware (HW) and computational constraints.

TABLE 2: REQUIREMENTS OF USES CASES FOR POSITIONING

Use case		Horizontal Accuracy	Vertical accuracy	Position availability	Sources
Regulatory and legal applications	**Emergency services**	50 m (80%)	3m	95%	Annex A of 3GPP TR 38.882
	Lawful Interception (LI)	macro cell size granularity up to 5-10 km diameter	macro cell size granularity up to 5-10 km diameter		
	Public Warning Service (PWS)	macro cell size granularity up to 5-10 km diameter	macro cell size granularity up to 5-10 km diameter		
	Billing/charging	macro cell size granularity up to 5-10 km diameter	macro cell size granularity up to 5-10 km diameter		
Automotive vehicles and Transportation		10 cm (90 %)		99,9%	
Precision Agriculture		10 cm		99,9 %	
Maritime Navigation		1-10 m (95%)		99,9%	
Asset tracking		10 cm		99%	

Focusing on the integrity illustrated in Figure 11, whether the target application puts human safety at stake or not is a very important driver for the design of relevant next generation hybridised receiver. A major challenge in these cases arises from the use of potentially non

solution certified positioning technologies, as GNSS is a tremendous innovation and a cornerstone for all positioning applications today.

Yet, the positioning and navigation service provided by current GNSS constellations in standalone mode is reaching some limits. The following figure summarizes the main known limitations and threats of GNSS systems.

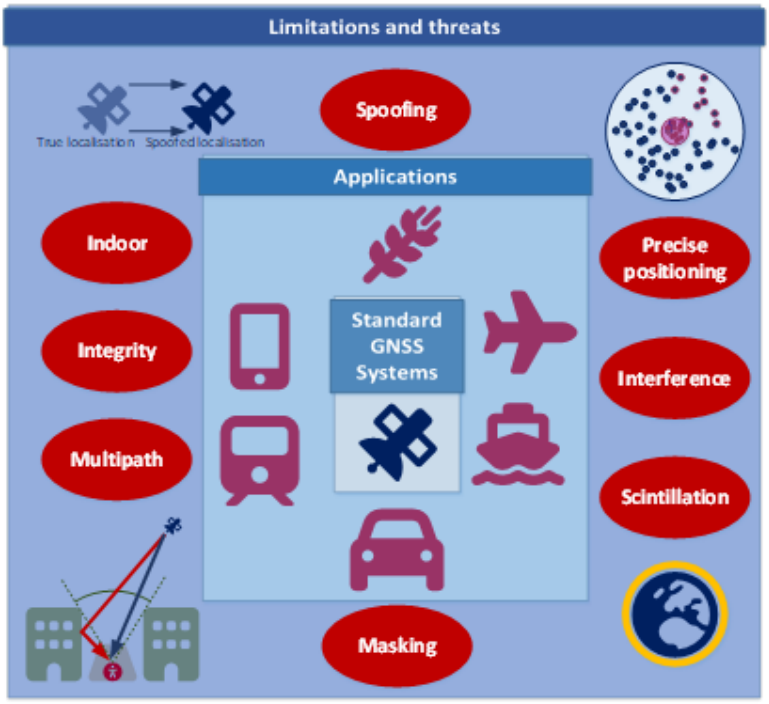

FIGURE 11: GNSS ECOSYSTEM AND MAIN LIMITATIONS

All these limitations and threats make standalone GNSS vulnerable. If innovative standalone solutions exist to tackle some of them: larger bandwidth signal for multipath, multi-antenna for interference and spoofing, they are often expensive and complex, and do not cover all types of environments relevant for the user scenarios of concern here. In that context, 6G NTN-based positioning solutions are essential to provide a reliable and precise ubiquitous positioning solution. This complementarity is expected to improve the robustness against threats.

2 ANALYSIS OF THE STATE OF THE ART FOR POSITIONING

2.1 POSITIONING IN TN AND NTN

To offer a comprehensive understanding of the status and future developments of positioning systems in TNs and NTNs we start by providing a detailed overview of the evolution of positioning systems across various cellular standards using RAT, with particular focus on current 5G efforts in NTN-based location verification that rely on coarse position estimates.

2.1.1 POSITIONING IN 5G TN

The positioning methods used in traditional terrestrial mobile communication systems 5G TN [8] can generally be categorized into two main types: i) angle-based methods, such as Angle of Arrival (AoA) and Angle of Departure (AoD), are particularly suitable for Frequency Range 2 (FR2), which operates in the millimeter-wave (mm-Wave) spectrum. These methods exploit the high-frequency characteristics of FR2 to achieve highly accurate positioning; ii) distance-based positioning. In distance-based positioning, distance information can be either absolute or differential.

- Absolute distance directly reflects the range between the transmitter (a ground-based station or satellite) and the device to be located. In this case, the device is located on a sphere centered at the transmitter with a radius equal to the measured distance. When multiple absolute distance measurements are available, the intersection of their respective spheres can be used to determine the device's position.
- Differential distance reflects the difference in distance between a single device and multiple transmitters. The device lies on a hyperboloid defined by the two transmitters as foci and the distance difference as the real semi-axis. The intersection of multiple such hyperboloids allows for the determination of the device's location.

5G leverages time of flight and angular resolution to bring multiple positioning techniques for different deployment scenarios and use-cases. It can support highly precise positioning in the vertical and horizontal dimensions, with the narrower beam and wider bandwidth in FR2 frequencies lending to high precision in angle and timing in future 6G TN.

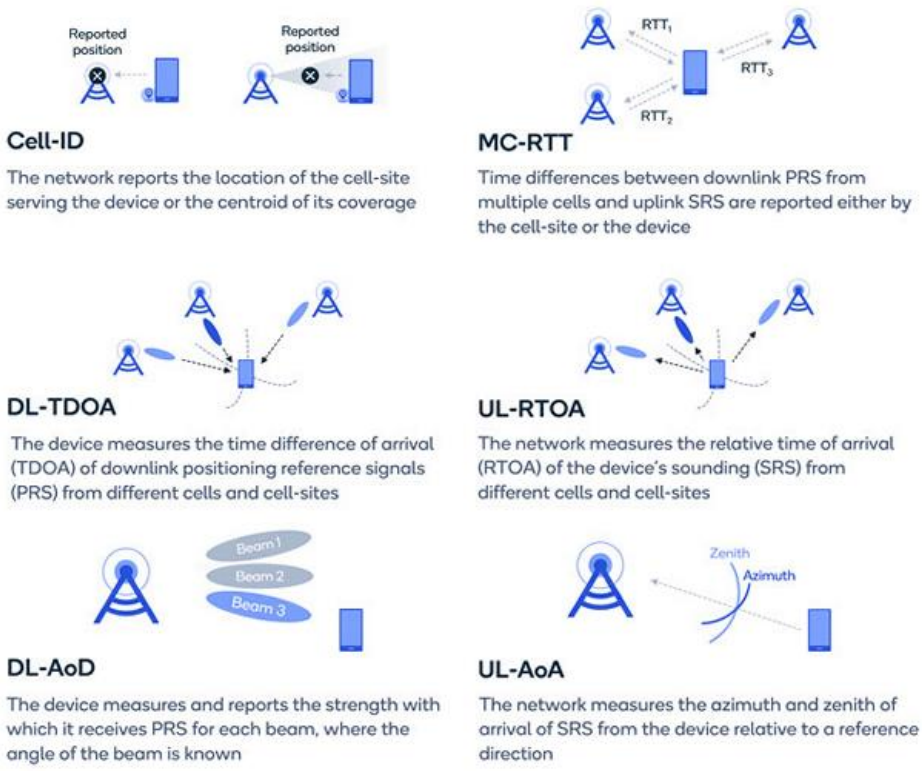

FIGURE 12: 5G BRINGING PRECISE POSITIONING TO THE CONNECTED INTELLIGENT EDGE [9]

According to the Release 16 detailed in section From 5G to 6G NTN, positioning is applicable to any target UE, whether or not the UE supports location services, but with restrictions on the use of certain positioning methods depending on UE capability. The standard 3GPP positioning methods support both frequency division duplexing and time division duplexing, and include the following positioning techniques illustrated in Figure 12:

- **Network-assisted GNSS positioning**, in which the UE position is estimated using GNSS measurements (e.g. pseudo-ranges, pseudo Doppler, carrier phase ranges, etc.) and assisted data such as atmospheric models, satellite ephemeris, visible satellite list, etc.
- **E-CID,** in which the UE position is estimated with the knowledge of the geographical coordinates of its serving base station (BS). The signal measurements can be the reference signal received power (RSRP), reference signal received quality (RSRQ), RTT or any combination of them.
- **Downlink TDOA (DL-TDOA),** in which the reference signal time difference (RSTD) is measured by the UE from downlink signals received from multiple BSs. The measurements are used along with their relative downlink timing and the knowledge of the geographical coordinates of the BSs to locate the UE in relation to the neighboring BSs.
- **Uplink TDOA (UL-TDOA),** in which the relative time of arrival (RTOA) is measured at multiple BSs from uplink signals transmitted by the UE. The measurements are used along with their relative uplink timing to estimate the UE position.
- **Downlink AoA (DL-AOD),** in which the RSRP per beam is measured by the UE from downlink signals received from multiple BSs. The measurements are used to determine the AOD for each BS-based on the UE beam location. Based on the AODs and the knowledge of the geographical coordinates of the BSs, the UE position can be estimated.
- **Uplink AoA (UL-AOA),** in which the azimuth of arrival (AOA) and zenith of arrival (ZOA) are measured at multiple BSs from uplink signals transmitted by the UE. The AOA and

ZOA are determined by each BS-based on the beam the UE is located in. Based on the AOAs and the knowledge of the geographical coordinates of the BSs, the UE position can be estimated.

- **Multi-cell RTT**, in which the UE and the BSs perform the difference between the transmission and the reception time. The measurements are used to determine the round-trip time of each cell and estimate the UE position.

2.1.2 SATELLITE-BASED POSITIONING

A satellite positioning system consists of a constellation of satellites that transmit signals, which are used to determine the position of a receiver. The general term for such a system is GNSS. Satellite systems are one type of positioning technique used in NTN networks.

GNSS refers to MEO satellites that offer global or regional coverage and it is used for navigation as well as other applications such as geology and geophysics. There are several types of GNSS, including the Global Positioning System (GPS), Galileo, Global Navigation Satellite System (GLONASS), and BeiDou [10]. Each system has its own satellite constellation, coverage area, and accuracy levels. GPS, being the oldest and most widely used GNSS, provides global coverage and is available in most countries. [4] provides a general description of the GPS system for localization and navigation, including an explanation of its operation. In this section, a description of the existing satellite positioning solutions and their accuracy positioning will be given in Table 3.

TABLE 3: COMPARISON OF DIFFERENT GNSS SYSTEMS FOR POSITIONING

GNSS	GPS	Galileo	GLONASS	Beidou
Frequency (MHz)	L1/L2 1575.42/1227.6	E1/E15a (1575.42/1176)	L1 (1,6 GHz) et L2 (1,2 GHz)	B1/B2(11561.098/1207.14)
Satellite constellation	31	30	24	45
Country	USA	Europe	Russia	Chinese
Constellation Type	*MEO*	*MEO*	*MEO*	MEO+IGSO+GEO
Accuracy(civilian)	*~5-10 metes*	*~ 1- 3 meters*	~2- 5 meters	~ 2.5 – 5 meters

GNSS systems are essential for delivering accurate positioning and timing for a wide variety of civil and military purposes. However, GNSS signals are prone to both unintentional and intentional interference, largely due to their naturally weak signal strength. This vulnerability makes it possible for attackers to disrupt location- and time-dependent applications through spoofing attacks, where fake GNSS signals can mislead receivers and cause them to calculate incorrect positions or times.

2.1.3 MAIN RANGING ERRORS CONTRIBUTION TO SATELLITES POSITIONING

Ranging errors are inaccuracies in the measured pseudo range between a GPS satellite and a receiver. They come from several sources and are grouped into six main classes [11] illustrated in Table 4:

- **Ephemeris Data Errors** occur when the transmitted satellite position (ephemeris) is inaccurate.

- **Satellite clock errors,** due to inaccuracies in the satellite's onboard clock, which affect all users equally. These are independent of satellite direction.
- **Ionosphere errors,** Caused by signal delay through the ionosphere; dependent on electron density and signal frequency.
- **Tropospheric errors,** Due to signal delay from water vapor and air pressure variations in the lower atmosphere.
- **Multipath errors** occur when reflected signals (off buildings, terrain, etc.) reach the receiver in addition to the direct path.
- **Receiver errors,** due to receiver thermal noise, software inaccuracies, and channel biases.

TABLE 4: STANDARD ERROR MODEL

	One-sigma error, m		
Error source	Bias	Random	Total
Ephemeris data	2.1	0.7	2.1
Satellite clock	2.0	0.7	2.1
Ionosphere	4.0	0.5	4.0
Troposphere	0.5	0.5	0.7
Multipath	1.0	1.0	1.4
Receiver measurement	0.5	0.2	0.5
User equivalent range			
error (UERE), rms	5.1	1.4	5.3
Filtered UERE, rms	5.1	0.4	5.1
Vertical one-sigma errors2	VDOP= 2.5		12.8
Horizontal one-sigma errors -HDOP	HDOP = 2.0		10.2

Each class is briefly discussed in the following sections. Representative values for these errors are used to construct an error table in a later section of this chapter.

2.1.3.1 EPHEMERIS DATA ERRORS

Ephemeris errors occur when the GPS message fails to convey the satellite's true position. Typically, the radial component of this error is the smallest, while the tangential and cross-track components can be up to an order of magnitude larger. However, these larger components have a smaller impact on ranging accuracy. When this is multiplied by the unit satellite direction vector. Only the component of the satellite position error projected along the line of sight contributes to the ranging error. Since satellite position errors are based on predicted positions, they tend to increase with time after the last control station update. It is also possible that part of the deliberate Selective Availability (SA) error is added to the ephemeris data. However, because satellite trajectories are smooth and predictable, ephemeris errors change slowly over time, which limits the effect of SA on these predictions.

2.1.3.2 SATELLITES CLOCKS ERRORS

Satellite clock errors are a fundamental source of GPS ranging inaccuracies, as the one-way ranging process depends directly on the precision and stability of the satellite's onboard clock.

These timing errors affect both C/A-code and P-code users equally. (See Appendix APPENDIX)

Importantly, satellite clock errors are independent of the satellite position or direction, which is particularly advantageous when differential correction techniques are applied. In such methods, all differential stations and users experience and correct the same satellite clock error, improving overall positioning accuracy. A major contributor to apparent clock error is Selective Availability (SA), an intentional variation introduced to degrade clock predictability. SA caused the satellite clock to vary unpredictably over intervals longer than approximately ten minutes, leading to additional uncertainty in ranging measurements.

2.1.3.3 IONOSPHERE ERRORS

Ionosphere errors arise from the effect of the Earth's ionosphere on GPS signal propagation. As GPS signals travel from the satellite to the receiver, they pass through this electrically charged layer of the atmosphere, where variations in electron density cause signal delays. The amount of delay depends primarily on the total electron content (TEC) along the signal path, as well as on the frequency of the transmitted signal. Because the ionosphere is a dispersive medium, higher-frequency signals are delayed less than lower-frequency ones. This property allows dual-frequency GPS receivers to measure and correct most of the ionosphere delay by comparing the phase and travel time of the two signals (L1 and L2). Single-frequency receivers, however, must rely on ionosphere models broadcast by the GPS system, which estimate the delay based on time, location, and solar activity.

Ionosphere errors are strongly influenced by solar radiation, geomagnetic activity, geographic latitude, and time of day. They tend to be greatest during periods of high solar activity, near the equator, and around noon local time. Under such conditions, uncorrected ionosphere delays can reach several tens of meters, significantly degrading the positional accuracy if not properly compensated for.

2.1.3.4 TROPOSPHERIC ERRORS

The troposphere, often described as the neutral part of the Earth's atmosphere, is the closest atmospheric layer to Earth's surface. The troposphere is started up to an altitude of about 50 km, where the refractive index is always greater than one. In consequence, tropospheric delays are expected in signals emitted by satellites on low Earth orbits. Variations in tropospheric delay depend on temperature, atmospheric pressure, humidity, and water vapor.

This delay also depends on the receiver's geographic location as well as the satellite elevation angle relative to the receiver. In terms of LEO systems based positioning, identical empirical models currently used in GNSS can be used for frequencies below 15 GHz. A possible gain is related to decorrelation of the troposphere during the estimation process. Indeed, the line-of-sight changes much faster for LEO transmitters than MEO ones. This geometric gain may greatly affect time.

2.1.3.5 MULTIPATH CHANNEL ERRORS

LEO constellations can offer higher signal power than MEO. Nonetheless, multipath effects reduce signal quality and power when NLoS propagation dominates.

Outdoor multipaths may be dealt with in a similar way to classic GNSS systems. However, given the possibility of indoor positioning, we discuss the transmission of RF signals into buildings and introduce satellite-to-indoor channel models developed in this environment.

Unlike the reception of GNSS signals outdoors, where the line of sight (LoS) propagation dominates the communications between satellites and end user, indoor reception includes additional local interactions of materials and signals on spatial scales ranging from just a few meters to hundreds of meters.

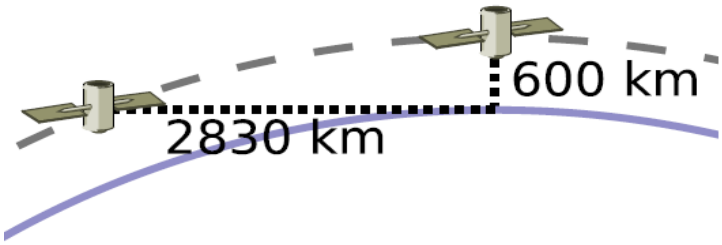

FIGURE 13: TWO LEO SATELLITES (ALTITUDE 600 KM), ONE AT NADIR AND THE OTHER NEAR THE HORIZON

The smaller spatial scales allow direct experimentation with a building system in response to excitation by externally applied electromagnetic radiation. The use of the channel impulse response method has been central to several measurement and modelling activities. Results from observation and analysis activities [12] [13] have demonstrated that:

- Indoor received signals vary as a function of the azimuthal and polar/altitude angles associated with the transmitter/receiver geometry, see Figure 14, and building materials.
- Signal-level fluctuations can be as high as 30 dB over periods of several hundred milliseconds within various locations in a single room.
- There is multipath activity with contributions of 20 to 35 wave fronts and associated delays up to 100 ns relative to the LoS signal.

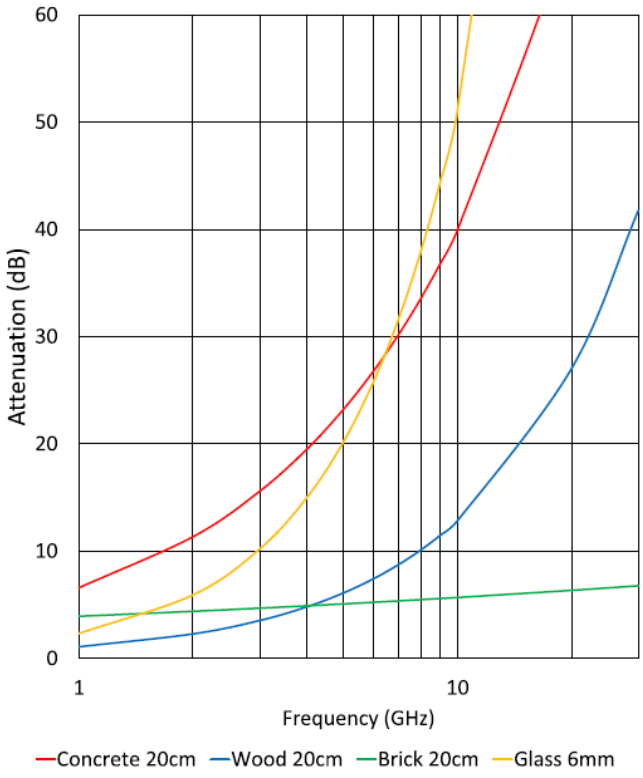

FIGURE 14: RF SIGNAL ATTENUATION CAUSED BY ABSORPTION CHARACTERISTICS OF COMMON BUILDING MATERIALS.

As shown in Figure 15, electromagnetic waves from LEO antennas travel a few hundred kilometers along the LoS. Waves may hit the different objects on earth (buildings, trees, cars, etc.) and propagate into different directions due to scattering, diffraction, and reactions. Furthermore, waves can penetrate the building's roof or walls, resulting in losses that depend on the construction material. In general, wave propagation indoors will be mainly in the form of multipath, and the impulse response of multipath wireless channels can be modelled as the path delays indoors are smaller than those observed from the outdoor environment.

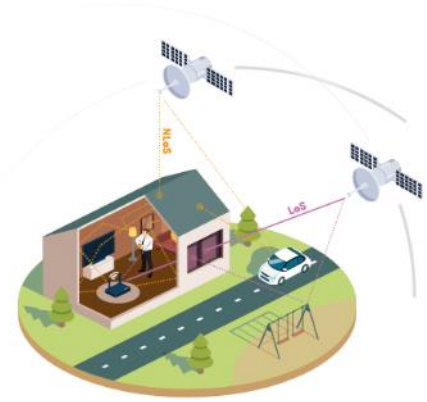

FIGURE 15: CONCEPTUAL DEPICTION OF LOS AND NLOS SIGNALS PROPAGATING FROM LEO SATELLITES TO AN INDOOR ENVIRONMENT.

$$h(t,\tau) = \sum_i \alpha_i(t) e^{-j\theta_i(t)} \delta\left(\left(t - \tau_i(t)\right)\right)$$

The summation is performed over the waves' path components. Each path has its specific gain α_i, angle θ_i, and delay τ_i.

Due to the associated uncertainty; it is convenient to consider the parameters of the channel impulse response as random processes. The signal strength usually decreases inversely with the distance between the transmitter and receiver (in free space, the power gained obeys an inverse square law). However, due to the multipath environment, it could easily be shown that the power attenuation with distance can be higher than 2 and is usually between 3 and 5 or even more. In some exceptional indoor scenarios, the power-law factor may be less than 2; this is known as the waveguide effect, but a power-law factor of 3 to 4 is more common in indoor applications. In a real environment, the channel model depends on a vast number of factors. Hence, it is feasible to find an accurate deterministic model that could be used to express the general channel model to express the multipath channel uncertainties. The models best known for this purpose are the Rician, Rayleigh and Nakagami-m channel models.

The Rician channel model is used for a strong LoS beam beside multipath components, as when the LEO satellite is on a small horizontal angle, the electromagnetic wave might propagate indoors with a strong LoS path through the windows. On the other hand, the Rayleigh

$$P_r = \frac{G_{rt}\sigma\eta}{d^{\alpha}} P_t$$

Where P_r and P_t are the received and the transmitted power respectively, G_{rt} is the multiplication of transmitter and receiver antenna gains, d is the distance between the transmitter and the receiver, σis the shadowing can be modelled as random process with lognormal distribution, but passed through a narrow band linear filter shadowing represents

slow losses such as those caused by entering buildings or being a big object. On the other hand, η represents a small-scale factor generally results from multipath. It can be modelled as the square of a random process (Rayleigh, Rician, or Nakagami) passed through a linear filter representing the Doppler filter.

2.1.4 SUMMARY OF STATE OF THE ART

The most ionosphere channel models for GNSS positioning do account for the ionosphere delay from the ground up to approximately 800 and 20,200 Km of the extra ionosphere content in such models, which requires dedicated ionosphere models for single-frequency systems. Another point is ionosphere scintillation has been one of the main barriers to achieving sub-decimeters' accuracy for precise GNSS positioning. Therefore, it is a great opportunity for upcoming 6G NTN systems to mitigate ionosphere scintillation by increasing signal frequency.

6G NTN-based LEO satellites for positioning systems can also provide a significant means for mitigation of the tropospheric effects. Due to the faster speed of LEO compared to MEO satellites, the spatial-temporal decorrelation of the tropospheric delay estimation is better achieved as the line-of-sight geometry changes faster.

In the analysis of positioning in the literature, it is essential to distinguish between TN positioning methods and satellites positioning. GNSS, such as GPS, Galileo, GLONASS, and BeiDou, rely on satellite constellations orbiting the Earth to provide absolute global positioning. These systems determine the user's location by measuring the time of arrival of signals transmitted from multiple satellites, typically requiring line-of-sight conditions, and a dedicated GNSS receiver integrated within the UE. However, GNSS performance degrades significantly in environments with signal blockage, multipath propagation, or interference, such as dense urban areas or indoors. In contrast, cellular based called positioning advantages the TN infrastructure such as base stations to estimate the UE's location. Using techniques like OTDOA, AOA, UTDOA, and E-CID, cellular systems can determine position either through network-based calculations or through UE-assisted measurements. Because these methods rely on existing RAN signaling, cellular positioning can operate independently of GNSS, even in UEs without GNSS hardware.

Moreover, 5G TN methods-based positioning offers several advantages over GNSS. It provides better coverage in challenging environments e.g., indoors, tunnels, or urban canyons), can leverage network synchronization and reference signals, and allows for integration with other services like emergency response, IoT tracking, and vehicular communications. The continued evolution of 5G and upcoming 6G standards is further enhancing the accuracy and reliability of cellular positioning, enabling standalone operation and complementing or even replacing GNSS in certain scenarios.

Therefore, when combining both aspects of the 5G/6G networks, the positioning service, and the NTN, there are several benefits such as: an independent and complete communication and navigation system under a 6G single network, higher accuracy on the positioning framework solution than previous generation, global coverage for joint navigation and communication, higher resilience on the positioning estimation, or new services offered. However, in TNs, the propagation time is short enough that the synchronization of the uplink depends directly on that of the downlink. However, in NTN networks, this time is much longer and exceeds the duration of a transmission slot.

2.2 REVIEW OF NTN POSITIONING STANDARDS

2.2.1 FROM 5G TO 6G NTN

To provide a comprehensive understanding of the current and future landscape of user positioning in 5G NTN through LEO satellite, we provide in the following sections a detailed overview of the evolution of positioning systems across different cellular standards, with specific emphasis on the current 5G activities on NTN.

Figure 16 [4] summarizes the evolution of positioning/ranging in various 3GPP standards, from 1G to 5G advanced.

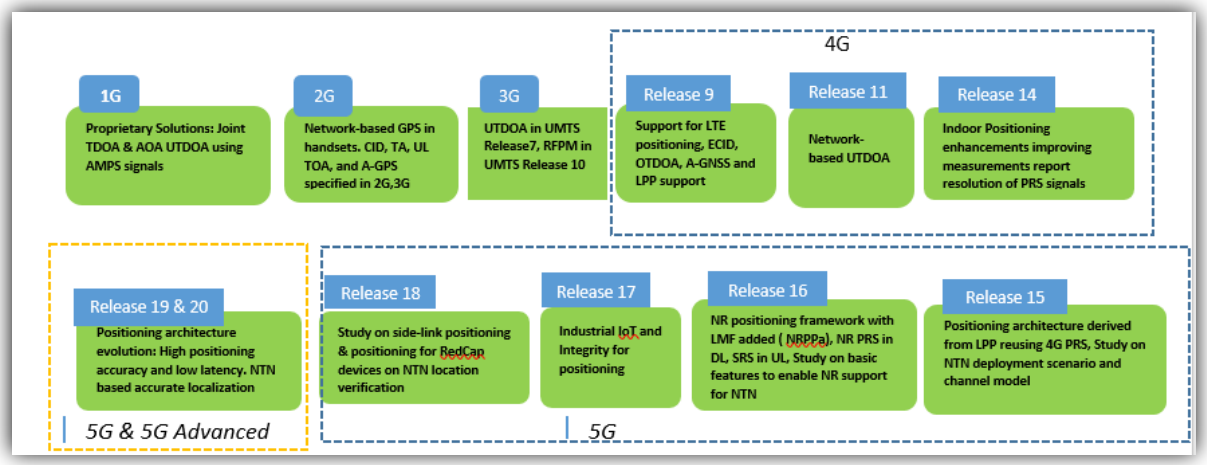

FIGURE 16: THE EVOLUTION OF POSITIONING OF 3GPP STANDARDIZATION [4]

In 1G, positioning was used primarily for intelligent vehicle highways systems and emergency services, relying on proprietary solutions using joint TDOA, and UTDOA.

The initial 2G network did not focus on positioning. Nevertheless, positioning becomes more crucial for emergency services with the FCC of the United States approving locations requirements on 911 emergency calls. Consequently, UE-based positioning techniques such as GPS were supported in terminals. Assisted GPS was introduced to help GPS with navigation messages and different corrections. The effort was continued to develop a functional description of LCS for 2G and 3G networks. To implement LCS, positioning schemes such as CID, TA, and UL-TOA were specified. Later in 3G, UTDOA was specified in Release 7, while RFPM was included in Release 10 to progress. Based location verification requires a coarse location estimate. While 5G cellular positioning methods retain some fundamental elements from the past, regarding architecture and protocol, the evolution really started from 4G. In 4G, to assist GNSS, some RAT methods were developed as an alternative for positioning. Different positioning methods such as E-CID, OTDOA for LTE, and PRS for LTE were specified. In later releases, UTDOA support was added by using UL reference signal (SRS). In 4G, the LCS signaling in the network (CN) was standardized. The LMF was introduced to interact with external clients (i.e. application, UE,) with location request/response and send localization assistance information with eNBs and UE.

2.2.2 IMPLEMENTATION IN 5G

The LCS signaling and LMF continue to be the central theme of the 5G positioning architecture. An LCS session may be initiated upon a location request from UE or external client via the GMLC, or CN node e.g. AMF. The LMF interacts with the UE using the LPP, and gNBs using the NRPPA.

The UE receives the required radio configuration from the NG-RAN over RRC via the NR-Uu interface. Leveraging the centralized unit (CU) and distributed unit (DU) split introduced in 5G

NR, both LPP and NRPPa protocols are transported over the control plane of the NG interface (NG-C) via AMF. The gNB CU is connected to a gNB DU over the F1 interface. The TRP in 5G-RAN, a central part of a gNB DU, is an abstract node that can transmit PRS in downlink and perform SRS measurements in uplink. Using the DL and UL measurements from the UE and TRPs, the LMF may compute the UE location using RAT-dependent positioning methods like TDOA, multi-RTT, DL AOA, UL AOA, and E-CID

The implementation of 5G positioning is facilitated using an optimized architectural design for the transmission of location signals between gNB and UE and the exchange of location measurements with the LMF. The architectural specifications for the positioning of 5G are contained in 3GPP TS 23.273. As depicted in Figure 17 the composition of the 5G positioning architecture encompasses the following components: UE that may carry out measurements of downlink signals from the NG-RAN, which may be time or angle-based, depending on the chosen positioning methodology.

- NG-RAN, comprised of gNB and ng-eNB network elements, which may contribute to the calculation of position estimates through radio signal measurements and convey these measurements to the LMF;
- The AMF, which is responsible for handling connection and mobility management tasks including positioning for a target UE;
- LMF, which is responsible for managing and supporting a range of location services for target UEs, including computation of user position and the delivery of assistance data.
- The ESMLC provides location information to the network, processes and combines location data from multiple sources, and transmits the position information to the requesting entity;
- The SLP is a server-based technology for providing secure and accurate location services to mobile devices. It is part of the SUPL specification developed by the OMA for delivering LBS in mobile networks.

In particular, the LMF receives location requests for a target UE from the serving AMF and interacts with the NGRAN to obtain both uplink and downlink position measurements. The LMF may also directly engage with the target UE to provide requested assistance data or calculate a location estimate. The LMF determines the positioning methods to be employed based on various factors such as the LCS, Client type, the desired QoS class (see [15]). UE positioning capabilities, and NG-RAN positioning capabilities, and involve these methods in the UE and serving NG-RAN. The positioning methods may result in location estimates for UE-based methods and positioning measurements for UE-assisted and network-based methods.

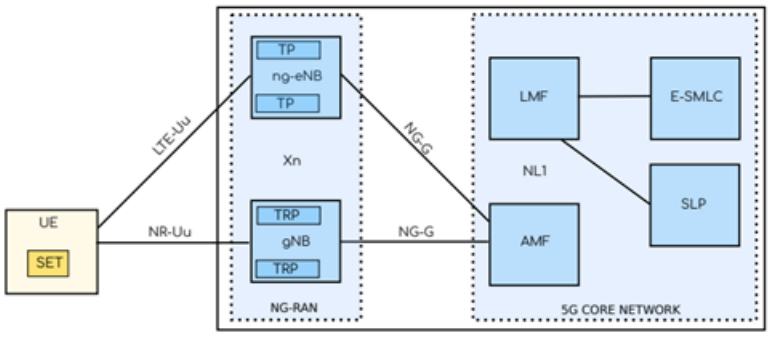

FIGURE 17: 5G POSITIONING ARCHITECTURE DISCUSSED IN 3GPP

In Release 18 [2], 3GPP continues NR positioning evolution by investigating different solutions to improve accuracy performance. Although, the positioning evolution is still focused on TNs 5G TN.

2.2.3 NTN DEPLOYMENT AND ASSOCIATED POSITIONING ACTIVITIES

NTN was introduced in Release 17 [14] through for various communications channels, from IoT to 5G communications. However, at least up to Release 19, the use of GNSS was considered mandatory for the UEs, as well explained in [16].

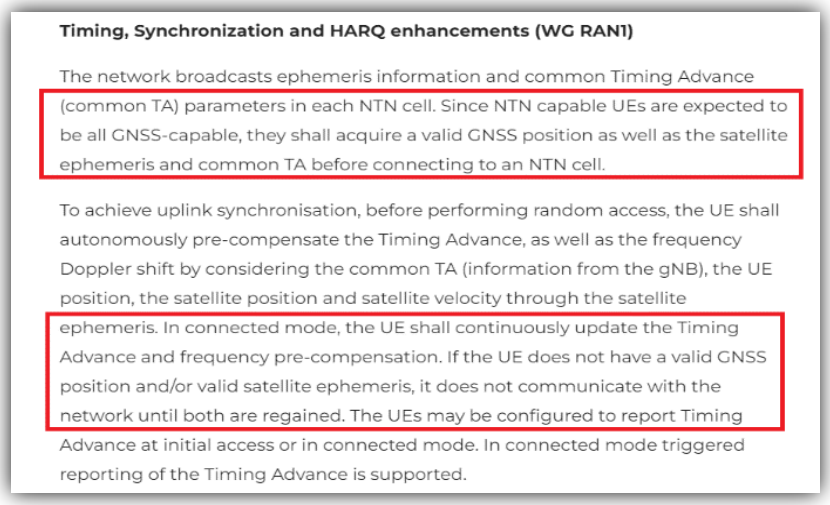

Timing, Synchronization and HARQ enhancements (WG RAN1)

The network broadcasts ephemeris information and common Timing Advance (common TA) parameters in each NTN cell. Since NTN capable UEs are expected to be all GNSS-capable, they shall acquire a valid GNSS position as well as the satellite ephemeris and common TA before connecting to an NTN cell.

To achieve uplink synchronisation, before performing random access, the UE shall autonomously pre-compensate the Timing Advance, as well as the frequency Doppler shift by considering the common TA (information from the gNB), the UE position, the satellite position and satellite velocity through the satellite ephemeris. In connected mode, the UE shall continuously update the Timing Advance and frequency pre-compensation. If the UE does not have a valid GNSS position and/or valid satellite ephemeris, it does not communicate with the network until both are regained. The UEs may be configured to report Timing Advance at initial access or in connected mode. In connected mode triggered reporting of the Timing Advance is supported.

FIGURE 18: EXTRACT OF 3GPP DOCUMENTATION FOR NTN

The first standardized version completed in Release 17 is addressing:

Identified issues due to long propagation delays, large Doppler effects, and moving cells in NTN.

- NG-RAN architecture enhancements and related procedures.
- Service continuity from TN to NTN and from NTN to TN systems.

The 5G NTN architecture focuses on transparent architecture and covers both Earth moving and Earth fixed radio cells. NR NTN based on LEO and GEO has an implicit compatibility to support HAPS (High Altitude Platform Station) and ATG (Air o Ground) scenarios.

The Release 17 defines that the UE part of NTN System has GNSS capabilities for the proper system computation for the Timing Advance and Doppler compensation.

In the overall 5G NTN System performance budget, the following assumptions are made:

- The UE GNSS positioning accuracy is better than 30 m.
- The 5G NTN Satellites broadcast their ephemerides with a maximum error as follows:
  - Max ranging Error < ±120m;
  - Max Doppler Error: <±1.5 m/sec
  - 5G NTN serving-satellite positioning estimation accuracy < 34 m

Since R18, 3GPP has begun exploring NTN-based positioning research and established a UE position validation research project to investigate how the network can effectively perform position verification in cases where the UE reports inaccurate positions. This ensures that the services provided by the network comply with local laws and regulations and meet regulatory requirements.

At the 109th meeting of the Radio Access Network (RAN) Working Group 1 (RAN1), discussions focused on the feasibility and theoretical accuracy of various NR-based positioning schemes in NTN, the specific challenges in NTN scenarios such as low overlap coverage, low signal-to-noise ratio, high operating frequency bands, and insufficient CP length with large subcarrier spacing. At the 110th meeting of RAN1, the discussions mainly covered basic positioning scenarios, the positioning methods employed, and the necessary simulation parameters. During the 110 bis meeting of RAN1, further analysis was conducted on the DL-TDOA and Multi-RTT positioning algorithms. Subsequent meetings further examined issues such as positioning accuracy under different geometric configurations and with UE clock drift. These discussions culminated in the conclusion of the relevant research at the 115th meeting of RAN1 [11-16].

However, due to the prioritization of other topics, further enhancements in 5G NTN positioning were not included in 3GPP Release-19, leaving GNSS as the primary positioning method. Looking ahead, 3GPP Release 20, which is recognized as the first release initiating pre-studies for 6G, is expected to revisit and expand NTN-based PNT solutions in response to evolving use cases and industry-driven demands.

The specific topic of NTN positioning is very well shown by section 6.4.10 of document TS 22.261 (Service requirements for the 5G system; Stage 1, Release 20).The standardization aspects for next Release 20 et 21 will be presented in WP6.

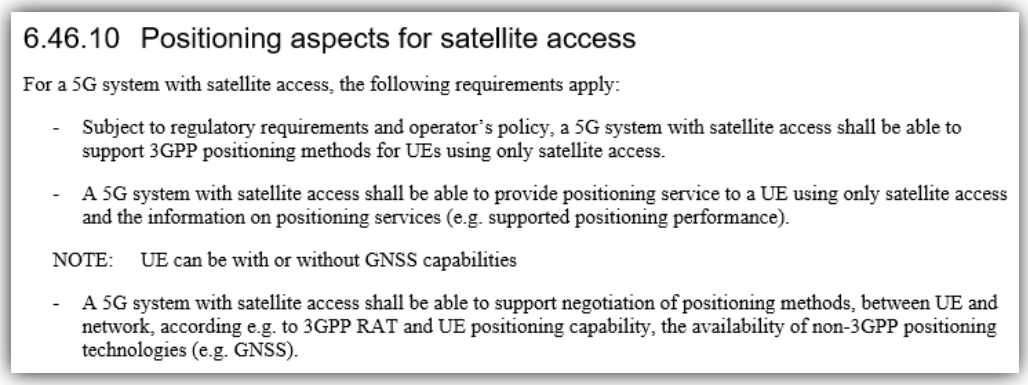

6.46.10 Positioning aspects for satellite access

For a 5G system with satellite access, the following requirements apply:

- Subject to regulatory requirements and operator's policy, a 5G system with satellite access shall be able to support 3GPP positioning methods for UEs using only satellite access.
- A 5G system with satellite access shall be able to provide positioning service to a UE using only satellite access and the information on positioning services (e.g. supported positioning performance).

NOTE: UE can be with or without GNSS capabilities

- A 5G system with satellite access shall be able to support negotiation of positioning methods, between UE and network, according e.g. to 3GPP RAT and UE positioning capability, the availability of non-3GPP positioning technologies (e.g. GNSS).

FIGURE 19: EXTRACT OF REL. 20 SERVICE REQUIREMENTS

In the future 6G releases (Release 20 and beyond), the focus will not only be on improving terrestrial-based positioning but on enhancing the positioning capabilities in hybrid environments, combining TN and NTN. This will be crucial for ensuring global coverage with high-precision services, as well as location-based services with real-time accuracy even in challenging environments. The challenges in the standardization of NTN-based positioning for 6G will revolve around latency, signal reliability, accuracy, and the ability to seamlessly integrate satellite constellations with TNs.

Achieving cm accuracy using 6G NTN-based positioning will be a key target, with applications in autonomous systems, reliable positioning. 3GPP Release 20—recognized as the first release to initiate 6G pre-studies—is expected to revisit and extend NTN-based PNT solutions in response to emerging use cases and growing industry demands.

2.3 NTN POSITIONING SECURITY RISK ANALYSIS RELATED TO GNSS

2.3.1 5G NTN RISK ANALYSIS RELATED TO GNSS

5G NTN relies on GNSS to access the 5G NTN network. Nevertheless, verification or stand-alone positioning with 5G satellite networks, potentially hybridized with 5G TNs, is necessary for Law Enforcement, Emergency, User Charging, and PLMN selection.

The document *"**Study on requirements and use cases for network verified UE location for Non-Terrestrial-Networks (NTN) in NR***. This document is related to this challenge.

Positioning Security Risk Analysis has been provided in 3GPP TR 38.857 V17.0.0 (2021-03) tackling the RAT independent security risk. The 3GPP TR 38.857 analysis integrates already a process with Galileo/GPS authenticated signals and a RAT dependent timing solution to detect spoofing.

It is understood that the here considered feared event is a tampering of the UE with a corruption of the GNSS data uplinked to the 5G NTN, while the receiver still pre-compensates the correctly the signals (Timing Advance, Doppler) uplinked with the correct GNSS solution inputs (see Figure 20Figure 20).

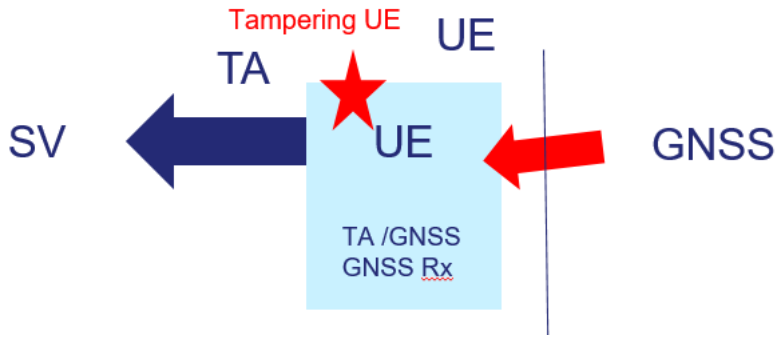

FIGURE 20: 5G NTN FEARED EVENT RELATED TO GNSS USE WITHIN USER EQUIPMENT

Additional security rules apply to the system functional chain "UE positioning", as follows:

- "The 5G positioning services shall be able to protect, by some mechanism, the UE's privacy and the privacy of the UE's user or owner, including the respect of its consent to the positioning services.
- "The 5G System shall support mechanisms to protect positioning-related data against tampering and spoofing.
- The 5G System shall support mechanisms to detect tampering and spoofing attempts on the position-related data."

Going further into the details, the UE may send GNSS measurements to the RAN over RRC, but this has at least the following drawbacks:

- The UE reported location information (for example, determined with its GNSS receiver) could be erroneous due to intentional (e.g., maliciously tampering by the user or by 3rd party) or unintentional (e.g., interference) causes, hence it cannot be considered trusted by network operators.

- Sending GNSS measurements over RRC before AS security is set up raises security and privacy issues as illustrated in Figure 20.

The 5G NTN System shall support mechanisms to protect positioning-related data against tampering and spoofing. Nevertheless, the UE equipment can be subject to tampering leading to inconsistent GNSS information and/or telecommunication-based measurement.

The compliance of 5G/ 6G NTN UE/System to these security requirements is critical and shall be solved. The security analysis shall be studied in future work.

3 REVIEW OF MEGA CONSTELLATION FOR RELIABLE POSITIONING

3.1 STARLINK CONSTELLATION OVERVIEW

Starlink is the world's largest satellite mega-constellation today, with more than 6750 satellites currently active in orbit as of February 2025. Starlink satellites operate in Low Earth Orbit (LEO) below 600 km altitude. The Starlink constellation uses Ku-band (10.7 GHz to 12.7 GHz) to transmit downlink signals to user terminals [17] Ka-band is mostly used for satellite-to-Gateway links. The parameters of Starlink constellation are summarized in Table 5.

TABLE 5: PARAMETERS OF THE STARLINK CONSTELLATION

Parameter	Value
Altitude [km]	540-570
Current number of active satellites in-orbit	6750
Planned number of satellites	30000
Downlink frequency sat-to-user [GHz]	Ku-band: 10.7-12.7
Modulation	OFDM
Frame duration	4/3 ms

Like all LEO satellite constellations, Starlink signals are received at a much higher SNR than the classical GNSS signals, essentially because of lower Free Space Loss (FSL). FSL is directly proportional to Sat-Receiver distance (e.g., satellite altitude) and to the signal frequency as can be seen in equation below.

$$FSL = \left(\frac{4\pi df}{c}\right)^2$$

Where:

- d is the distance between the satellite and the receiver in m;
- f is the carrier frequency in Hz;
- c is the speed of light c = 3·10^8 m/s.

Table 6 compares values of FSL for a typical GNSS MEO satellite and a Starlink LEO satellite.

TABLE 6: COMPARISON BETWEEN GNSS AND STARLINK FSL

	Carrier frequency	**Satellite altitude**	**FSL**
GNSS MEO	*1.2 GHz (L-band)*	20000 Km	180.05 dB
Starlink LEO	*11.7 GHz (Ku-band)*	550 Km	168.62 dB

As can be observed, Starlink constellation provides FSL values 31 dB lower than the GNSS constellation.

3.1.1 HIGH SATELLITE VISIBILITY

Another big plus is the number of visible satellites from any location on earth at any point of time. [18] shows the total number of Starlink satellites above a given region at any time. In

Figure 21 It can be observed that more than 50 satellites are always present above a non-polar region.

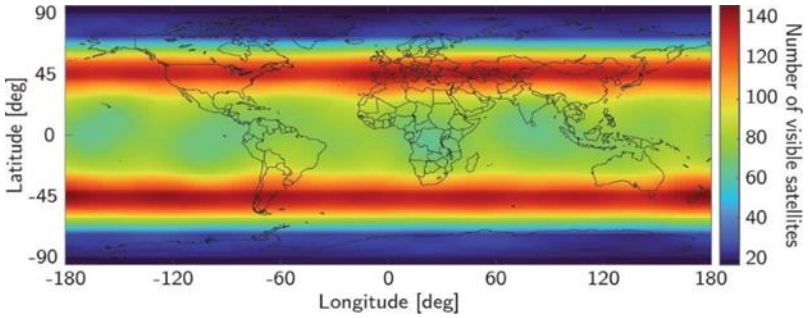

FIGURE 21: NUMBER OF VISIBLE SATELLITES

However, only a very small subset of these visible satellites are simultaneously active to provide data for user terminals. Figure 22 shows an experimental data set providing the number of visible active Starlink satellites for a receiver located in Columbus, OH, USA in July 2024. As shown in [19].There is always one active Starlink satellite overhead, and, on average, three satellites are simultaneously active. According to [19], the duration of satellite visibility (visible arc duration) falls within a 4-8 min range with an average value of 5,7 min with a minimum elevation angle of 5°.

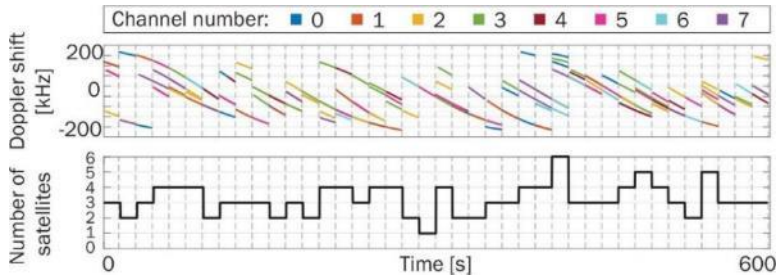

FIGURE 22: EXPERIMENTAL DATA SET SHOWING THE NUMBER OF ACTIVE VISIBLE STARLINK SATELLITES FOR A RECEIVER LOCATED IN COLUMBUS, OH, USA IN JULY 2024.

3.1.2 STARLINK SIGNAL MODEL

This section discusses the model of Starlink's Ku-band downlink signals based on [20].

Consider, to be the baseband signal transmitted by a Starlink satellite, where C is the transmitter's carrier power in Watts, $s_{III}(t) \equiv \sum_{k=-\infty}^{\infty} s(t - kT_0)$ is the repetitive beacon stream, s(t) is a deterministic beacon of duration T_0 seconds, and $n_d(t)$ is the random user data. The received signal after mixing with Local Oscillator (LO) frequency at the receiver can be written as:

$$r(t) = \sqrt{C} s_{III}\left(t - \tau(t)\right) e^{j\theta\,(t)} + n(t);$$

Where $\theta(t)$ is $\tau(t)$ is the code phase.

We suppose the received signal sampled at time instants t_k, then the Taylor series expansion at time t_k of carrier and code phase can be written as

$$\theta_{k(t)} = \theta(t + t_k) = \theta(t_k) + \dot{\theta}(t_k)t + \frac{\ddot{\theta}(t_k)}{2}t^2 + \cdots$$

$$\tau_k\,(t) = \tau(t + t_k) + \cdots \approx \tau_k$$

With:

- $f_D(t) = \frac{\dot{\theta}(t)}{2\pi}$ is the Doppler shift;
- $\dot{f}_D(t) = \frac{\ddot{\theta}(t_k)}{2\pi}$ is the Doppler rate;
- τ_k is the Doppler stretch factor.

The received signal after estimating and correcting with phase and code phase estimates $\hat{\theta}_k$ and $\hat{\tau}_k$, respectively, can be expressed as:

$$\tilde{r}_k(t) = r_k(t + \hat{\tau}_k) exp\left[-j\hat{\theta}_k(t)\right] w_{T_0}(t)$$

$$= \sqrt{C} S_{III}(t - \tilde{\tau}_k) exp\left[j\tilde{\theta}_k(t)\right] w_{T_0}(t) + \tilde{n}_k(t)$$

Where $\tilde{\theta}_k$ and $\tilde{\tau}_k$ are the residual phase and code phase errors, respectively.

The estimates of the code and carrier phase that are fed to the numerically controlled oscillator are obtained from:

- A determined set of search values when the receiver is in the acquisition stage or,
- The tracking loops when the receiver is locked to the source.

The operations in the last equation are referred to as the code and carrier wipe-off.

3.1.3 STARLINK CHALLENGES FOR POSITIONING

The main challenges for using Starlink satellites downlink signals for positioning are the following:

➲ **Limited information on signal structure**

While the orbits, frequencies, polarization, and beam patterns of Starlink satellites are a matter of public record through the licensing databases of the U.S. Federal Communications Commission, the details on the signal waveform and timing performance of the hardware generating it are not publicly available.

Some existing studies depicted some of the waveform characteristics through reverse engineering. For example:

- In [20], the authors captured Starlink downlink signals on the Ku-band and were able to identify the signal modulations, the frame structure & duration as well as the exact synchronization sequences embedded on the first two symbols of the frame: Primary Synchronization Sequence (PSS) & Secondary Synchronization Sequence (SSS). These sequences can be used to derive pseudo range measurements.
- In a more recent study [18] (March 2025), the authors revealed for the first time, the full Starlink orthogonal frequency division multiplexing (OFDM) beacon, which spans the whole time-frequency resource grid and not only the first two symbols.

➲ **Very high Doppler dynamics of LEO satellites in Ku-band**

Doppler models for LEO satellites in Ku-band must include both a Doppler shift, a Doppler rate and a Doppler stretch (a.k.a code phase) as shown in the signal model in the previous section.

➲ Doppler shift and Doppler rate dynamics

Figure 23Figure 23 from [21] shows an illustration of the communication failure due to the Doppler shift (failed: static) and Doppler rate (failed: dynamic) in a DtS IoT scenario. As stated in [22] the Doppler shift, also called static Doppler, degrades communication performance at the lowest elevation angles and the maximum link distance. On the other hand, the Doppler rate, also referred to as dynamic Doppler, causes packet losses at high elevation angles, when the satellite is positioned just above the end-device on the ground, resulting in the closest link distance.

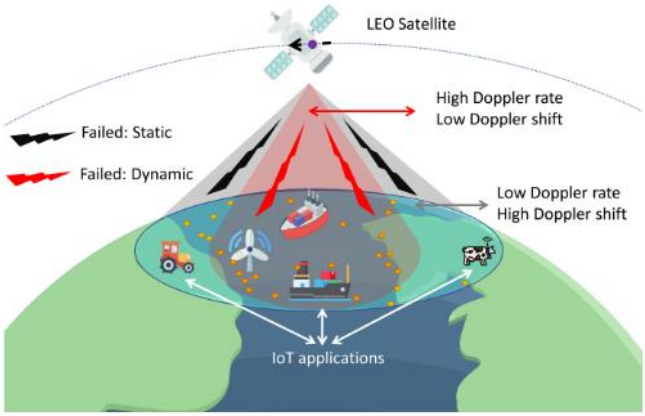

FIGURE 23: ILLUSTRATION OF THE COMMUNICATION FAILURE DUE TO DOPPLER SHIFT (FAILED: STATIC) AND DOPPLER RATE (FAILED: DYNAMIC) IN DTS IOT SCENARIO.

As explained in [21], mathematically, at a given instant of time (t), the difference between the transmitted carrier frequency F_C and the received carrier frequency $F_R(t)$, the latter varying in time owing to the satellite motion, is known as Doppler shift, given by :

$$F_D(t) = F_R(t) - F_C,$$

Whereas its derivative is called the Doppler rate:

$$\Delta F_D(t) = \frac{d(F_D(t))}{dt}$$

Details on the computation of $F_D(t)$ and $\Delta F_D(t)$ are given in [22].

A typical maximum value of Doppler shift for a LEO satellite at 550 km in Ku band is around $\frac{v_{sat}}{c} f_0 = 296\ kHz$ [23] with a Doppler rate peaking at 1609 Hz/s during passes [24] .

3.1.4 STARLINK PNT SUMMARY TABLE

TABLE 7: STARLINK SUMMARY TABLE

Average number of satellites visible active above any location	**3**
Average duration of one satellite pass with a minimum elevation angle of 5° (visible arc duration)	5.7 min
Maximum Doppler shift	296 KHz
Maximum Doppler rate	1609 Hz/sec
Doppler stretch (code phase) factor considering Rx/Tx clock quality with TCXO	2.5 x 10^-5
Best reliable PNT observable from [18]	Doppler shift
PNT performance from [18]	3 active satellite, 3D error = 2 m in 20 seconds

3.2 KUIPER CONSTELLATION

Kuiper constellation is an Amazon initiative planning to deploy a constellation of LEO satellites for broadband connectivity. According to [25], the initial satellite constellation design includes 3232 satellites. In April 2025, in the context of full-scale deployment of Kuiper's constellation, Amazon launched and tested connectivity with 27 satellites [26]. Up to this day, there are over 102 launched Kuiper satellites. Kuiper's satellites orbit at around 630 km altitude. The orbital speed of a Kuiper's satellite is is 7.54 km/s. Kuiper's terminals are designed to receive signals on the Ka-band (17.7-20.2 GHz). Parameters of Kuiper's constellation are summarized in Table 8.

TABLE 8: PARAMETERS OF THE KUIPER CONSTELLATION

Parameter	Value
Altitude [km]	630
Current number of active satellites in-orbit	102
Planned number of satellites	3232
Downlink frequency sat-to-user [GHz]	Ka-band: 17.7-20.2

Unfortunately, there is no available online information about Kuiper's downlink signal structure, which makes it very hard to assess PNT for the time being.

3.3 ONEWEB CONSTELLATION

Initially Eutelsat OneWeb's satellite communications network is intended to feature more than 630 satellites along 12 carefully synchronized orbital planes 1200km above, in low Earth orbit (LEO). As of January 2023, OneWeb has launched 544 satellites, with 542 being functional [27]. OneWeb satellites transmit and receive in Ku-band frequencies (10.7–12.7 GHz). The orbital speed of one web satellite 7.25 km/s.

Parameters of the OneWeb constellation are summarized in Table 9.

TABLE 9: PARAMETERS OF THE ONEWEB CONSTELLATION

Parameter	Value
Altitude [km]	1200
Current number of active satellites in-orbit	542
Planned number of satellites	630
Downlink frequency sat-to-user [GHz]	Ku-band: 10.7-12.7

- **Higher SNR**

Like any LEO constellation, OneWeb satellites provide higher SNR compared to traditional GNSS signals due to lower FSL. By computing the FSL in both cases, it is possible to see that OneWeb FSL is 5 dB lower than that typical of GNSS satellites.

- **High number of visible satellites from a given location**

Furthermore, due to the high number of satellites in the constellation, one user has a visibility of a multitude of satellites from a single location on earth. In [28] it is mentioned that the minimum number of visible satellites above 7.5° elevation mask can go up to 19 satellites. However, it is worth noting that in [28] the authors considered OneWeb constellation to have 720 satellites as was intended by the constellation design at the moment of writing the paper, therefore this number shall be smaller with the present constellation of 542 active satellites.

➲ **OneWeb Signal Model**

As described in [29] OneWeb received signal model is very similar to the Starlink model described in Section "Starlink signal model". The authors in [29] model the received signal r(t) after modulating the incoming signal with a numerically controlled oscillator as explained below.

For a given estimate of the carrier phase $\hat{\theta}_k\ (t)$ and code phase $\hat{\tau}_k$, the output signal at the kth accumulation is given by:

$$\tilde{r}_k(t) = r(t\ +\ t_k\ +\ \hat{\tau}_k\ )\ exp\left[-j\hat{\theta}_k\ (t)\right]w_{T0}\ (t)$$

$$=\ s_{III}(t-\tilde{\tau}_k)\ exp\left[\ j\tilde{\theta}_k(t)\right]w_{T0}\ (t) + \tilde{n}_k(t)$$

Where:

- $\tilde{\theta}_k(t) = \theta_k(t) - \hat{\theta}_k\ (t)$ is the carrier phase error;
- $\tilde{\tau}_k = \tau_k - \hat{\tau}_k$ is the code phase error;
- $\tilde{n}_k(t) = n(t + t_k + \hat{\tau}_k)\ \exp\left[-j\hat{\theta}_k\ (t)\right]\ w_{T0}\ (t)$;
- $w_{T0}(t)$ is a window function that is unity within the interval [0, T0] and zero elsewhere.

The phase modulation of r (t) by the estimated carrier phase $\hat{\theta}_k(t)$ is known as the carrier phase wipe off. Similarly, the time-domain modulation of r(t) by the estimated code phase $\hat{\tau}_k$ is referred to as the code phase wipe off. The code phase wipe off in this case is simply a time shift.

➲ **Positioning studies on OneWeb signal**

The authors in [29] present an exhaustive study on the blind acquisition of OneWeb beacons and how to use them for PNT based on phase measurements, see Table 10.

The main contributions of the paper are:

- Beacons are estimated in a blind fashion;
- A fast acquisition approach is presented for Ku-band signals received from LEO satellites with high Doppler, to reduce computational complexity;
- Use the estimated beacons to identify OneWeb's beam structure and C/N0;
- Development of Kalman filter-based tracking loops to track code and carrier phase of 9 satellites;
- A positioning solution with OneWeb signals is proposed, based on carrier phase measurements collected from 9 visible satellites, and using a Weighted Non-Linear Least Squares (WNLS) estimator.

The main results of this paper are:

- Faster acquisition with Doppler search complexity reduced by 80%;
- Final 2D positioning error = 30.4 m using observables from nine satellites passing over the receiver, one at a time, during a period of 30 minutes.

In [30], the authors propose a pseudorange based PNT method using signals from Oneweb satellites in a context of a network-aided approach.

The motivation behind using pseudorange observables for PNT is that they provide better timing accuracy than Doppler based methods, which is a common requirement for many practical applications existing today.

The challenge is that pseudorange based PNT is limited by the clocks mismatch at the receiver and the satellite, especially that recent work showed that clocks on-board of LEO satellites may not meet PNT requirements [31] [32]. This is why the authors propose a network-aided opportunistic solution, using two types of ground stations:

- A Reference Station RS with known position and reliable timing. A network of reference stations provides corrections to pseudorange, Doppler, or carrier-phase measurements of existing LEO satellite signals. It can also provide additional payload symbols to extend the integration period. In the simplest embodiment, the network is a single reference station.
- UE: a low cost terminal that uses RSs shared information to measure correctly the TOA.

The paper assumes that the signal structure of Oneweb constellation is known based on a soon to be released paper written by the same authors [33]. To this day no available public info can be found on this signal structure.

The main contributions of this paper are the following:

- Evidence that clock corrections from the RS could be used for PNT within at least one beam footprint;
- Establishing the framework for PNT information exchanges between UE and RS located in the same beam footprint;
- Running a field experiment with live signals.

The main result is that a 2-D positioning error of 0.35 m could be achieved using data collected from 12 satellites over a period of 30 min, with a timing resolved in only 69 ns. The solution is contained within a 95% error ellipse with a semi-major of 36.38 m and a semi-minor of 2.40 m.

TABLE 10: ONE WEB SUMMARY TABLE

Average number of visible satellites above any location	**14**	
Average duration of one satellite pass (visible arc duration)	5-15 min	
Maximum Doppler shift	283 KHz	
Doppler stretch (code phase) factor considering Rx/Tx clock quality with TCXO	2.42 x 10^-5	
Positioning method	Doppler shift	Pseudo-range (network-aided)

Initial UE position estimate fed to PNT solution	50 km away from the true position with a vertical error of 10 km.	250 km away from the true position
Positioning performance	Final 2D positioning error = 30.4 m using multi-epoch observables from a total of 9 satellites passed over the receiver, one at a time, during a period of 30 min [28]	2D positioning error of 0.35 m using data collected from 12 satellites over a period of 30 min, with a timing resolved in only 69 ns [29]

3.4 IRIDIUM CONSTELLATION

A recent study in [34] explored using TOA methods for positioning using Iridium satellites and compared them to FOA methods. TOA methods, although more sensitive to time drifts, provide better positioning in mobile scenarios and are less dependent on parameter initialization than FOA based methods.

The paper shows that the theoretical positioning errors for the TOA and FOA methods are 280.7 m and 361 m, respectively. These values are several times smaller than the actual TOA and FOA positioning errors of 644.0 m and 1173.8 m, but the relative error magnitudes between the two methods remain consistent. See Table 11.

TDOA positioning reduces this error down to around 181 m for 2-D and 3-D positioning.

In another paper [35], the authors explore positioning with instantaneous Doppler measurement. The main contributions are:

- Presentation of the characteristics and components of the Iridium signal opportunity positioning positioning system;
- Proposed positioning algorithm using SOPPs: Instantaneous Doppler positioning algorithm;
- Analysis of the effects of measurement errors and satellite orbital errors on the positioning solution;
- Analysis of the influence of constellation geometrical distribution on positioning performance;
- Simulations for theoretical verification;
- Real data experiment with IRIDIUM NEXT signals.

The receiver can see 7 IRIDIUM NEXT satellites during 30 min, and at most 2 satellites can be viewed simultaneously. With this assumption, 2D position accuracies of approximately 22 m (1σ) can be achieved when the static receiver has a complete view of the sky.

TABLE 11: IRIDIUM SUMMARY TABLE

Average number of visible satellites above any location	2
Average duration of one satellite pass (visible arc duration)	5-10 min
Maximum Doppler shift	~ 26 kHz
Doppler stretch (code phase) factor considering Rx/Tx clock quality with TCXO	N/A

PNT observable	TOA [36]	Instantaneous Doppler [35]
PNT performance	Final 2D positioning error = 644 m with TOA (gain in computation complexity)	2D positioning error of 22 m using data collected over a period of 30 min

3.5 SYNTHESIS AND RELEVANCE TO THE 6G NTN RELIABLE POSITIONING

The emerging mega-constellations of LEO networks such as Starlink, Kuiper, and OneWeb are primarily designed for broadband communications rather than for navigation or positioning purposes. Recent research investigated how existing communication signals can be exploited for navigation, for example by utilizing Doppler shift measurements, time-of-arrival (TOA) or time-difference-of-arrival (TDOA) estimation techniques. Such methods can achieve positioning accuracies ranging from a few centimeters to 100 meters, as summarized in Table 12.

TABLE 12: COMPARAISON BETWEEN MEGA SATELLITES CONSTELLATIONS PERFORMANCES

Constellation	Band	Reference signal model	Positining algorithm	Average number of visible satellites	Position accuracy	Assumptions
Starlink for broadband (VSAT) [18]	Ku	• OFDM beacon with 4G PRS like sequences. • Receiver BW = 5 MHz. • Frame length T0 = 1,33 ms. • Frame transmissio n ratio ~ 50%	**Doppler** shift tracking with weighted batch nonlinear least squares (WNLS) estimator	3 active satellites	3D at 90%: • **2m in 20 sec** • 10m in 8 sec	• 10-minute total observation period, with signals collected from 63 Starlink satellites • No Doppler biases in this data set • Stationary receiver but the results show it can support positioning in mobile applications

						with inertial aiding. • **No timing estimation**
Oneweb	Ku	[28] • Repetitive beacon with length and period T0 = 10 ms • Receiver BW = 2,5 MHz	**Carrier phase** measurements with Kalman filter and WNLS estimator	Not clear: data recorded from 9 satellites over 30 min (each satellite passing over UE one at a time)	**2D of 30,4m**	• Initial estimate 50 Km away • The SV positions were obtained from TLE SGP4 propagation, with the TLEepoch time being adjusted a priori such that it minimizes the range residuals for each SV to account for ephemeris errors. • Stationary receiver • **No timing estimation**
		[30] • Single carrier QPSK • Frame repeats each 10 ms • Receiver BW = 25 MHz	**Pseudo range** estimation with least squares algorithm for PNT	Data recorded from 12 satellites over 30 min (each satellite passing over UE one at a time)	**2D of 35 cm** **Timing resolved within 70 ns**	• **Network aided with a Reference Station** (RS) providing the UE with corrections to the satellites'observables • RS decodes fames coming from satellites so that UE can

						create local replicas for pseudorange estimation • RS sends to UE Time of Transmission (TOT) of each frame • UE position initialized 250 Km away from true position • Stationary receiver
Iridium	L-band	• Proprietary to Iridium • Max signal duration: 4.96 ms • Symbol rate = 25 KBaud • Signal repeats each 4.32 sec	[34] MMSE algorithm for **pseudo-range** estimation with TOA or FOA, assisted with data decoding of satellite ID	During 29 min, 7 satellites visible within 5-10 min each (each time epoch, 1 or 2 satellites visible)	TOA: **2D of 491.7m** FOA: 2D of 1007.5 m (3D & differential accuracies available in paper)	• Initial postion errors at the 25 Km level; • Base receiver with known position is used for differential algorithms
			[35] Instantaneous Doppler shift measurement	During 30 min, 7 satellites visible (at most 2 satellites visible simultaneously)	**2D of 22m**	• Static receiver with complete view of the sky

Currently, these constellations are primarily focused on providing high-speed internet access, especially in rural or remote areas, and they mainly use LEO satellites.

However, there are limitations in their use for positioning and navigation services, particularly due to limited signal access and the types of modulation used. Some limitations for positioning and navigation are listed below:

- **Signal access and modulation**

Currently, constellations like Starlink and Kuiper are not designed to be used as positioning systems (like GNSS). This means:

- The signals emitted by these satellites are not optimized for real-time position tracking, and the modulation of the signals used by these constellations for internet connectivity is different from that used by GNSS systems.
- For example, Starlink satellites use high-speed modulation and millimeter-wave frequencies (such as Ku and Ka bands) to provide broadband data services, but these types of signals are not designed for positioning accuracy. They lack GNSS-specific signal characteristics, such as code periods or phase range, which are essential for determining position.

- **Non-Dedicated Navigation Services:**

Constellations like Starlink and Kuiper do not currently provide services dedicated to navigation or positioning. The signals are adapted for data transmission, but do not include positioning information typically found in GNSS systems.

- **Limitation of Location Information:**

Unlike GNSS systems, which transmit precise time and satellite position information, the satellites in mega-constellations do not directly transmit this information to receivers. In GNSS systems, receivers determine their position by using signals from multiple satellites broadcasting synchronization and position data. In contrast, Starlink and Kuiper's LEO satellites do not currently fulfill this role.

4 RANGING BASED POSITIONING

4.1 POTENTIAL RANGING-BASED POSITIONING SOLUTIONS

4.1.1 GENERAL INTRODUCTION TO RANGING-BASED POSITIONING

The ranging-based positioning solutions are the ones used:

- in GNSS systems (GPS, Galileo, …)
- for OTDOA positioning solutions in TN

The principle is:

- The user evaluates a Time-of-Arrival on a reference signal pattern,
- The user gets information on where the satellite was when the reference signal pattern was sent and on when the signal was transmitted.

From this, the user can transform the time-of-arrival information into a ranging information. By combining ranging information from several satellites, it may estimate its position and time (PVT).

The transition from time-of-arrival to ranging may include the resolution of an ambiguity, for instance 1ms on GPS L1 C/A. The resolution of the ambiguity is part of the process.

The reference positioning method, used in particular for the assessment of navigation system performances, is usually a 3D snapshot position, for which simultaneous ranging information from at least 4 satellites are collected, and the position is estimated by a weighted least-square resolution. In some cases, for instance autonomous driving, it may be interesting to consider a 2D positioning method, which requires one less satellite (or the same number of satellites but for a better accuracy). This reference method will be firstly applied for the analysis of overall performances.

In this context, the accuracy depends on:

- The ranging error budget (see Section 2.1.3)
- The geometry of the constellation, which usually depends on latitude.

Examples for this method will be detailed in Section 4.3.

4.1.2 IMPROVEMENT SOLUTIONS

As seen in the GNSS context, but also in the LEO-PNT FR1 context seen below, the order of magnitude of the achieved accuracy with the reference positioning method is within a few meters.

There are several means to improve the accuracy from this reference snapshot position:

- Cumulate measurements over time, and integrate them within a position filter, usually a Kalman Filter (EKF). This approach is particularly efficient when combining the measurements with additional sensors, such as inertia, which allows to cover the

effect of position evolution over time. The main advantage of the approach is that it is possible to filter most of the user receiver noise, however in the short-term it has no major impact on the other contributors to the ranging budget, in particular atmosphere impacts and steady-state errors in the receiver measurements. It is worth noting that in a LEO context, the dynamics are much higher than in MEO, so the benefits of such approach appear faster in a LEO context than in a MEO context, within tens of seconds and not within minutes.

- Use of phase-measurements: As soon as phase tracking is feasible (reasonable Doppler drift and reasonable clock drift), the phase measurements are much more accurate than the ranging measurements: the stability is achieved for noise around 15°, so less than 1cm for L-band measurements (wavelength ~20cm). However, the main problem is that the phase measurements have an ambiguity of the wavelength, much smaller than the ranging error. It is then necessary to find a solution to improve the ranging uncertainty below the wavelength, in order to directly "jump" to cm accuracy thanks to the phase measurements. There are mainly two ways to achieve this:
  - RTK: Use a differential approach wrt reference stations. In this case, the convergence can be very fast, but the solution is demanding in terms of infrastructure. In addition, communication between the RTK stations and the users is necessary, which adds more complexity to the user device.
  - PPP: Wait enough time to get the ranging measurement accuracy improved and the error sources (user error, ephemeris error, atmosphere) to be clear enough in order to get an autonomous PPP. In MEO context, this method requires additional information to reduce as far as possible the error on some contributors, in particular satellite ephemeris and other discrepancies (code and phase errors), to concentrate on the user-related ones (mostly atmosphere). Those corrections are retrieved either by a communication mean, or directly through GNSS signal thanks to the Galileo HAS service. The main limitation of this approach is that in MEO-only context, the convergence time remains long (10 to 20 minutes) due to the slow motion of the satellites in sky. A key advantage of the LEO-PNT layer is that thanks to higher dynamics, a LEO + MEO PPP algorithm is expected to converge in much faster time, lower than 30s.
- Amongst the main contributors of the error budget, both ionosphere and ranging errors are reduced when considering large bandwidth transmissions in FR2 frequencies, as ionosphere evolves in $1/f^2$ (f = central frequency) and as ranging accuracy varies in 1/B (B = bandwidth). Transmission in FR2 then tends to improve accuracy for these aspects. However, some contributors remain the same (troposphere, ephemeris) and other contributors tend to increase, in particular effects of Doppler such as steady-state errors, but also higher difficulties to properly track the signal phase, and the accurate management of clock in the payloads becomes more complex. In addition, the wavelength becomes so small that even when the phase measurements are available, the wavelength ambiguity cannot be solved, so that only ranging measurements can be used.

In the next paragraphs 4.1.3.2 and 4.3, a proof-of-concept in FR1 (2.2 GHz) is introduced, and associated positioning performances are analyzed based on the reference positioning method described in 4.1.1. Discussion on achievement of centimetric accuracy is done in 4.4.

4.1.3 PRS, SRS AND OTHER SOOP

4.1.3.1 POSITIONING REFERENCE SIGNAL (PRS)

PRS as a SoOP signal is constructed using pseudo-random sequences that have good autocorrelation proprieties and small cross-correlation to ensure accurate timing measurements. The pseudo-random sequence used is a gold sequence of length 31. PRS sequences are sent in at least one subframe and one sub-carrier.

PRS uses OFDM with CP as a modulation technique. A 5G frame has a duration of 10 ms and consists of 10 subframes with durations of 1 ms each. A frame can also be decomposed into two half-frames, with sub-frames 0 to 4 form half frame 0 and sub-frames 5 to 9 form half-frame 1. In the time-domain, each subframe breaks down into numerous slots, each of which contains 14 OFDM symbols for a normal CP length, as illustrated in Figure 24.

The number of slots per subframe depends on the subcarrier spacing. The subcarrier spacing is flexible and is defined as $\Delta f = 2^{\mu} \cdot 15$ [kHz], where μ is a pre-defined numerology such that $\mu \in \{0, \cdots, 4\}$.

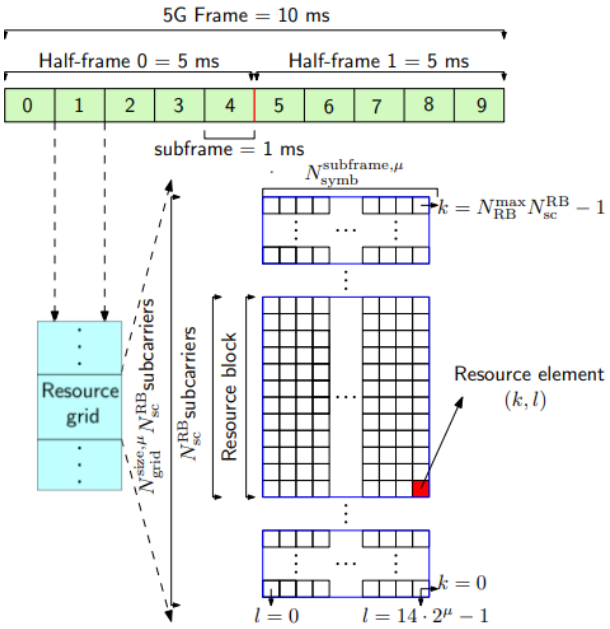

FIGURE 24: 5G NR MODULATION SLOT

In FR1, subcarrier spacing of 15 and 30 kHz are used, i.e., $\mu = 0$ and $\mu = 1$. In the frequency-domain, each sub frame is divided into numerous resource grids, each has multiple resource blocks with 12 subcarriers each. The number of resource grids in the frame is provided to the UE from higher level signaling. A resource element is the smallest element of a resource grid that is defined by its symbol and subcarrier number. Figure 25 summarizes the 5G frame structure.

μ	$\Delta f = 2^{\mu} \cdot 15$ [kHz]	FR1	FR2	T_s (μs)	T_{CP}(μs)	$T_{CP} + T_{CP}$ (μs)	N_{slot}^{frame}	T_{Slot} (ms)
0	15	✓	x	66.67	4.69	71.35	10	1
1	30	✓	x	33.33	2.34	35.68	20	0.5
2	60	✓	✓	16.67	1.17	17.84	40	0.25
3	120	x	✓	8.33	0.57	8.92	80	0.125
4	240	x	✓	4.17	0.29	4.46	160	0.0625

FIGURE 25: SUPPORTED FLEXIBLE TRANSMISSION NUMEROLOGY IN 5G-NR

On the fact that a PRB is defined as 12 continuous subcarriers in frequency domain, the PRBs allocated to PRS in TS 38.214 have the granularity of 4 PRBs, a minimum of 24 PRB and maximum of 272 PRBs. 5G-NR transmissions are more flexible than their predecessor technologies. 5G -NR signals can be transmitted using different numerology, which is summarized in the numerology that is parameterized using an index parameter.

In the following table, Δf stands for sub-carrier spacing, T_s for symbol duration, T_{CP} for the Cyclic Prefix (CP) duration, N_{slot}^{frame} for the number of slots per frame, and T_{slot} for the slot duration.

The available Frequency Ranges (FR) for 5G NR are also flexible. FR ranges can be divided in two, namely FR1 for frequencies below 6 GHz and FR2 for frequencies above 24 GHz.

The PRS signal is modeled as:

$$r(m) = \frac{1}{\sqrt{2}}(1 - 2c(2m)) + j\frac{1}{\sqrt{2}}(1 - 2c(2m+1))$$

Where c is

$$c_{\text{init}} = \left(2^{22} \left\lfloor \frac{n_{\text{ID,seq}}^{\text{PRS}}}{1024} \right\rfloor + 2^{10}\left(N_{\text{symb}}^{\text{slot}} n_{\text{s,f}}^{\mu} + l + 1\right)\left(2\left(n_{\text{ID,seq}}^{\text{PRS}} \bmod 1024\right) + 1\right) + \left(n_{\text{ID,seq}}^{\text{PRS}} \bmod 1024\right) \right) \bmod 2^{31}$$

$$l = l_{\text{start}}^{\text{PRS}}, l_{\text{start}}^{\text{PRS}} + 1, \ldots, l_{\text{start}}^{\text{PRS}} + L_{\text{PRS}} - 1$$

The bandwidth can be divided into a maximum of 3300 subcarriers. The effective number of subcarriers is defined by the subcarrier spacing (SCS), with possible values listed in Figure 27, SCS values greater than 120 kHz cannot be used for the PRS.

The number of slots per sub-frame is a function of the SCS. Indeed, the principle of OFDM is to ensure orthogonality between the subcarriers by transmitting data blocks with a duration of 1/SCS. Thus, for an SCS of 15 kHz, there will be one slot per sub-frame i.e., 14 OFDM symbols for an SCS of 30 kHz, two slots per sub-frame i.e., 28 OFDM symbols, as illustrated in Figure 26.

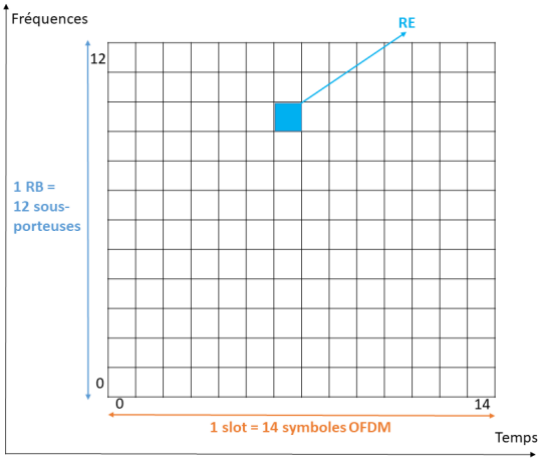

FIGURE 26: PRS RESSOURCES ELÉMENTS ALLOCATION

PRS supports four comb forms, namely Comb 2/4/6/12, as illustrated in Figure 27 in the frequency domain, and four symbol number configurations, i.e., Symbol 2/4/6/12, in the time domain. PRS supports the time-domain patterns with the RE offset KPRS offset = 0, which indicates that the mapping mode is not supported. The comb structure of PRS is to control the interference of PRS signals transmitted by multiple transmitters.

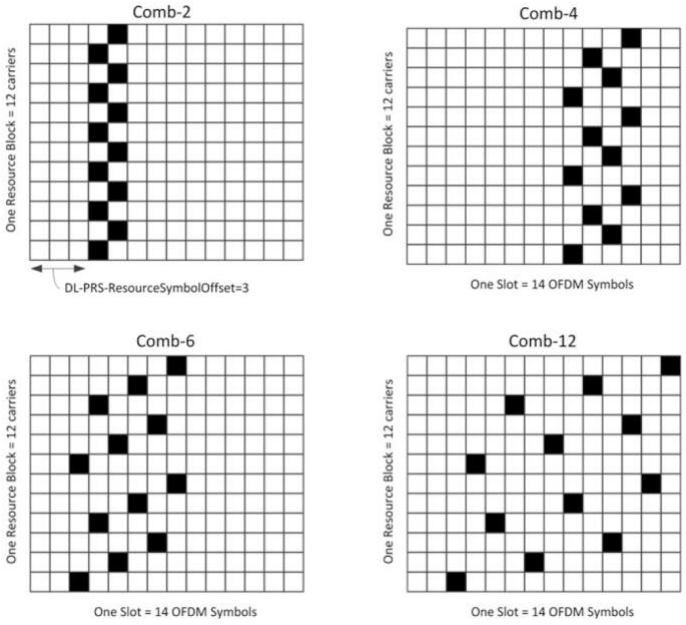

FIGURE 27: EXAMPLES OF PRS CONFIGURATIONS SIGNALS WITH DIFFERENT COMB

More details on PRS generation and sequence mapping are given in Section 4.2.1.

4.1.3.2 UPLINK SOUNDING REFERENCE SIGNAL (SRS)

In the uplink direction, 3GPP introduced the SRS for positioning in 3GPP Release 16. This new signal resolves two aspects specific to positioning. Since positioning involves measurements from multiple receiving base stations, the new signal must have enough range to reach not only the serving base station to which the UE is connected, but also the neighboring base stations involved in the positioning process. The SRS was also designed to cover the full bandwidth, where the resource elements are spread across the different symbols so as to cover all subcarriers. Therefore, SRS is also designed with a comb-based pattern similar to the PRS.

The underlying structure of the SRS is based on a sequence of discrete symbols that have very specific properties in terms of a constant time-domain envelope, in order to ensure a low peak-to-average power ratio (PAPR). Such symbols belong to the Zadoff-Chu family and have the property that their frequency domain representation, after applying the Fourier transform, is also a Zadoff-Chu sequence with similar constant envelope properties. Apart from the constant envelope property, the Zadoff-Chu sequences conveyed by the SRS are orthogonal one with each other, thus enabling to separate different SRS sequences coming from different BS. The mapping to physical resources is done as follows. An SRS sequence spans Nsym=1, 2, 4, 8, or 12 consecutive OFDM symbols which can be located anywhere within the slot. In the frequency domain, the SRS sequence is allocated according to a comb-like pattern every KTC=2, 4, or 8 subcarriers.

The following shows an example of the frequency-time structure of an SRS sequence in the case when the transmission comb number is KTC=4, the number of OFDM symbols allocated for SRS transmission is Nsym=8, and the index of the first OFDM symbol in the SRS within a slot is l0=3, respectively. Note that SRS transmissions from different devices can be frequency multiplexed within the same frequency range by being assigned different combs corresponding to different frequency offsets. Hence, for KTC=4, that is, up to four different SRS sequences can be frequency multiplexed.

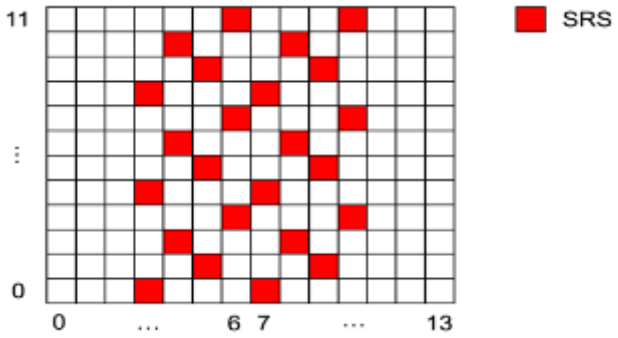

FIGURE 28: EXAMPLE OF THE RESOURCE ELEMENT ALLOCATION FOR AN SRS

In Figure 28, the following parameters have been selected: transmission comb number KTC=4, number of OFDM symbols allocated for SRS transmission Nsym=8, and the index of the first OFDM symbol in the SRS within a slot is l0=3

In the time-domain, the SRS can be configured for:

Periodic transmission: The configured SRS transmission occurs with a certain periodicity TSRS and a certain offset Toffset within that periodicity, which are both configurable,

Semi-persistent transmission: The actual SRS transmission can be activated or desactivated from higher protocol stack layers. If activated, the SRS transmission occurs periodically

according to the configured periodicity and offset. Otherwise, there is no transmission until it is explicitly reactivated,

Aperiodic transmission: The SRS transmission is explicitly triggered by means of signalling in the DCI.

Additionally, frequency hopping can be enabled to achieve frequency diversity in uplink transmissions: the data in the first set of OFDM symbols in the slot are transmitted on the RB indicated by the scheduling grant, whereas the data in the remaining OFDM symbols are transmitted on a different set of RBs given by a configurable offset from the first set. Uplink frequency hopping can be dynamically controlled using a bit in the DCI scheduling the transmission.

4.1.3.3 OTHER SOOP

The PRS and SRS signals described above are dedicated signals for positioning and thus they become the preferred signals to work with in this activity. However, there are also other reference signals which can provide supplementary performance gain, for example, in terms of accuracy, continuity, latency, and/or energy efficiency. Besides PRS and SRS, positioning algorithms can benefit from at least the following reference signals:

SSB in downlink

Repetitive broadcasting of necessary cell information

Limited bandwidth (240 subcarriers)

Available also in idle state operation of the UE as part of mobility management measurements

CSI-RS in downlink

Primary reference signal for channel measurements during the connected UE state (e.g., scheduling decisions and beam management)

Can be allocated to full bandwidth regardless of the allocated user data bandwidth.

DMRS in downlink and uplink

Assisting reference symbols for demodulation and detection of received signals

Available only within the allocated user data band (distributed evenly over the allocated band)

PTRS in downlink and uplink

Assisting reference symbols for demodulation and detection of received signals under phase noise.

Available only within the allocated user data band (limited frequency coverage, but dense allocation in time).

Although PRS and SRS can be considered the main reference signals for positioning, depending on the scenario, the above-described additional reference signals can be exploited separately or jointly in order to achieve the desired performance criteria. Table 13 gives a comparison between all signal location.

TABLE 13: COMPARISON OF DIFFERENT SIGNALS

	SS	DMRS	CSI-RS	PRS
Signal location	SS is located in the Synchronization Broadcast Block (SSB)	DMRS exists in various physical channels, including downlink and uplink physical channel	CSI-RS can only be sent on downlink symbols, not on the overlapped PRB with SSB	The signal dedicated to downlink positioning, which cannot be mapped to the resource particles allocated to the SSB
Sequence generation	PSS is a 127-length M sequence, and SSS is a 127-length Gold sequence.	Gold sequence	Gold sequence	Gold sequence with a length of 4096
Time-frequency Resources	PSS and SSS use the first and third symbol in an SSB respectively, occupying 127 subcarriers with the number of sequences from 57 to 183 among 144 REs in the frequency domain	Front-load DMRS can occupy 1/2 OFDM symbols in the time domain. The DMRS of physical broadcasting channel (PBCH) occupies up to 20 PRBs in the frequency domain	CSI-RS can support up to 32 different antenna ports, which allows multiplexing in one PRB. The time domain can occupy 1/2/4 OFDM symbols, and the bandwidth can occupy up to 52 PRBs.	The frequency domain has a comb-shaped pilot structure, the bandwidth can occupy a maximum of 272 PRBs, and the time domain can occupy multiple consecutive time slots

It can be summarized that the time-frequency resource allocation for PRS is flexible, so that multiple different downlink PRS signals from multiple base stations are multiplexed on different subcarriers in a comb-like manner. Thus, the comb structure of PRS is to control the interference of PRS signals transmitted by multiple BSs. It is also necessary to distinguish signals through different time-frequency structures to reduce interference. Positioning Reference Signal is the Downlink that can be configured at two levels, whitin a slot and at multi slot level. Within a slot, the starting resource element in time and frequency from a TRP can be configured. Across multiple slots, gaps between PRS slots for their periodicity and density whiten for a period can be configured.

Maximum Bandwidth: The PRS footprint on the time frequency grid is configurable with a starting PRB and PRS bandwidth. The PRS may start at any PRB in the system bandwidth PRS may start at any PRB in the system. The PRS may start at any PRB in the system bandwidth and can be configured with a range of 24 to 276 PRBs in steps of 4 PRBs. This amounts to a maximum bandwidth configuration of about 100 MHz for 30 KHz subcarrier spacing and to about 400 MHz for 120 KHz subcarrier spacing. It is the maximum supported bandwidth that determines the resolution of TOA, the flexibility affect other parts such as efficiency etc.

Resource and resource sets: The PRS can be transmitted in beams. A PRS beam is referred to as a PRS resource while the full set of PRS beams transmitted from a TRP on the same frequency is referred to a as a PRS resource set as illustrated in Figure 29. The different beams can be time-multiplexed across symbols or slots. To assist UE RX beamforming, the DL PRS

can be configured to be quasi-co-located with a DL reference signal from serving neighboring cells, signaling that the same RX beam used by the UE to receive said reference signal can be used by the UE to receive said reference signal.

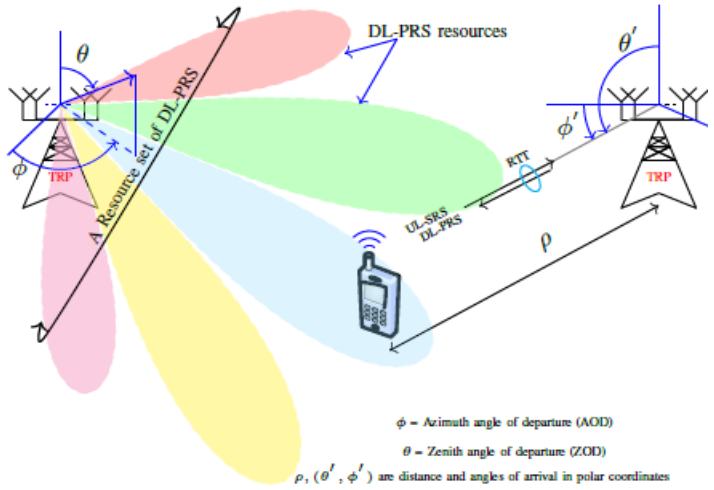

FIGURE 29: AN ILLUSTRATION SHOWING A FEW POSITIONING ELEMENTS WITH NR. BEAMS ARE RESOURCES AND SET OF BEAMS AS RESOURCE SETS ARE SHOWN

The beam structure of the PRS improves coverage especially from mm-wave deployments and allows for AoD estimation, e.g., the UE may measure DL PRS received signal Time Difference (RSTD) par beam and report the measured RSTD including DL PRS Resource id (beam id) to the LMF.

- Repetition and Periodicity: To improve positioning accuracy, more measurements can be collected. Measurements collected per resource helps to collect more measurements. Measurements can be collected per resource. The repetition of resources can be done in two ways, repeat before sweep and sweep before repeat;

- Interference Suppression: The DL PRS is designed to allow the UE to perform accurate ToA measurements in the presence of interfering DL PRS from nearby TRPs. Each symbol of the DL PRS has a Comb structure in frequency; that is, the PRS has a comb structure in frequency; that is, the PRS utilizes every nth subcarrier. The com value N can be configured to be 2, 4, 6 or 12. The length of the PRS whiten one slot is flexible as long as the slots consist of at least N PRS symbols allows accumulation of contiguous sub-carriers across a slot, which improves correlation properties for ToA estimation.

- The resource element pattern can be shifted in frequency with a frequency offset of 0 to N– 1 subcarrier, thus allowing N orthogonal DL PRSs to utilize the same symbols. All configurable patterns cover every subcarrier in the configured bandwidth over the pattern duration, giving the maximum measurement range for the ToA measurement in Scenarios with large delay spreads.

4.1.3.4 SUMMARY

Table 14 presents a comparison between PRS, SRS, and broadcast reference signals.

TABLE 14: PRS, SRS, AND BROADCAST REFERENCE SIGNALS COMPARISON

In positioning Signal	Advantages for positioning and navigation	Disadvantages for positioning and navigation	Conclusion remarks
Reference signals	Broadcast mode No need to be connected to network Give good acquisition performance	Ranging performance is limited due to short sequences	Good candidate for acquisition with Doppler dynamics
PRS	Give good ranging performance Can be configured over time/frequency resources in a flexible manner	Require terminal connection to network Not well suited for acquisition in the actual 6G NTN configuration with Kcomb	**Good candidate for refining ranging estimation, especially if Kcomb configuration is modified**
SRS	Can be used for GNSS assistance with DoA localization algorithms	Require network connection Problems of multi-user interference Only one satellite is used for localization (sometimes two)	Not the best candidate for the moment

4.2 PROOF OF CONCEPT TOOLS TO ASSESS THE CANDIDATE POSITIONING

The PoC tool proposed is based on a Matlab software doing Monte Carlo simulations. It is validated later by theoretical performance equations. Contrarily to a lab experiment, a simulator based PoC allows to validate the positioning performance while enabling the configuration of different performance tradeoff metrics which can only be derived from a statistical approach. This is the reason why the development of a specific test lab platform was abandoned in order to put more emphasis on a software based simulator.

The objective here is to model the PRS signal in baseband and estimate the accuracy with which a time-of-flight estimate can be derived. The PRS model is coupled with a channel model from allowing for the consideration of essential propagation parameters in an NTN context.

The use case chosen for this proof of concept is a GNSS assisted PRS positioning for NB-IoT terminals in S-band.

Note 1: this use case uses the FR1 frequency range (S-band) and not the usual Ku/Ka or C band proposed in LEO mega-constellations, as Wideband Data Rate Services (< 10 Mbps), which are supported by FR1, are expected from 2029 onwards, and enabled by 3GPP Release 17/18 standards. For C-band or Ku/Ka band adaptation the analysis found hereafter still applies with some modified considerations to make on the acquisition procedure specially for code phase as it might be higher.

Note 2: the work focuses on low energy terminals as it provides a worst case scenario from the frequency resources point of view. However, the trade-offs made can still be valid for non NB-IoT uses cases.

Note 3: the work focuses on 4G PRS for sake of simplicity as narrow band PRS exists only in 4G, but a performance comparison has been done with 5G PRS to show that the results in terms of pseudo-range computation are similar.

Note 4: the opportunistic approach corresponding to GNSS assisted positioning presented here can also be viewed as network-aided, which allows estimation of LEO satellite ephemeris, clock, and clock rate errors just as it occurs under typical 3GPP network assisted positioning approach. In effect, the receiver acts as its own reference station during the initialization phase, holding over key estimated values during the GNSS-denied phase.

4.2.1 PRS MODELING: 4G, 5G AND NB-IOT

As previously stated, 5G NR introduces new signals for positioning to improve the UE position reliability and precision. These signals are called Positioning Reference Signals (PRS). These signals already existed in 4G (LTE) however the sequences used to generate them were different and their mapping to time and frequency resources was less flexible. PRSs are used for ranging estimation.

Advantages: predefined Gold sequences designed to support interference. Longer sequences than reference signals so better link budget for ranging estimation.

Disadvantages: they are transmitted at terminal request so they require that the terminal is already connected to the network.

NB-PRS (Narrow band PRS for low energy terminals): they are modelled the same as normal 4G PRS but occupy smaller BW.

4.2.1.1 PRS IN 4G

4G PRS is detailed in Section 6.10.4 of 3GPP TS 36.211.

It is only defined for a subcarrier spacing of 15 KHz, and it is transmitted in pre-configured subframes.

4.2.1.1.1 PRS SEQUENCE GENERATION

A PRS sequence on one subframe contains 14 OFDM symbols. Each OFDM symbol contains only two active subcarriers per Resource Block (RB). Each RB occupies 180 KHz bandwidth.

A complex Pseudo Random Noise (PRN) sequence is generated for each symbol, therefore the length of the PRN sequence for each symbol is equal to $2 \times N_{RB}^{max,DL}$, where $N_{RB}^{max,DL}$ is the maximum number of resource blocks on the DL Bandwidth, defined at 110 for 3GPP LTE (see Section 6.2.1 of TS 36.211).

The sequence generator is initiated with c_{init} which depends on the cell ID, the OFDM symbol number {0,…,13} and the slot number {0,19}. Thus, the PRN sequences repeat themselves on each frame period.

4.2.1.1.2 MAPPING TO RESOURCE ELEMENTS

The mapping of PRS sequences on frequency/time resource elements for each resource block on each subframe is shown in Figure 30 below.

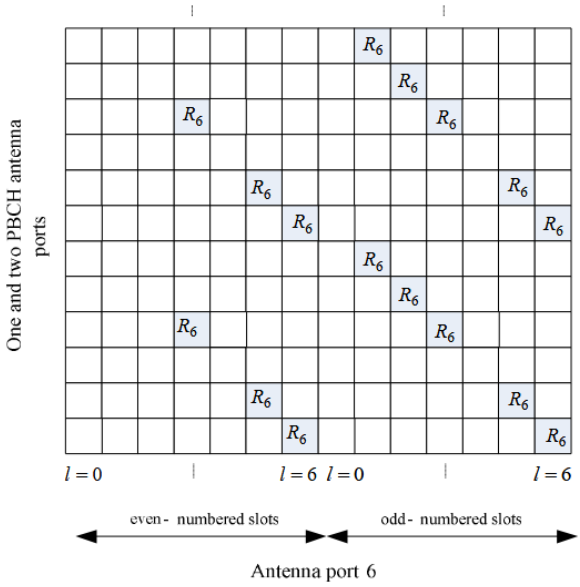

FIGURE 30: MAPPING OF POSITIONING REFERENCE SIGNALS (NORMAL CYCLIC PREFIX) FROM SECTION 6.10.4.2 OF TS 36.211

4.2.1.2 PRS IN 5G

3GPP 5G standard made modifications to the 4G PRS sequences and their mapping to make them more robust and with flexible configuration over the resource blocks as described in the following.

5G NR PRS for wide band communications is defined in Section 7.4.1.7 of TS 38.211 v19.1.0. A positioning frequency layer consists of one or more downlink PRS resource sets, each of which consists of one or more downlink PRS resources as described in Section 6 of TS 38.214.

5G NR introduces the concept of numerology to define subcarrier spacing and slot size. Table 15shows the supported numerologies and their associated subcarrier spacing Δf and cyclic prefix.

TABLE 15: SUPPORTED TRANSMISSION NUMEROLOGIES (FROM TABLE 4.2-1 OF TS 38.211 V.19.1.0)

μ	$\Delta f = 2^{\mu} \times 15$ [KHz]	Cyclic prefix
0	15	Normal
1	30	Normal
2	60	Normal, Extended
3	120	Normal
4	240	Normal
5	480	Normal
6	960	Normal

The number of OFDM symbols per slot in 5G NR, $N_{symb}^{slot} = 14$ symbols, contrarily to 4G where it was equal to 7 symbols. Table 16 shows the number of OFDM symbols per slot, slots per frame and slots per subframe for normal cyclic prefix.

TABLE 16: NUMBER OF OFDM SYMBOLS PER SLOT, SLOTS PER FRAME, AND SLOTS PER SUBFRAME FOR NORMAL CYCLIC PREFIX FROM TABLE 4.3.3-1 IN TS 38.211

μ	N_{symb}^{slot}	$N_{slot}^{frame,u}$	$N_{slot}^{subframe,u}$
0	14	10	1
1	14	20	2
2	14	40	4
3	14	80	8
4	14	160	16
5	14	320	32
6	14	640	64

4.2.1.2.1 SEQUENCE GENERATION

The 5G standard adds more flexibility to the PRS sequence so that the it can be allocated a flexible number of subcarriers and not only 2 subcarriers among 12 as done in 3GPP LTE. The PRS sequence generation in 5G is described in Section 7.4.1.7.2 of TS 38.211.

The parameter defining the number of subcarriers used per OFDM symbol is a configurable parameter denoted by Kcomb = {2, 4, 6, 12}. When Kcomb = 2, it means that all one every 2 subcarriers in a resource block are used per OFDM symbol, when Kcomb = 4, it means one every 4 subcarriers is used per OFDM symbol, etc. Hence, the equivalent Kcomb for LTE PRS is Kcomb = 6 (one every 6 subcarriers = 2 subcarriers per OFDM symbol).

For each OFDM symbol, the subcarriers are filled by chosing elements from a PRN sequence (2 for each I/Q symbol). The PRN sequence is defined by the same length-31 Gold sequence used for 4G PRS but with a different c_{init} . Like 4G PRS, the PRN sequence is unique for each cell ID, each OFDM symbol and each slot. However, when the slot number re-initializes to zero on the next frame, the PRN sequence is repeated.

4.2.1.2.2 MAPPING TO RESOURCE ELEMENTS

Mapping of the symbols on the frequency/time grid of one slot is described in Section 7.4.1.7.3 in TS 38.211. As shown in Table 17, each OFDM symbol has an offset in number of subcarriers where the symbol starts, that depends on:

- The symbol number inside the slot;
- The value of $Kcomb \in \{2,4,6,12\}$;
- A common configurable frequency offset $k_{offset}^{PRS} \in \{0,1,\dots,Kcomb-1\}$ fixed for all PRS symbols.
- A symbol-dependent frequency offset denoted by k' defined in function of the symbol number as shown in Table 17.

TABLE 17: FREQUENCY OFFSET K' IN FUNCTION OF SYMBOL NUMBER (FROM TABLE 7.4.1.7.3-1 IN TS 38.211)

	Symbol number											
Kcomb	**0**	**1**	**2**	**3**	**4**	**5**	**6**	**7**	**8**	**9**	**10**	**11**
2	0	1	0	1	0	1	0	1	0	1	0	1
4	0	2	1	3	0	2	1	3	0	2	1	3
6	0	3	1	4	2	5	0	3	1	4	2	5

12	0	6	3	9	1	7	4	10	2	8	5	11

A mapping example is shown in Figure 9 in [37] for Kcomb = 4 and $k_{offset}^{PRS} = 2$.

4.2.1.3 PRS FOR LOW ENERGY

4.2.1.3.1 NB-IOT PRS SIGNAL DEFINITION

The 3GPP LTE standard (TS 36.211 Section 10.2.6A) defines Positioning Reference Signals for Narrow Band applications called NPRS.

The difference between narrowband PRS defined for LEOPNT IOD and normal 3GPP PRS is that the total useful BW per satellite is limited to 1 resource block = 180 KHz.

Similarly to normal PRS, each NPRS on one resource block consists in a series of OFDM symbols each containing 12 I/Q elements to be distributed on 12 subcarriers of 15 KHz each.

3GPP FDD frame structure (frame structure type 1), as defined in Section 4.1 of 3GPP TS 36.211, is used. As shown in Figure 31 below, each frame has a duration of 10 ms and contains 10 subframes. Each subframe contains 2 slots. The slot number increases sequentially within a radio frame from 0 to 19. Consequently, the slot number depends on both the subframe number and its position within the frame. Here's how the slot numbers increment:

- For subframe 0, slots 0 and 1
- For subframe 1, slots 2 and 3
- For subframe 2, slots 4 and 5

And so forth, up to subframe 9, which has slots 18 and 19.

After the 19th slot, the slot number resets at the start of the next radio frame. Therefore, the slot number increases with the subframe number within each frame, and the frame itself resets the sequence every 20 slots.

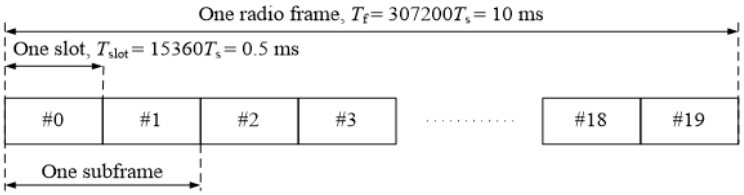

FIGURE 31: TS 36.211 FIGURE 4.1-1 : FRAME STRUCTURE TYPE 1.

Figure 32 below shows the time/frequency configuration of a NPRS subframe.

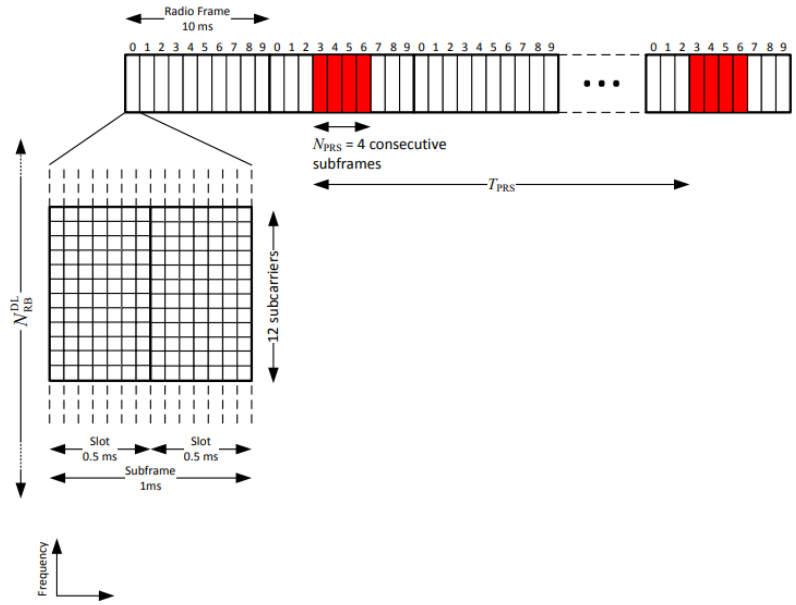

FIGURE 32: PRS TRANSMISSION SCHEDULE (FROM [42])

Each slot contains 7 OFDM symbols in time (1 subframe = 14 OFDM symbols), and each OFDM symbol occupies 12 subcarriers in frequency of 15 KHz each.

Each OFDM symbol is constituted of a Pseudo-Random Noise (PRN) sequence of length 12x2 for I & Q samples.

Originally, as seen in Section 4.2.1.1, 3GPP LTE PRS sequence uses only 2 subcarriers per OFDM symbol among the available 12 subcarriers. However, in the context of NTN, we propose to use Kcomb=1 because in legacy 4G terrestrial systems, using higher Kcomb values has been proposed to allow different eNodeBs to share the frequency resources in order to avoid PRS collisions in time. This phenomena rarely applies to satellites systems as the risk of simultaneous transmissions by different satellites is much lower and for positioning purposes specifically, sometimes multi-epoch algorithms are applied, meaning that the same satellite TOA is observed at different times.

Therefore, it is proposed to modify the NPRS so it occupies all 12 subcarriers and limit the number of NPRS subframes transmitted to achieve an equivalent ranging performance.

4.2.2 CHOICE OF THE SIGNAL MODEL

The signal model proposed to be studied in the following for impact analysis and positioning simulations, is based on 3GPP-LTE NPRS waveform.

The difference with respect to the standard 4G-NPRS as shown in Section 4.2.1.3.1, is in the sequence mapping to resource elements where it is proposed to add a comb pattern similar to the one in 5G-NR with Kcomb having values in {2,4,6,12} plus adding Kcomb = 1 for trade-offs comparison.

The subcarriers offset of each symbol on a slot are given in Table 18.

TABLE 18: 4G PRS SUBCARRIER OFFSET IN FUNCTION OF KCOMB AND THE SYMBOL NUMBER INSIDE A SLOT.

	Symbol number						
Kcomb	**0**	**1**	**2**	**3**	**4**	**5**	**6**
2	0	1	0	1	0	1	0
4	0	3	2	1	0	3	2
6	0	5	4	3	2	1	0
12	0	11	10	9	8	7	6

The representation of the Tx waveform model is shown in Figure 33, with the following terminologies explained:

- PRS occasion: a duration at the beginning of the each Tx signal over which NPRS frames are transmitted. In the figure, this duration is equal to 40ms but will be configurable in the simulations.
- Reference signals: signals transmitted on dedicated subframes on which neither NPRS nor data are allowed to be transmitted as per the 3GPP standard. The reference signals are: N-MIB, N-PSS & N-SSS. They form what is called in 3GPP the Signal Synchronization Block (SSB). Their subframe positions are shown in Figure 34 on a zoomed interval of two frames. These subframes positions are the same for each two frames duration.
- PRS occasion period: the transmission period of the PRS occasion. This period is not relevant in this PoC as the positioning algorithm is done over one snapshot.

For example, a Tx signal with a number of NPRS frames = 4, contains in the PRS occasion part:

- A total of 40 ms of NPRS plus reference signals:
  - 30 ms of NPRS;
  - 10 ms of reference signals.

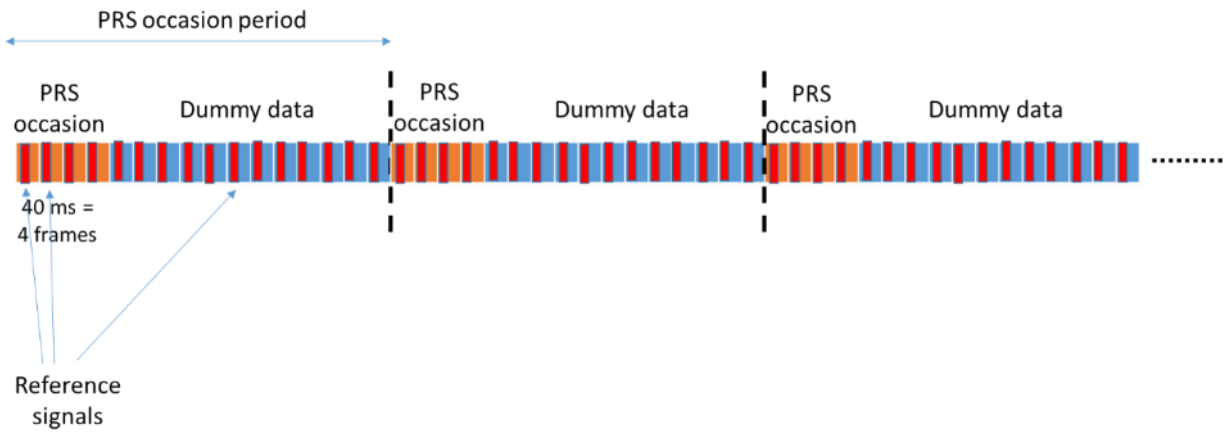

FIGURE 33: TEMPORAL REPRESENTATION OF THE 4G TX WAVEFORM CONTAINING NPRS, REFERENCE SIGNALS AND DATA.

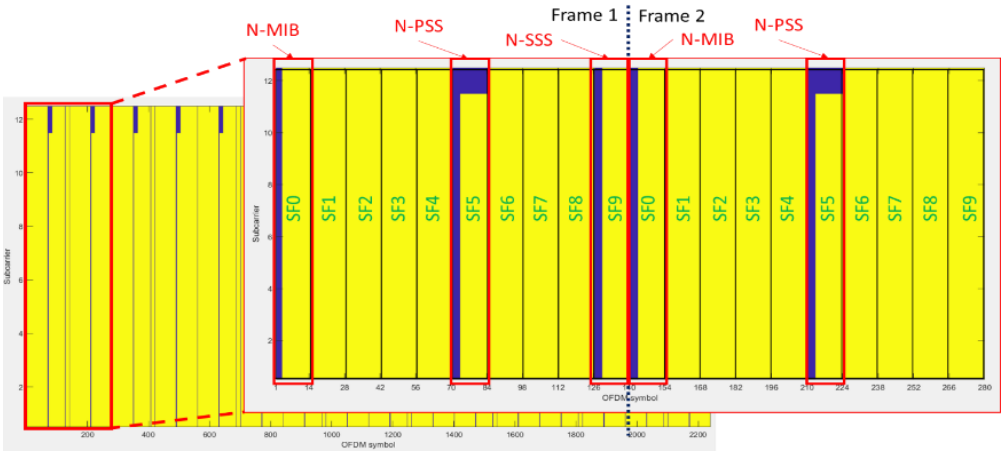

FIGURE 34: TX GRID WITH REFERENCE SIGNALS: NMIB, NPSS AND NSSS (BLUE IS FOR EMPTY SYMBOLS, YELLOW FOR FILLED).

4.2.3 IMPACT ANALYSIS METRICS

The impact analysis metrics contributing to measure the trade-offs on the ranging performance are listed in Table 19.

TABLE 19: IMPACT ANALYSIS METRICS

SNR value	36-46 dB
Kcomb parameter	1-2-6-12
Doppler consideration for ranging	Perfectly compensated
Target SNR for ranging	~40 dB
Target ranging performance (rms value)	100-180 nanoseconds

4.2.4 OVERALL RECEIVER FUNCTIONS

Let's recall the receiver procedure at the user terminal:

- The user knows approximately its position (ref loc + ref time + ref frequency) & the satellite ephemeris;
- It can then deduce the expected received frequency and pre-compensate most of the Doppler drift to get quite long coherent acquisition;
- The signal is supposed to have perfect acquisition at the receiver side at the assumed C/N0 working point.
- Once the peak position is known, the user performs a refined TOA measurement with larger bandwidth (zero-padding) and if needed a longer duration, to compute the pseudo-range.
- The procedure is repeated on several satellites (and if needed several epochs) for positioning.

4.2.5 RANGING PROCEDURE

Monte Carlo simulations are conducted to evaluate the ranging (pseudo-distance) estimation when a PRS signal transmitted by one satellite and acquired at the ground terminal receiver side.

For each simulation run, the simulations steps are described below and shown in figure 35.

1- Transmission
   a. We generate a signal s1 containing reference signals and PRS sequences modulated according to 4G NB-IoT. The number of transmitted NPRS subframes is configurable.
   b. We add a random delay τ_1 to the signal s1 to obtain: $s1_{\tau_1}(t) = s1(t - \tau_1)$
2- Channel
   a. AWGN is added according to a predefined level of C/N0: y(t) = $s1(t - \tau_1) + n(t)$, with n(t) being the AWGN samples.
3- Reception
   a. We suppose that the acquisition step is done as shown in Section 4.2.7 and Doppler and frequency offsets have been compensated at the receiver
   b. The received signal y(t) is correlated with the known signal s1(t) at the receiver side (reference signals are omitted when testing NPRS signal alone).
   c. Polynomial fitting with polynom p is applied around the supposedly known correlation peak in order to refine the ranging estimation
   d. Ranging estimate a.k.a TOA estimate $\widehat{\tau_1}$ is obtained where dp/dx=0.

At the end of N simulation runs, the ranging standard deviation is computed as:

$$Ranging\ std = \sqrt{\frac{1}{N}\sum_{n=1}^{N} |\widehat{\tau_1}|^2}$$

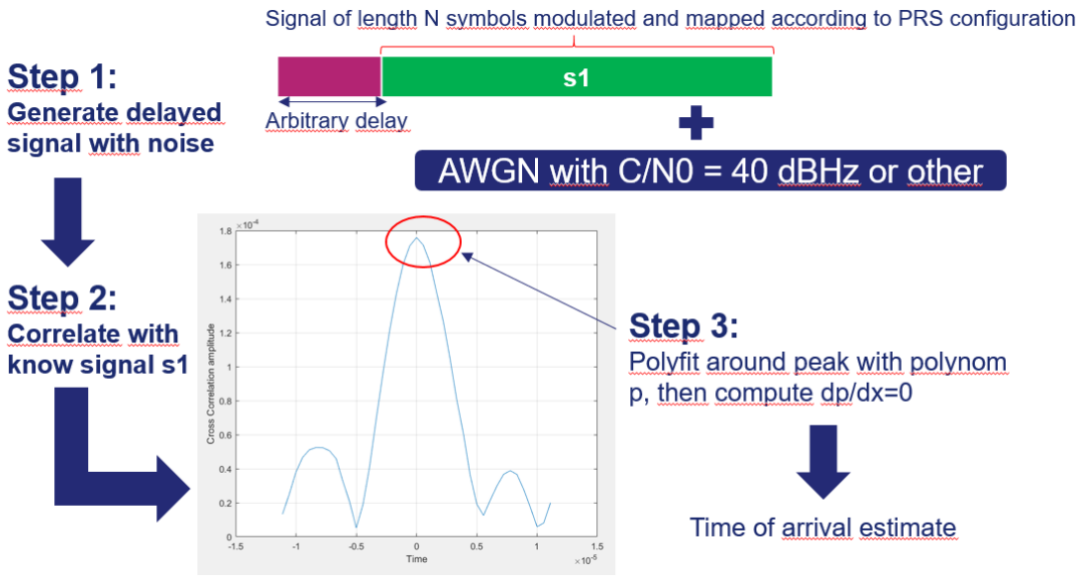

FIGURE 35: SIMULATION STEPS FOR REFINING TIME OF ARRIVAL ESTIMATE USING PRS.

4.2.5.1 ASSUMPTIONS

The simulation inputs assumptions are listed in Table 20.

TABLE 20: GENERAL SIMULATIONS ASSUMPTIONS

Number of runs N	1000
C/N0	Configurable
Subcarrier spacing	15 KHz
Nfft = sampling rate	128
Sampling frequency	1.92 MHz
Number of subcarriers per OFDM symbol	12
Number of transmitted RBs in frequency domain	1
Number of transmitted subframes	Configurable
Number of OFDM symbols per subframe	14
Cyclic prefix vector (normal CP)	[10 9 9 9 9 9 9 10 9 9 9 9 9 9]
Subframe duration (OFDM symbols + cyclic prefixes)	1 ms
Slot duration (OFDM symbols + cyclic prefixes)	0.5 ms

4.2.5.2 RESULTS

The ranging performance is computed by varying the following parameters:

- Kcomb values
- C/N0 values
- Number of transmitted PRS frames

This analysis is done in order to:

1- determine the loss in dB induced when Kcomb is increased and make sure it is proportional to kcomb values.
2- Validate that the performance is acceptable for the target C/N0.
3- Determine the recommended number of PRS frames to transmit in order to achieve the target ranging performance.

4.2.5.2.1 RANGING IN FUNCTION OF NUMBER OF PRS FRAMES

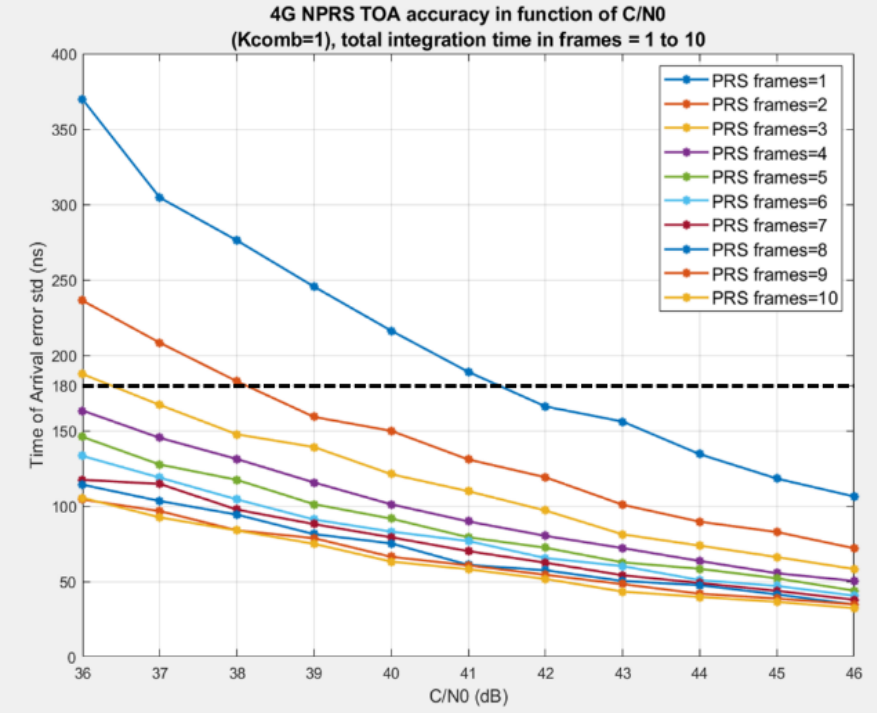

FIGURE 36: 4G RANGING PERFORMANCE IN FUNCTION OF C/N0 AND NUMBER OF PRS FRAMES (KCOMB=1)

Figure 36 shows the TOA std error obtained with different number of NPRS frames used for correlation at the receiver for an interval of C/N0 from 36 to 46 dB. It is assumed here that reference signals are transmitted inside the NPRS frames but they are not used in the ranging procedure at this step. The value of Kcomb=1.

It is observed that increasing the number of PRS frames used for integration (from 1 to 10) consistently improves TOA accuracy. The improvement is steep between 1–3 frames but gradually saturates beyond around 7–8 frames.

Regarding performance limits, The highest curve (PRS frames = 1) shows large errors, from ~380 ns at 36 dB-Hz down to ~110 ns at 45 dB-Hz. The lowest curve (PRS frames = 10) achieves TOA errors below 60 ns across most C/N_0 values above 40 dB-Hz, at the cost of higher integration complexity at the receiver side, hence higher power consumption.

The black dashed horizontal line at 180 ns represents an acceptable upper bound of a target TOA accuracy threshold. This target is satisfied when the number of PRS frames used for correlation is higher or equal to 4 frames at C/N0 ≥ 36 dB-Hz. (Note that four frames is equivalent to a total of 30 ms of PRS as the rest is for reference signals).

4.2.5.2.2 RANGING IN FUNCTION OF KCOMB AND C/N0

The PRS signal used for the correlation is shown in Figure 37.

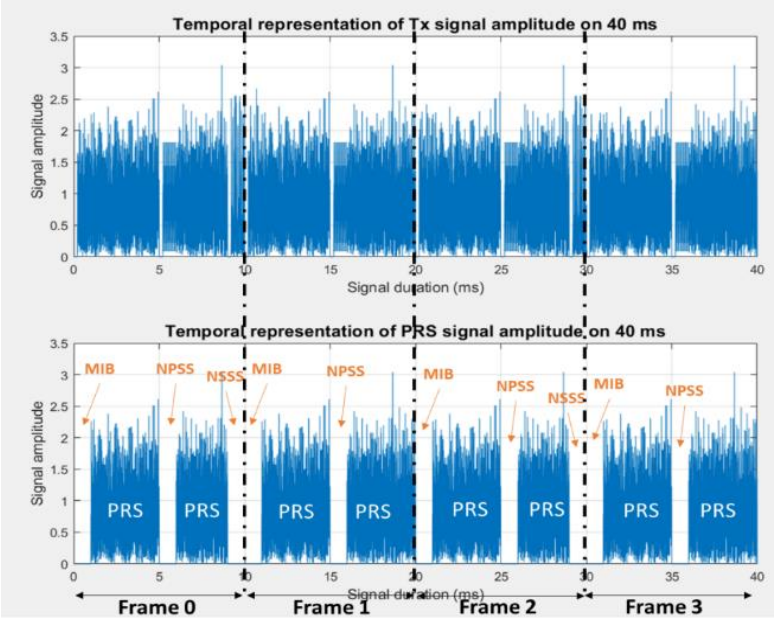

FIGURE 37: TEMPORAL REPRESENTATION OF PRS SIGNAL W.R.T TX SIGNAL ON 40 MS.

The ranging performance results are traced in Figure 38, in function of C/N0 and several Kcomb values for a fixed value of available correlation frames equal to 4 frames including MIB, NPSS, NSSS and PRS subframes. The performance curves are obtained with a ranging correlation done using only the PRS subframes totaling a duration of 30 ms.

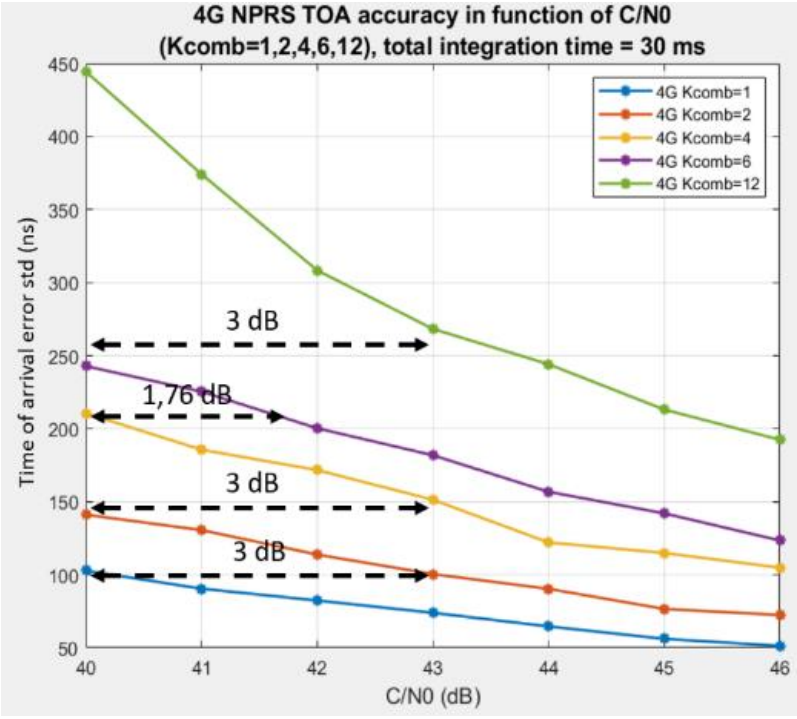

FIGURE 38: 4G RANGING PERFORMANCE IN FUNCTION OF C/N0 AND KCOMB USING PRS ONLY CORRELATION.

Several key observations can be made:

- Effect of C/N0:
  - An increase of 3 dB in C/N0 results in a decrease of the TOA error std by the factor $\frac{1}{\sqrt{2}}$ which is in line with the Cramer Rao theory (see Section on MCRB below).
- Effect of Kcomb:
  - For each C/N0 value, increasing Kcomb (from 1 up to 12) increases TOA error. This indicates that using more NPRS frequency resources produces finer positioning resolution under the same integration time.
  - The curve for Kcomb=1 exhibits the lowest TOA error (highest accuracy), while Kcomb=12 achieves significantly worse TOA accuracy, reflecting the trade-off in NPRS resource allocation.
  - Decreasing Kcomb from 12 to 6 to 4 to 2 and to 1, results in a C/N0 gain in dB equivalent to the Kcomb ratio in dB. Therefore using PRS with Kcomb=2 for example requires 3 dB more in C/N0 or two times longer PRS frames, to achieve the same TOA accuracy as using Kcomb = 1.

4.2.5.2.3 RANGING WITH PRS AND SSB

To enhance the ranging performance we can also make benefit of the synchronization signals in the SSB (NSSS and NPSS). The results using these additional signals are shown in Figure 39.

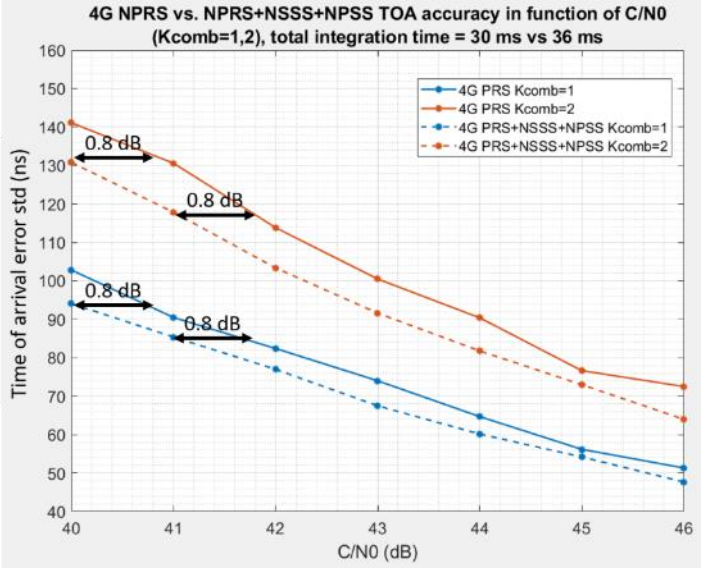

FIGURE 39: 4G RANGING PERFORMANCE IN FUNCTION OF C/N0 AND KCOMB USING PRS VS. PRS + REFERENCE SIGNALS.

The key observation from this plot is that increasing correlation time by using the reference signals as well as the NPRS results in an increased accuracy for the same C/N0. Thus, for a

certain target accuracy using only PRS requires increasing the C/N0 of 0,8 dB which is equivalent to the ratio $10log10\left(\frac{duration\ of\ PRS+NSSS+NPSS}{duration\ of\ PRSonly}\right) = 10log10\left(\frac{36}{30}\right)$.

4.2.5.2.4 MCRB

The modified Cramer-Rao (MCRB) bound [Zanier_2008] & [Wixu et al.] has been utilized in the link budget to estimate the NB-IoT NPRS timing error from which the position accuracy is derived. In particular:

$$MCRB(\tau) = \frac{\sigma^2}{8\pi^2\ f_{sc}^2\ \sum_{l=0}^{N_{symb}^{PRS}} \sum_{k=-\frac{N_{sc}}{2}}^{\frac{N_{sc}}{2}} k^2 |s_l(k)|}$$

Where:

- σ^2 is the noise variance over the ranging integration time T_{obs},
- f_{sc} is the OFDM sub-carrier frequency bandwidth,
- N_{sc} represents the number of OFDM sub-carriers,
- N_{symb}^{PRS} is the total number of PRS symbols which are effectively used for the ranging measurement
- $s_l(k)$ is the signal allocated on the kth subcarrier of the lth OFDM symbol.

Naming N_0 the AWGN noise power spectral density, we derive:

$$\sigma^2 = \frac{N_0}{T_{obs}}$$

In practice T_{obs} corresponds to the number of observed NPRS symbols time the OFDM symbol duration including CP, $T_{symb,CP} = T_{symb} + T_{CP} = \frac{1ms}{14}$, i.e.

$$T_{obs} = N_{sym}^{PRS} * T_{symb,CP}$$

Developing the sum

$$\sum_{l=0}^{N_{sym}^{PRS}} \sum_{k=-\frac{N_{sc}}{2}}^{\frac{N_{sc}}{2}} k^2 |s_l(k)| = N_{sym}^{PRS} * |s| * \sum_{k=-N_{sc}/2}^{N_{sc}/2} k^2,$$

With $|s| = C * \frac{1}{N_{sym}^{PRS}} * \frac{1}{N_{SC}} * \left(\frac{T_{symb,CP}}{T_{symb}}\right)^2$, being the normalized symbol power taking into account CP addition, and:

$$\sum_{k=-N_{sc}/2}^{N_{sc}/2} k^2 = \frac{N_{sc}}{6}(N_{sc}+1)\left(\frac{N_{sc}}{2}+1\right)$$

and after replacing the above elements in the MCRB equation, we get:

$$MCRB(\tau) = \frac{\sigma^2}{8\pi^2 \; f_{sc}^2 \; C \; \frac{1}{N_{sc}} \left(\frac{T_{symb} + T_{CP}}{T_{symb}}\right)^2 \sum_{k=-N_{sc}/2}^{N_{sc}/2} k^2}$$

$$= \frac{3}{4\pi^2 \; f_{sc}^2 \left[\frac{C}{N_0}\right] N_{sym}^{PRS} \, T_{symb,CP} \; (N_{sc} + 1) \left(\frac{N_{sc}}{2} + 1\right) \left(\frac{T_{symb} + T_{CP}}{T_{symb}}\right)^2}$$

The relation between MCRB and the minimum theoretical TOA error in seconds is given below:

$$TOA \; accuracy \; (\sigma) = \sqrt{MCRB(\tau)}$$

To verify if the simulation results presented previously are valid, the plot in Figure 40 traces simulation results versus the minimum bound on TOA accuracy $\sqrt{MCRB(\tau)}$, obtained with a number of PRS frames equal to {1, 4, 10} and C/N0 values from 40-46 dBHz. The parameters used for plotting the results are reported in Table 21.

TABLE 21: PARAMETERS USED TO PLOT MCRB THE RESULTS

Number of PRS frames	1, 4, 10
Subcarrier spacing f_{sc}	15 KHz
C/N0	40 – 46 dBHz
Number of PRS_subframes in even frames	7
Number of PRS_subframes in odd frames	8
Number of symbols per subframe	14
Subframe duration	1 ms
Number of subcarriers N_{sc}	12
T_{symb}	1/fSC = 1/15KHz

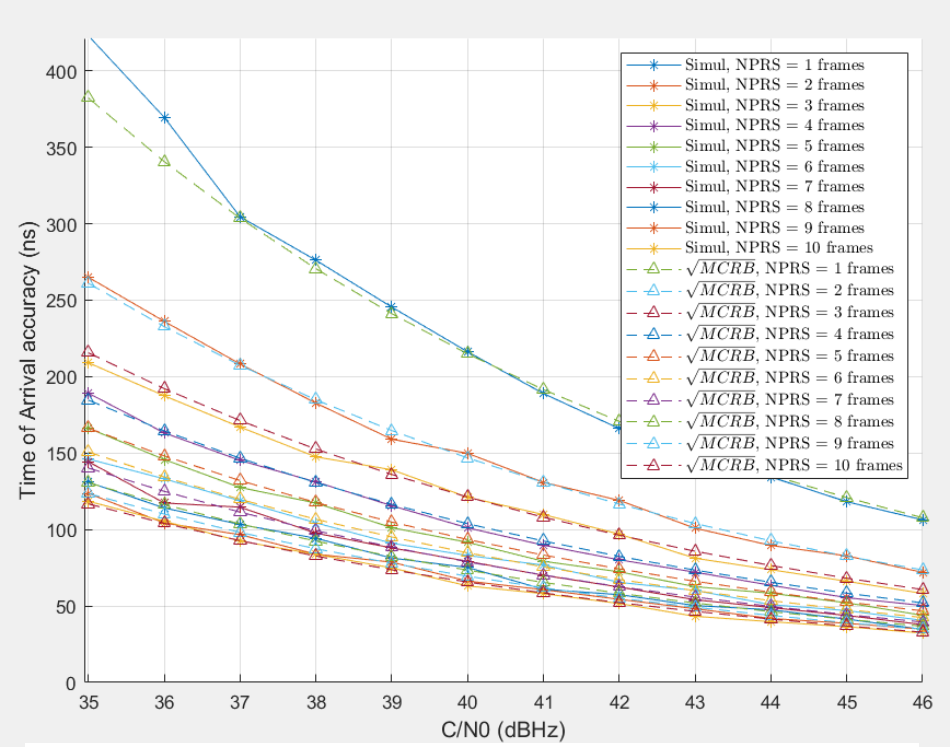

FIGURE 40: TOA ACCURACY SIMULATED VS. MCRB

Regarding simulation vs. $\sqrt{MCRB(\tau)}$ (theoretical bound), we can observe that for each NPRS duration, the simulated results lie very close to the theoretical bound, with the gap remaining relatively consistent. This demonstrates that the simulations are realistic and approach the theoretical minimum error. The gap tightens when the number of NPRS frames used in the correlation increases, showing that the MCRB approximation holds especially when NPRS $\geq$ 2 frames.

4.2.5.3 CONCLUSIONS

Given the ranging performance results presented above, the go-to solution when it comes to the choice of Kcomb is Kcomb = 1, as it gives the best timing accuracy while requiring the lowest C/N0. Furthermore, the use of Kcomb=1 is privileged in NTN systems.

The required number of NPRS frames to achieve a target ranging performance of around 100 ns at C/N0=40 dB, is equal to 4 frames. Additional reference signals can be used in the correlation to gain a margin of 0.8 dB.

Finally, the MCRB approximation of TOA accuracy for NPRS frames $\geq$ 2 holds very close to simulation results making MCRB a good simplification for positioning performance analysis.

Table 22 summarizes the main ranging accuracy performances with NPRS.

TABLE 22: MAIN RANGING ACCURACY PERFORMANCES WITH NPRS

Number of frames in PRS occasion	Number of PRS subframes	1-sigma accuracy (ns)	1-sigma ranging error (m)= 1-sigma accuracy (ns)*SpeedOfLight
-	10	180	54
1	7	216	65

2	15	150	45
3	22	121	36
4	30	101	30
5	37	92	28
10	75	65,6	20

4.3 POSITION PERFORMANCE WITH TEST CONSTELLATIONS

4.3.1 HYPOTHESIS

4.3.1.1 POSITIONING METHOD

We consider that the user is connected to network so that it knows approximately where it is and it knows visible satellites ephemerises.

PRSs are used to enable OTDOA positioning as shown in Figure 41 except that eNodeBs in NTN case are the LEO satellites in visibility (gNodeBs).

The procedure of OTDOA can be summarized as follows:

- Several synchronized satellites simultaneously transmit the PRSs.
- The UE estimates the time of arrival (TOA) of signals received from multiple eNBs. This is also called ranging estimation (see previous Section).
- OTDOAs are formed by analyzing the differences between the arrival time instances.
- UE positions can be found by calculating the intersections of the hyperbolas created by each time differences.

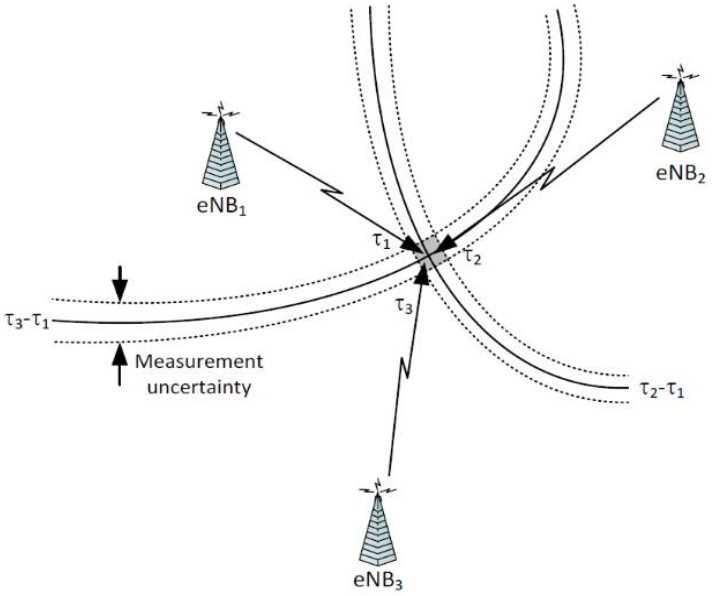

FIGURE 41: OTDOA POSITIONING

In order to build a first results iteration, the following assumptions are taken:

- Only TOA measurements are used
- The standard 2D/3D TOA snapshot algorithm is used

4.3.1.2 ERROR MEASUREMENT BUDGETS

Three ranging budget scenarios are considered:

- SC1 : Low-energy scenarios (NB-IoT in FR1)
- SC2 : Standard NR scenario (FR1)
- SC3 : Large bandwidth scenario (FR2)

The list of contributors has been introduced in 2.1.3. The performance simulator takes into account an evolution of the ranging error as a function of elevation. In Table 23 the values at horizon (10° elevation) are provided.

TABLE 23: ERROR MEASUREMENT BUDGET

Error source (m)	SC1	SC2	SC3	Comment
Ephemeris data	0.5	0.5	0.5	State of the art of dual frequency dual constellation GNSS Rx in LEO. Dependency on elevation due to along-track higher error.
Satellite clock	1.0	1.0	3.0	Roughly 3ns error for GNSS Rx + 3ns (SC1 or SC2) or 10ns (SC3) due to quality of transmission stability (more difficult with beams)
Ionosphere	2.0	2.0	0.1	Single-frequency measurements, evolution in $1/f^2$
Troposphere	0.7	0.7	0.7	
Multipath	1.4	1.4	1.4	
Receiver measured error	20.0	2.0	1.0	**For SC1, see 4.2.5.3** For SC2, same formulas than for SC1 but applied to a larger bandwidth signal (5 MHz) For SC3, estimation of steady-state errors and effect of shorter measurement durations
Total (rms)	**20.2**	**3.4**	**3.6**	

For the sake of simplicity, the simulations for SC2 and SC3 below have been merged, and aligned on a total error of 3.5m.

4.3.1.3 TEST CONSTELLATIONS

The performances have been tested with 3 reference constellations:

- Constellation 1:
  - Altitude 1200 km
  - 263 satellites :
    - Walker 120/12/1 at 89° inclination
    - Walker 143/11/1 at 55° inclination
- Constellation 2:
  - Altitude 900 km
  - 364 satellites :
    - Walker 364/18/1 at 73° inclination
- Constellation 3:
  - Altitude 600 km
  - 1458 satellites :
    - Walker 1458/27/1 at 89° inclination

Rationales:

- The constellation 1 corresponds to typical OW2/Iris² configurations.
- The constellation 2 corresponds to a reference LEO-PNT standalone design
- The constellation 3 corresponds to a massive low-LEO constellation

4.3.2 POSITIONING PERFORMANCES

All simulations have been done with mask = 10°.

4.3.2.1 VISIBILITY

The visibility (statistics on the visible number of satellites for a given latitude) only depends on the geometry, and then on the constellation, and not on the ranging error budget.

The curves for the 3 constellations are provided in Figure 42:

Constellation 1 (1200km)	Constellation 2 (900 km)	Constellation 3 (600km)
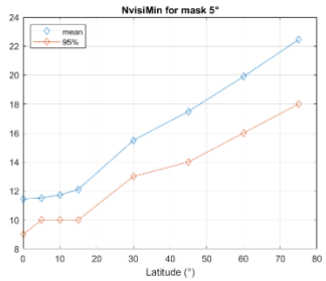	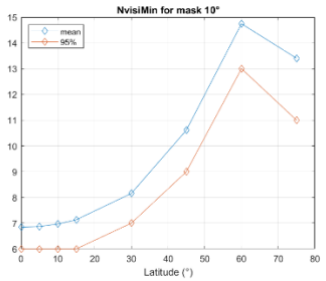	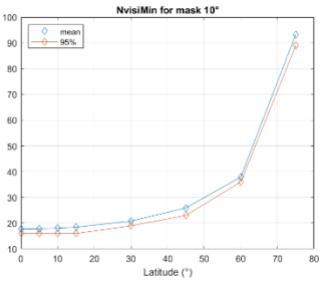

FIGURE 42: SATELLITES VISIBILTY ANALYSIS FOR CONSTELLATIONS 1, 2 AND 3.

4.3.2.2 SCENARIO 1 (LOW-ENERGY, 20.2M RMS RANGING ERROR)

The positioning accuracies in meter (y-axis) based on the ranging error budget presented in Table 23 are presented in the following for Scenario 1.

4.3.2.2.1 HORIZONTAL ACCURACY FOR 2D POSITIONING

Constellation 1 (1200km)	Constellation 2 (900 km)	Constellation 3 (600km)
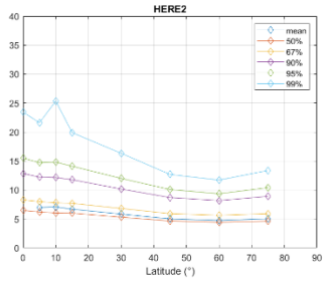	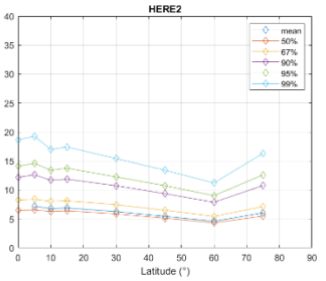	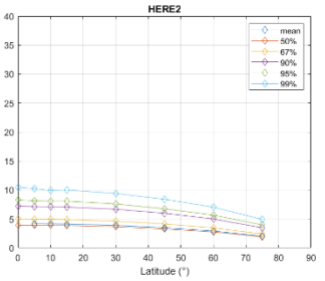

4.3.2.2.2 HORIZONTAL ACCURACY FOR 3D POSITIONING

Constellation 1 (1200km)	Constellation 2 (900 km)	Constellation 3 (600km)
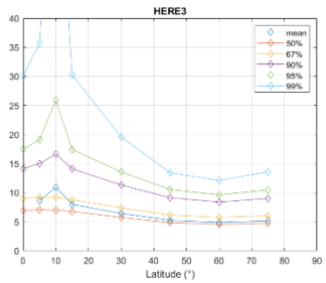	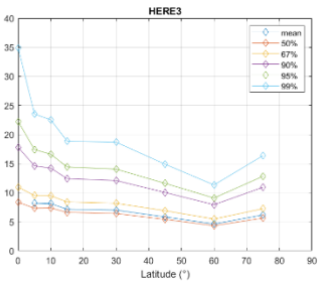	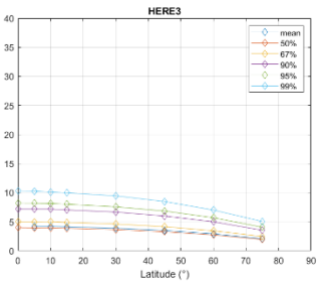

4.3.2.2.3 VERTICAL ACCURACY FOR 3D POSITIONING

Constellation 1 (1200km)	Constellation 2 (900 km)	Constellation 3 (600km)
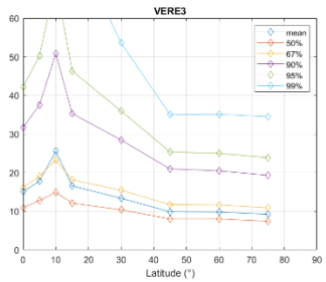	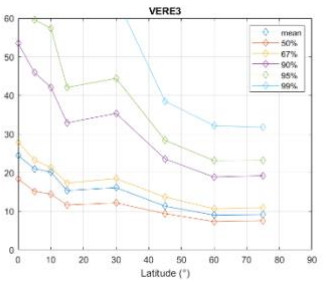	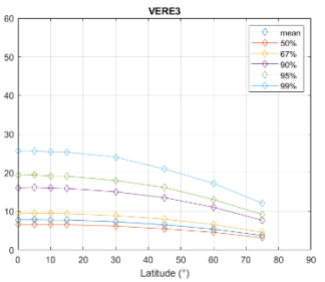

4.3.2.3 SCENARIOS 2/3 (NR, 3.5M RMS RANGING ERROR)

The positioning accuracies in meter (y-axis) based on the ranging error budget presented in Table 23 are presented in the following for Scenarios 2/3.

4.3.2.3.1 HORIZONTAL ACCURACY FOR 2D POSITIONING

Constellation 1 (1200km)	Constellation 2 (900 km)	Constellation 3 (600km)
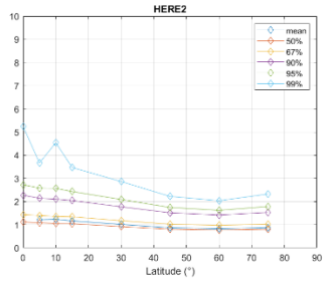	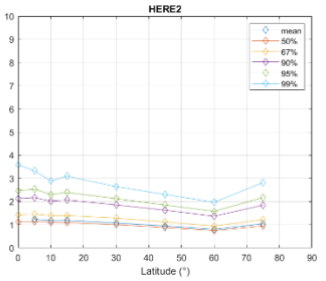	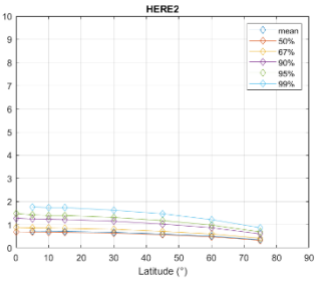

4.3.2.3.2 HORIZONTAL ACCURACY FOR 3D POSITIONING

Constellation 1 (1200km)	Constellation 2 (900 km)	Constellation 3 (600km)
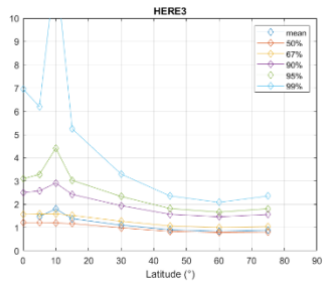	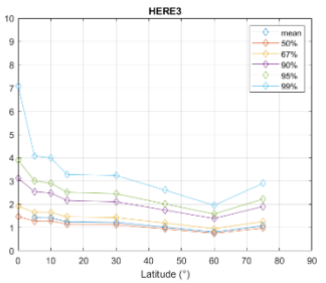	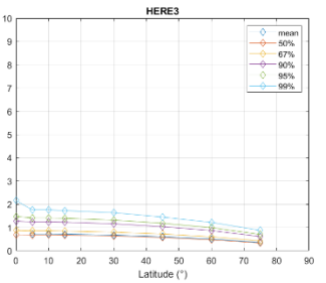

4.3.2.3.3 VERTICAL ACCURACY FOR 3D POSITIONING

Constellation 1 (1200km)	Constellation 2 (900 km)	Constellation 3 (600km)
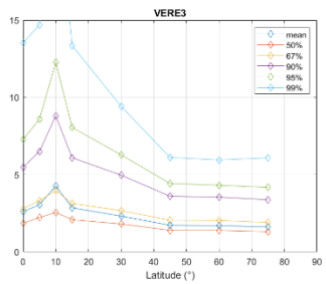	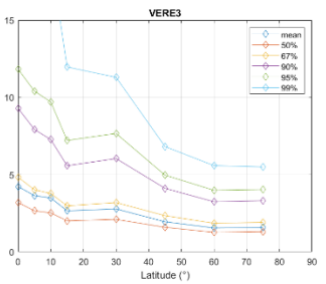	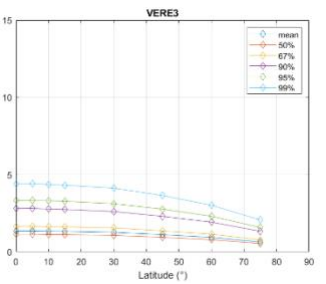

4.4 SUMMARY AND CONCLUSIONS

Through these simulations, simple conclusions can be driven:

- It is possible to implement satellite ranging measurements on 3GPP signals, based on PRS design. The nature of the measurements is very similar to the ones in GNSS.
- With large LEO constellations (around 300 satellites, depending on the altitude), it is possible to reach enough satellites in visibility to reach performance similar to the one achieved with the MEO GNSS, around a few meters.
- If the target accuracy is around 50m @95%, low-energy NB-IoT signals (180 kHz) can be used, but the resulting measurement accuracy is the driver of the overall ranging error budget, and then the driver of the positioning accuracy. With larger bandwidths such as 5 MHz it becomes possible to align the receiver measurement error to other contributors.
- Not considering this low-energy case, the main drivers for performance are the measurement accuracy (noise) and the ionosphere delay in FR1, and the measurement accuracy (Doppler steady-state errors) and the payload synchronization in FR2. With such solutions, it is possible in this context to reach horizontal positioning error @95% below 3m and vertical error @95% below 10m for all latitudes.
- With even larger constellations (constellation 3 above), the error can be as low as 1.5m (horizontal error @95%), but it is not improved enough to pass below 1m and reach centimeter level.
- In order to reach centimetric level, it is necessary (as in GNSS context) to consider more complex positioning methods, as introduced in 4.1.2, and more specifically:
  - For FR1:
    - More accurate information on satellite errors by assistance or corrections (similar to Galileo HAS), which can be built for instance from a set of global or regional reference receivers ;
    - Averaging of noise over time, either by keeping the receiver static, or within a Kalman filter aided by inertia sensors, and estimating ionosphere delay contribution thanks to dedicated processing and observation over time ;
    - From these two conditions, possible centimetric accuracy could be expected with a minute, considering the high dynamics of LEO. This would however require further analysis and in-orbit tests, such as the one planned in the ESA Celeste-IOD context in 2027, knowing that for instance the wavelength in S-band will be smaller than in L-band making more demanding the improvement on ranging to solve the wavelength ambiguity allowing to use phase measurements for high accuracy.
  - For FR2:
    - More accurate information on satellite errors by assistance or corrections (similar to Galileo HAS), which can be built for instance from a set of global or regional reference receivers. This is even more

important in FR2 as the satellite errors are the main driver. It is also more challenging to implement as the estimation of the errors will have to be consistent with the beam management, and in particular if the reference station and the users are not in the same beam.

- For the user, the best implementation to improve measurements will be to implement ultra-tight aided-tracking, that is an assistance from the positioning to the tracking loops, in order to pre-compensate the Doppler. This creates a virtuous circle between tracking performance and positioning performance. Such method has already been successfully tested for high-dynamics users (aircrafts for instance) in the MEO context, but would have to be tailored to FR2 LEO-context.

In summary, the ranging methods are fully applicable to telecommunication signal for standard positioning methods (snapshot least square), allowing to reach accuracy of a few meters. It is also possible to implement improved technologies allowing to reach better accuracy (PPP and ultra-tight coupling), but they require a supporting infrastructure to provide corrections on the system (similar to Galileo HAS) and further in-orbit tests to demonstrate the feasibility. For FR1, such tests are expected to take place in ESA Celeste IOD project, but for FR2 the next opportunities remain to be defined.

The main weakness of these technologies is that they rely on the availability of signals from multiple satellites (as a minimum 4) at a time, which is not usually the sizing criteria for a satellite communication system is max 2 or 3 satellites in visibility.

Note: In the 6G-NTN D3.9 chapter entitled “NAVIGATION CAPABILITIES OF THE PAYLOADS”, the number of satellites in visibility by a user equipment has been assessed for the C band constellation at 600 km altitude. In Figure 6-6 of D3.9, the number of satellites in visibility ranges between 4 and 9 across the full service area. The highest number of satellites in visibility is seen in high latitude regions. With such constellation, the positioning accuracy could range between ~2 meters (for 9 satellites in visibility) and ~4 meters (for 4 satellites in visibility).

It is then necessary:

- either to adapt the beamforming transmission, with for instance the introduction of full-footprint broadcast mode with dedicated ranging signals. This approach appears for instance relevant for FR1, but appears more challenging for FR2, just mentioning the constraint of GSO protection as a point to address ;

- or to map the implementation of PNT through the beam-hoping approach, the measurements from the N satellites being achieved with N successive beam hops, synchronized between the satellites and the users.

  - Considering the duration of the hops (milliseconds), the impact on position accuracy is expected to be very limited (could be visible on the fastest users, but those users generally have complementary positioning means, such as inertia sensors, so that the desynchronization of the measurements between satellites is no longer disturbing).

  - Such approach requires at least a NTN system beam management optimization. In addition, if the PNT is used for entering into the network without knowing the position of the user, the acquisition process shall be reviewed in order to accommodate the combination of user and satellite beams.

The conclusion on the feasibility of ranging positioning is then positive, but the impacts on the NTN telecommunication system have to be refined. It is then interesting to also consider alternative solutions such as the solutions proposed in the next sections.

5 DOPPLER BASED POSITIONING

Ranging methods of positioning that GNSS uses involve the measurement of the distance between the UE and the satellite, whereas Doppler methods of positioning involve the measurement of the time-rate of range. Since Doppler is a function of the relative-velocity and relative-position between the satellite and the UE its measurement, together with the knowledge of the satellite's position and velocity, can be used to determine the UE velocity and position, or any combination thereof depending on the need. In the following we shall restrict our focus to determining the location of a stationery UE only; thus, in all the following models, UE's velocity is not considered – it must be taken to be a zero-vector.

Determination of Earth-location by using measurements of Doppler from satellites is not new – it predates even GPS. The TRANSIT satellite system was a Doppler-based LEO positioning system consisting of fewer than a dozen polar satellites at a height of 1100km, providing global coverage albeit discontinuously.[1] The point positioning accuracy was around 100–200 m using about 2 min of Doppler shift observations [38]. With broadcast ephemeris and 30-50 satellite passes, 2-3m accuracy was achievable for single-station point positioning, whereas this accuracy could be improved to 1m with precise ephemeris [39].

With the prospect of multiple large LEO constellations being heralded, many recent works have studied Doppler-based LEO positioning. For instance, Doppler-only positioning for the case of large satellite-constellations like Starlink was studied in [28], use of Doppler in conjunction with pseudorange was studied in [40] with a focus on Globalstar, Orbcomm, Iridium, and Starlink constellations, Doppler in conjunction with inertial navigation system (INS) was studied for the case of Iridium Next constellation in [41]. Many of these studies perceive these Doppler-measurements as signals-of-opportunity, where they can be measured by the UE that is not necessarily connected to the network of the constellation under consideration. That is, unintended navigation signals from communication satellites may be opportunistically used by the UE to measure Doppler and derive its location using the satellite ephemeris.

The scope of the Doppler study presented in this document is to analyze the expected performance and feasibility of Doppler-based positioning as applicable to mobile-phones from communication constellations that can offer one, or two, satellites in visibility at any time. The present analysis models only additive measurement noise and the XO-clock error but does not model other errors such as ionosphere-rate and tropospheric-rate. It also assumes error-free clock at the satellite.

5.1.1 NOTATION

Table 24 captures the notation used in this section.

TABLE 24: NOTATION FOR DOPPLER ANALYSIS

Symbol	Meaning
x_S, v_S	Position vector and velocity vector, respectively, of satellite s (the time epoch is not explicitly notated here, but will be made explicit when required)

[1] Consecutive satellite passes at an Earth location could be interspersed with gaps of no satellite-coverage that could extend from 2 hours at Equator to 30-mins near poles, on average.

$\boldsymbol{x}$	Position of the UE, to be determined
$\|\boldsymbol{p}\|$	Norm of the vector $\boldsymbol{p}$
$\langle \boldsymbol{p}, \boldsymbol{q} \rangle$	Dot-product of vectors $\boldsymbol{p}$ and $\boldsymbol{q}$
$\boldsymbol{c}$	Speed of light, 3e8 [m/s]
$\widehat{\boldsymbol{p}}$	$\frac{\boldsymbol{p}}{\|\boldsymbol{p}\|}$, unit vector in the direction of vector $\boldsymbol{p}$
$\overline{\boldsymbol{v}}_{\boldsymbol{s}}$	Velocity component of satellite s that is perpendicular to the LOS direction (the time epoch is not explicitly notated here, but will be made explicit when required)
	Partial derivative of the scalar function f with respect to the vector $\boldsymbol{x}$
$\boldsymbol{Tr}(\boldsymbol{A})$	Trace of matrix A
$\boldsymbol{\mu}$	Gravitational parameter of Earth ~ 3.986e14 m^3/s^2
$\boldsymbol{a_E}$	Earth radius = 6378137 [m]

5.1 SENSITIVITY OF THE DOPPLER OBSERVABLE

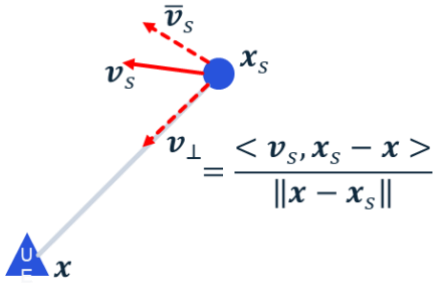

FIGURE 43: MEASUREMENT OF DOPPLER

Figure 43 shows a UE and a satellite in its view. In the ideal case, the UE measures the satellite Doppler given as the projection of the satellite velocity in the direction of the LOS-vector between the UE and the satellite. This is denoted by $\boldsymbol{v}_\perp$in the figure.

To determine the sensitivity of the measurement with respect to the UE location, we start with the definition of ideal Doppler measurement as:

$$cD = v_\perp = \frac{\langle \boldsymbol{v}_s, \boldsymbol{x}_s - \boldsymbol{x} \rangle}{\|\boldsymbol{x} - \boldsymbol{x}_s\|}.$$

Next, taking the gradient of the foregoing with respect to the UE location, we have:

$$c\frac{\partial D}{\partial \boldsymbol{x}} = -\frac{\boldsymbol{v}_s - \langle \boldsymbol{v}_s, \widehat{\boldsymbol{x}_s - \boldsymbol{x}}\rangle \widehat{\boldsymbol{x}_s - \boldsymbol{x}}}{\|\boldsymbol{x} - \boldsymbol{x}_s\|} = -\frac{\bar{\boldsymbol{v}}_s}{\|\boldsymbol{x} - \boldsymbol{x}_s\|},$$

where we note $\bar{\boldsymbol{v}}_s$ is the velocity of the satellite projected onto the plane that is perpendicular to the LOS vector.

Thus, the magnitude of the gradient of the Doppler observation, from the above, is given as:

$$c\left\|\frac{\partial D}{\partial \boldsymbol{x}}\right\| = \frac{\|\bar{\boldsymbol{v}}_s\|}{\|\boldsymbol{x} - \boldsymbol{x}_s\|}.$$

We shall denote the RHS of the foregoing equation as 'Doppler sensitivity'.

5.1.1 COMPARISON OF DOPPLER SENSITIVITY BETWEEN LEO AND MEO

We note that the range to the satellite $\|\boldsymbol{x} - \boldsymbol{x}_s\|$ in the case of LEO is smaller in comparison to that of MEO by a factor between 10 (LEO at 2000km altitude) and 40 (LEO at 400km), and max. $\|\bar{\boldsymbol{v}}_s\|$ is larger by a factor between 1.78 (LEO at 2000km altitude) and 1.94 (LEO at 400 km). In fact, Doppler sensitivity is a function of the elevation angle. Figure 44 illustrates the ratio of the Doppler sensitivity of a LEO to that of a MEO as a function of the elevation angle by considering a GPS satellite and two exemplar polar LEO orbits, at 400 km and 2000 km. We note that for the lower LEO-orbit, the Doppler sensitivity ratio ranges from nearly 40 at elevation angle 30-deg to nearly 125 towards the zenith direction, whereas of the higher LEO-orbit, the ratio ranges from nearly 20 at 30-deg elevation till about 40 in the zenith direction. These two example heights can be considered to represent the limits of the ratio; that is, for any other LEO-orbit its Doppler-sensitivity ratio with respect to GPS lies in the region between the two curves shown in the figure. Therefore, we see that LEOs exhibit much larger (at least 20-fold) Doppler-sensitivity in comparison to MEOs.

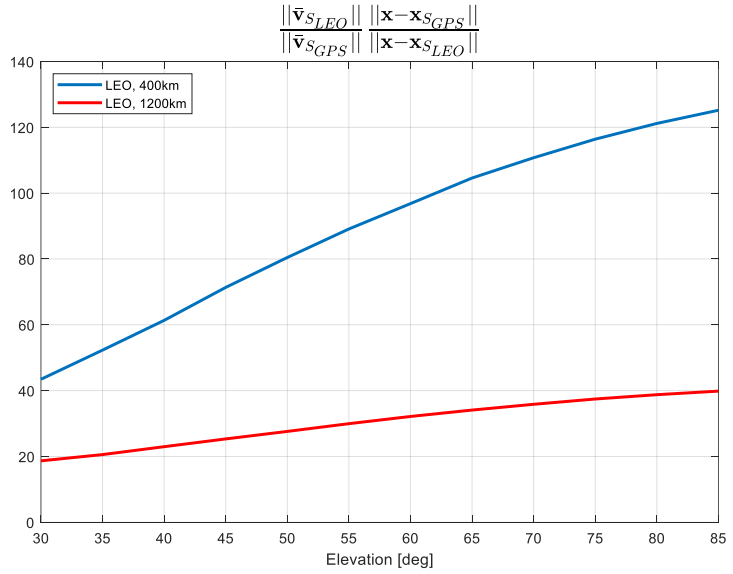

FIGURE 44: RATIO OF DOPPLER SENSITIVITY OF LEO TO THAT OF MEO AS A FUNCTION OF ELEVATION ANGLE.

5.1.1 ILLUSTRATION

An implication of the foregoing observation is that for the same amount of Doppler-measurement error in Doppler measurements from LEO and MEO satellites, the LEO measurement yields a smaller positioning error. Further, this positioning error improves with larger Doppler-sensitivity ratio. Stated differently, two UEs that are far separated on ground are likely to measure similar Doppler-values in the case of MEO satellites, but this is not the case for LEO satellite measurements. Thus, the spatial resolvability of position is much better in the case of Doppler measurements from LEOs than MEOs.

For an illustration of this principle, we compare the performance of Doppler-based positioning between LEOs and MEOs under the same measurement noise model. Specifically, this illustration considers simultaneous measurement of Doppler over time from two satellites. Positioning fix is determined upon the collection of all measurements. The Keplerian orbital elements of the two satellites for LEO and MEO (GPS) are given in Table 25.

TABLE 25: KEPLERIAN ORBITAL ELEMENTS FOR THE TWO LEO/MEO SATELLITES USED IN THE ILLUSTATION

Parameters	LEO	GPS
Semimajor axis, a [m]	6978137	26560e3
Longitude of ascending node, laan [deg]	-116, -123.5	212.85, 272.85
Inclination, i [deg]	87.2	55
Argument of periapsis, w [deg]	0	0
Mean anomaly, M [deg]	21, 19.67	345.23, 268.89
Eccentricity, e	0	0

The measurement model is:

$$o_{s_i}(k) = \frac{\langle \boldsymbol{v}_{s_i}(k), \boldsymbol{x}_{s_i}(k) - \boldsymbol{x} \rangle}{\|\boldsymbol{x} - \boldsymbol{x}_{s_i}(k)\|} + n_{s_i}(k), i = 1,2; 1 \leq k \leq N,$$

where $o_{s_i}(k)$ denotes the measured Doppler at time-step k from satellite i, whose position and velocity at time-step k is $\boldsymbol{x}_{s_i}(k)$ and $\boldsymbol{v}_{s_i}(k)$, respectively. $n_{s_i}(k)$ denotes the corresponding noise in the measurement, assumed to be independent and identically distributed (iid) additive zero-mean white Gaussian with standard deviation σ_n of 0.2 Hz at carrier frequency of 2 GHz (= 0.03 m/s). The noise standard deviation is the same for measurements from LEO and those from GPS. The total number of measurements per satellite is denoted by N. Further, let G denote the time-duration between consecutive time-steps.[2] Figure 45 shows the 80-percentile 3D positioning error for $N = 25$ as a function of G for both LEO and MEO.

[2] Note that k denotes time-step: a unit-less quantity, whereas G denotes the duration between consecutive time-steps, in units of seconds.

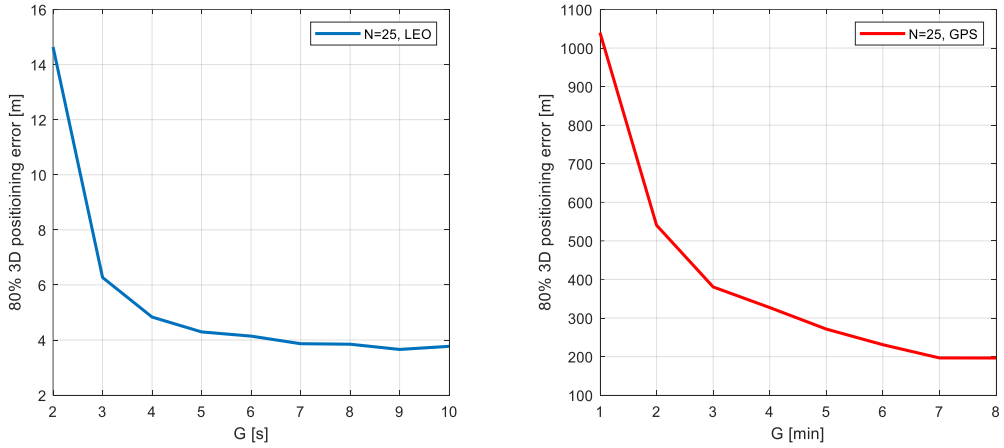

FIGURE 45: DOPPLER POSITIONING PERFORMANCE OF LEO AND MEO UNDER SAME OBSERVATION NOISE VARIANCE

The comparative plots illustrate the following. In both cases, performance improves with larger inter-observation duration G. This is attributed to better geometric diversity arising from satellite movement; in effect, larger G `decorrelates' the observation equations leading to better conditioning of the positioning matrix (for numerical invertibility) in the solution of the navigation equations. Note that for LEO, G is plotted in units of seconds, whereas for MEO, it is in units of minutes. This is because the satellite-geometry changes very slowly for MEO, and we need much larger G to obtain a well-conditioned positioning matrix. The eventual `flooring'/saturation of both plots refers to the fact the further geometric diversity cannot be gained once we have sufficiently spaced samples. Lastly, we note that the best performance in the case of LEO is seen to be about 4m, whereas for MEO the corresponding number is about 200m. This improved performance, with a factor of 50, reflects the superior Doppler-sensitivity of LEO observed earlier. Thus, with respect to Doppler-positioning, not only can we get quicker positioning fixes, but also much superior error-performance from LEOs, as compared to MEO. Therefore, Doppler observables are better suited for LEO than MEO given similar observation noise. This further motivates the study of Doppler-observables in the context of LEO positioning. It is also interesting to note that ranging-sensitivity is the same for MEO and LEO.

5.1 SIMULATION STUDIES

In this section we study Doppler-based positioning in the case of a constellation providing (i) only a single satellite in visibility at any time and (ii) two satellites in visibility at any time. The foregoing special cases are motivated by the consideration that constellations dedicated for satellite broadband are usually designed to maximize coverage with minimal number of satellites, thus, ensuring one (or two) serving satellite(s) in a cell. Thus, these studies document the expected performance in the case that such communication network also begins to provide positioning service. They can be envisioned as lower bounds on Doppler-positioning performance: a constellation, like GNSS, capable of providing 4 or more simultaneous satellites in visibility will only provide much better performance than the single/two satellite case. For both foregoing studies we consider constellations as described in Table 26.

TABLE 26: CONSTELLATION CONSIDERED IN SIMULATIONS. MEA IS ASSUMED TO BE 30-DEGREES FOR BOTH CASES.

Case	Constellation type	Inclination [deg]	Total number of satellites	Number of planes	Inter-plane phasing [deg]
Single-satellite visibility	Walker-star	87.2	476	17	7
Two-satellite visibility	Walker-star	87.2	912	16	6

In the following, we employ Doppler measurement noise standard deviation σ_n as a simulation parameter, where Doppler estimates are modeled to be corrupted from their ideal values by additive white Gaussian zero-mean measurement noise with standard deviation σ_n. In principle, Doppler can be estimated in the time-domain (exploiting CP-repetition) or in the frequency-domain (using frequency domain reference signals). In the latter case, any reference-signal can be employed, for example, PBCH-DMRS (SSB), tracking reference signal (TRS), and PRS. Estimation can be improved by fusing across multiple reference signals, whenever available. We do not delve on any specific reference-signal or its configuration in this study. The estimate variance σ_n^2 is, in general, inversely dependent on the SNR of the reference signal and the total number of frequency (Bandwidth) and time-domain resources it occupies. It is also directly proportional to the loop-bandwidth of the filter that is typically used to smoothen instantaneous estimates.

5.1.1 SINGLE-SATELLITE BASED DOPPLER POSITIONING

This scenario is the most challenging for any kind of positioning by a mobile phone UE. Since instantaneous availability of at least 4 measurements is impossible, we need to collect measurements over time and obtain positioning fix/refinement across time as more measurements are made. This case is made much more challenging owing to the poor stability of the clocks used in mobile phones. Further, measurements made from a single satellite pass lack geometric diversity and are hence augmented with measurements from multiple satellite passes.

5.1.1.1 XO MODEL

Typically, mobile phones contain a simple basic uncontrolled crystal oscillator (XO), whose timing error can have very large uncontrolled drifts over time owing to ambient temperature changes. We model the total fractional-frequency XO-error $e_{XO}(t)$ at time t as:

$$e_{XO}(t) = e_{XO,S}(t) + e_{XO,R}(t),$$

where $e_{XO,R}(t)$ denotes the random-error component and $e_{XO,S}(t)$ denotes the deterministic residual systematic error that is seen in baseband after compensation at the receiver front-end.[3] We adopt a third-order polynomial for temperature-dependence of $e_{XO,S}(t)$ as:

$$e_{XO,S}(t) = c_0 + c_1(T(t) - T_0) + c_2(T(t) - T_0)^2 + c_3(T(t) - T_0)^3,$$

where $\{c_i\}_{i=0}^{3}$ denote the post-compensation residuals whose maximum uncertainties are known, $T(t)$ denotes the temperature of the XO at time t, and T_0 denotes the nominal temperature of XO, which is specified by the manufacturer. For the temperature variation, we use a temperature-ramp model:

$$T(t) = T_A + \gamma t,$$

where T_A denotes the ambient temperature and γ is the rate of temperature change. The random error component $e_{XO,R}(t)$ is modeled with a power-law spectral density $S(f)$ of the fractional-frequency error given by:

$$S(f) = \frac{h_{-2}}{f^2} + \frac{h_{-1}}{f^1} + h_0, f > 0$$

where h_0 denotes the spectral density component for white frequency modulation (WFM) , $h_{-1}f^{-1}$denotes the Flicker frequency modulation (FFM) component, and $h_{-2}f^{-2}$ denotes the random-walk frequency modulation (RMFM) component.

5.1.1.2 OBSERVATION MODEL AND PROCESSING

The following describes the measurement collection strategy. Two Doppler measurements (observations) that are separated in time by g_1[s] are made every g_2[s] from the single satellite that is in view ($g_1 \leq g_2$). Figure 46 illustrates the foregoing.

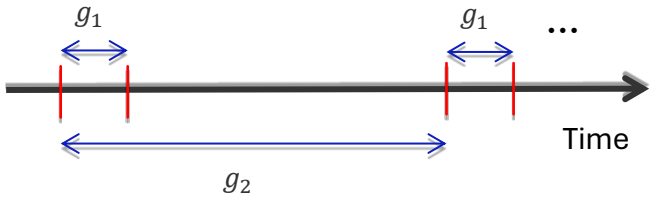

FIGURE 46: MEASUREMENT STRATEGY FOR SINGLE SATELLITE.

For $l \in \{0,1\}$ and $1 \leq k \leq N$, we index the time-epoch of measurement $(kg_2 + lg_1)$ as time-step (k, l). Thus, the Doppler-measurement $o_s(k, l)$ that is collected at time-step (k, l) from satellite s is:

$$o_s(k,l) = \frac{\langle \boldsymbol{v}_s(k,l), \boldsymbol{x}_s(k,l) - \boldsymbol{x} \rangle}{\|\boldsymbol{x} - \boldsymbol{x}_s(k,l)\|} + ce_{XO}(k,l) + n_s(k,l), l \in \{0,1\}, 1 \leq k \leq N,$$

where $\boldsymbol{x}_s(k, l)$ and $\boldsymbol{v}_s(k, l)$ denote the position and velocity of the single satellite s in view, $e_{XO}(k, l)$ is the (unknown) XO-error, and $n_s(k, l)$ is the additive white Gaussian measurement

[3] Compensation of the error is usually made by learning and recalibrating the XO's temperature variation parameters.

noise, all defined at time-step (k, l). The XO-error is sampled from the process model described in the foregoing. The measurements are differenced as below:

$$\tilde{o}_k = o_s(k,1) - o_s(k,0), 1 \leq k \leq N.$$

Note that we have dropped the indication of the satellite in the notation for brevity. We thus obtain N time-differenced measurements that are g_2[s] separated in time. It is also worth noting that for the time-differenced measurements in the single-satellite case the unmodelled errors such as ionospheric and tropospheric rates can be assumed to be effectively negligible, especially for small values of g_1.

Further, batch processing per satellite is assumed, where we collect all measurements from a satellite's pass and augment to the existing data in the solution engine. The solution engine takes the differenced measurements $\tilde{o}_k$ along with satellite ephemeris to solve for the user position $\boldsymbol{x}$.

Table 27 captures the various parameters in the XO-model that is used in the simulations. Figure 47 shows an example variation of the XO error using the foregoing parameters. We note that not only the fractional error increases over time, but the bias in it also increases, albeit at a slower rate. Thus, the (unknown) differential XO error also has a time-varying bias.

TABLE 27: PARAMETERS OF XO MODEL USED IN SIMULATION

Parameter [unit]	Value used in simulation
T_0 [degrees Celsius]	25
c_0[ppm]	0.25
c_1[ppm/degree]	0.02
c_2[ppm/degree^2]	1.2e-4
c_3[ppm/degree^3]	1.5e-5
T_A[degrees Celsius]	27
γ[degrees/s]	0.02
h_0[1/Hz]	1e-19
h_{-1}[1/Hz]	1e-19
h_{-2}[1/Hz]	1e-20

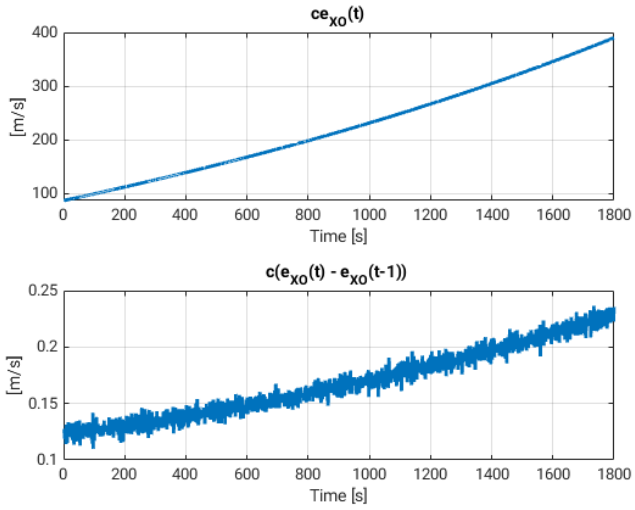

FIGURE 47: SAMPLE VARIATION OF XO-ERROR WITH THE CONFIGURATION PARAMTERS IN TABLE 11

5.1.1.3 PERFORMANCE

Figure 48 shows the 90-percentile positioning error as a function of measurement time measurement noise standard deviations $\sigma_n$of 0.1 Hz and 1Hz, using $g_1 = 2$s and $g_2 = 5$s.[4]

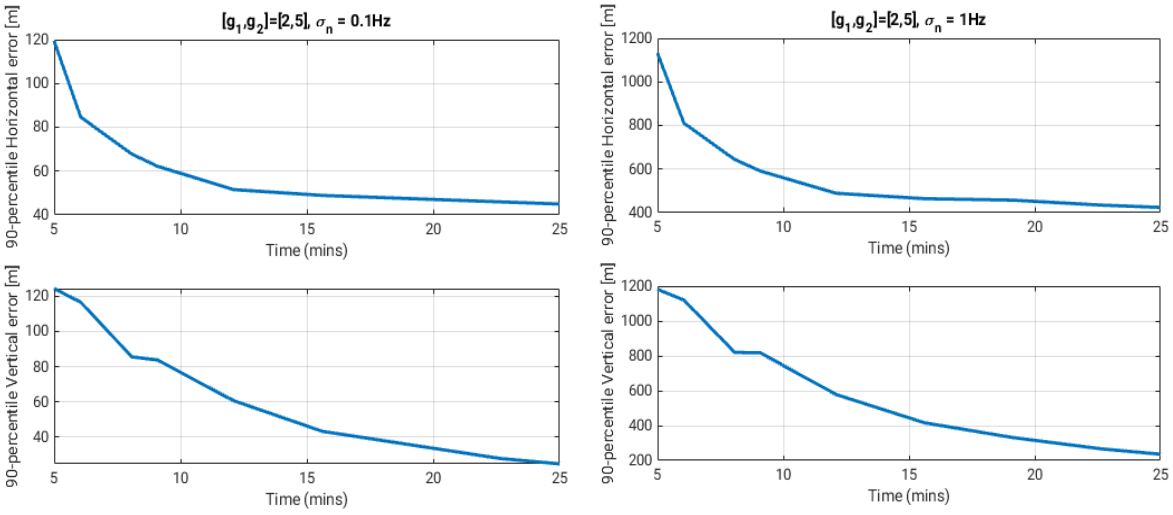

FIGURE 48: PERFORMANCE OF SINGLE-SATELLITE DOPPLER POSITIONING WITH XO-ERROR MODEL.

We note that as we measure more samples over time, better noise-averaging leads to improved error performance. After 10 mins of observations, a horizontal positioning error of 60[m] and a vertical positioning error of 75[m] can be achieved for the case of measurements with accuracy $\sigma_n = 0.1$Hz. If the measurement quality deteriorates, the positioning error too worsens drastically. For $\sigma_n = 1$Hz, the horizonal and vertical errors are at 460[m] and 416[m],

[4] The choice of $g_1 = 2$[s] in the simulation is a design illustration here. In general, it should not be so small that the change of satellite-UE geometry is insignificant in comparison to (measurement-AWGN + XO) noise during the interval g_1; it should also be not too large to allow a large differential (time-varying) XO-error. This tradeoff, in practice, must be evaluated wrt the device's true XO and measurement-noise limitations.

respectively, after 15 mins of measurements. Further averaging to 25 mins nearly halves the vertical error without significantly improving the horizontal error.

5.1.1 TWO-SATELLITE BASED DOPPLER POSITIONING

Next, we study the case of two satellites in view, under the assumption that simultaneous observations can be made from both satellites at any given time. Under this assumption, we can take difference measurements across satellites and eliminate the XO-error in all the differenced measurements. This is in contrast with the single-satellite case, where the XO-error is not eliminated in differenced measurements. This directly provides a huge advantage in positioning, where performance is governed primarily by the two-satellite geometry over time and measurement noise.

5.1.1.1 OBSERVATION MODEL AND PROCESSING

The measurement model in this case, with the XO-error introduced, is:

$$o_{s_i}(k) = \frac{\langle \boldsymbol{v}_{s_i}(k), \boldsymbol{x}_{s_i}(k) - \boldsymbol{x} \rangle}{\|\boldsymbol{x} - \boldsymbol{x}_{s_i}(k)\|} + ce_{XO}(k) + n_{s_i}(k), i \in \{1,2\}, 1 \leq k \leq N,$$

where $o_{s_i}(k)$ denotes the measured Doppler at time-step k from satellite s_i, whose position and velocity at time-step k is $\boldsymbol{x}_{s_i}(k)$ and $\boldsymbol{v}_{s_i}(k)$, respectively. The XO-error at time-step k is $e_{XO}(k)$, which is the same for both satellites being measured simultaneously. Finally, $n_{s_i}(k)$is the corresponding iid. white Gaussian measurement noise with standard deviation σ_n. We now difference across the satellites:

$$\tilde{o}_k = o_{s_2}(k) - o_{s_1}(k), 1 \leq k \leq N.$$

As before, we have dropped the indication of the satellite-index in the notation for brevity. We again obtain a total of N differenced observations that is input, along with satellite-ephemeris, to the solution engine.

5.1.1.2 PERFORMANCE

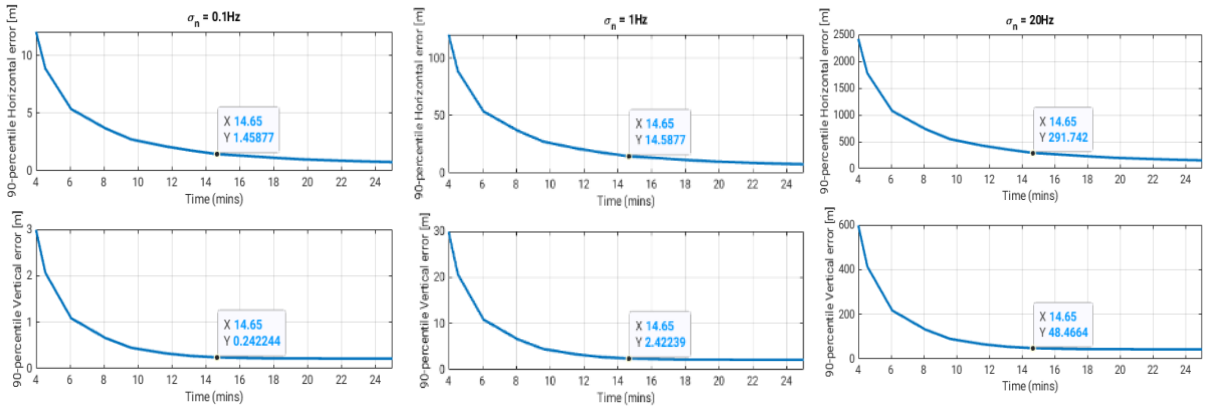

FIGURE 49: PERFORMANCE OF DOPPLER POSITIONING WITH TWO-SATELLITES IN VIEW.

Figure 49 shows the 90-percentile positioning error for two-satellite visibility scenario as a function of measurement time measurement for noise standard deviation $\sigma_n$of 0.1 Hz, 1Hz, and 20Hz. Consecutive measurements were obtained 5s apart. With the effect of the XO-error eliminated by differencing across satellites, we see a huge improvement in error performance in comparison to the single-satellite case. With σ_n = 0.1Hz, we see 1.5[m] of horizonal error

and 0.24[m] of vertical error after about 15mins of measurements. For σ_n=20Hz, the horizontal error increases to 291[m] and the vertical error increases to 48[m] for the same period of measurement. The error performance continues to improve in all cases with a greater number of observations (noise-averaging). A further interesting observation is that the vertical-positioning accuracy in all cases is seen to be much better, by an order of magnitude, than the horizontal-positioning accuracy. The same observation can be made of even the single-satellite positioning case.

5.1 DILUTION OF PRECISION ANALYSIS FOR JOINT RANGE-DOPPLER POSITIONING

In this section we provide an elementary dilution-of-precision (DOP) analysis to motivate the combination of range and Doppler measurements for LEO positioning. For this analysis, we restrict attention to the scenario of two-satellites in view, with differencing of the simultaneous observations between the satellites. As is common in DOP-analysis, we consider the linearization of the observables around the true UE location and relate the error-adjustment in positioning solution to the error in measurement through a DOP-metric.

In the case of ranging, the measured quantity is the distance $r_{s_i}(k)$ to the satellite at time-step k:

$$r_{s_i}(k) = \|\boldsymbol{x}_{s_i}(k) - \boldsymbol{x}\|, i \in \{1,2\}, 1 \leq k \leq N.$$

The difference between them is $\tilde{r}_k = r_{s_1}(k) - r_{s_1}(k)$. An error-adjustment $\delta\tilde{r}_k$ in the differenced observable relates to the error vector $\delta\boldsymbol{x}$ through the first-order derivative as (linearization):

$$\delta\tilde{r}_k = \langle(\boldsymbol{x}_{s_2}\widehat{(k)} - \boldsymbol{x}) - (\boldsymbol{x}_{s_1}\widehat{(k)} - \boldsymbol{x}), \delta\boldsymbol{x}\rangle .$$

We can collect all the forgoing equations in matrix notation by rewriting thus:

$$\delta\tilde{\boldsymbol{o}}_R = G_R\delta\boldsymbol{x},$$

Where $\delta\tilde{\boldsymbol{o}}_R$ is a Nx1 vector of $\{\delta\tilde{r}_k\}_{k=1}^N$ with units [m], $\delta\boldsymbol{x}$ is a 3x1 position error vector with units [m], and G_R is a dimensionless Nx3 matrix. We can define the range-DOP (RDOP) as:

$$RDOP = \sqrt{Tr((G_R^T G_R)^{-1})}.$$

In the case of Doppler-differencing, an error-adjustment $\delta\tilde{o}_k$ in the differenced observable relates to the error vector$\delta\boldsymbol{x}$ through the first-order derivative as (linearization):

$$\delta\tilde{o}_k = \langle\frac{\overline{\boldsymbol{v}}_s(k)}{\|\boldsymbol{x} - \boldsymbol{x}_{s_1}(k)\|} - \frac{\overline{\boldsymbol{v}}_s(k)}{\|\boldsymbol{x} - \boldsymbol{x}_{s_2}(k)\|}, \delta\boldsymbol{x}\rangle .$$

As previously, collecting all the equations above, we can write

$$\delta\tilde{\boldsymbol{o}}_D = G_D\delta\boldsymbol{x},$$

where $\delta\tilde{\boldsymbol{o}}_D$ is a Nx1 vector of adjustments $\{\delta\tilde{o}_k\}_{k=1}^N$, $\delta\boldsymbol{x}$ is the 3x1 position error vector, and $G_D$is a Nx3 matrix. Note here that $\delta\boldsymbol{x}$ is in units to [m], $\delta\tilde{\boldsymbol{o}}_D$ in [m/s] and the elements of G_D are in units of [1/s]. To obtain a dimensionless Doppler-DOP metric (DDOP) we introduce a scaling factor η with dimension [1/s] as follows:

$$\delta\tilde{\boldsymbol{o}}_D = (\frac{1}{\eta}G_D)(\eta\delta\boldsymbol{x}),$$

where we take η to be the maximum value of $\frac{\|\bar{v}_s(k)\|}{\|\boldsymbol{x}-\boldsymbol{x}_s(k)\|}$. For a satellite constellation at height h, this maximum value can be easily seen to be $\eta = \frac{\max\|\boldsymbol{v}_s(k)\|}{\min\|\boldsymbol{x}-\boldsymbol{x}_s(k)\|} = \sqrt{\frac{\mu}{(a_E+h)}}\frac{1}{h}$. For a 600-km orbit, $\eta = 0.012596$[1/s]. We can now define the scaled DDOP metric as:

$$DDOP(\eta) = \sqrt{Tr((G_{D,\eta}^T G_{D,\eta})^{-1})}.$$

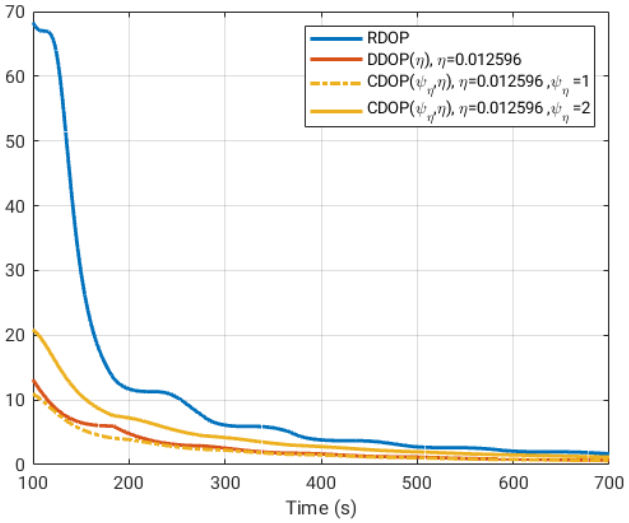

FIGURE 50: DILUTION OF PRECISION METRICS FOR RANGING, DOPPLER, AND COMBINED SCENARIOS. THESE ARE FOR TWO-SATELLITE SCENARIO WITH DIFFERENCED OBSERVABLES.

Figure 50 shows RDOP and DDOP(η) as a function of time for the case of two-satellite differencing over time. As expected, both metrics decrease over time since we gather more geometrically diverse observations over time. Suppose that the differenced range adjustments $\{\delta\tilde{r}_k\}_{k=1}^N$ be iid zero-mean Gaussian with standard deviation σ_R and the differenced Doppler adjustments $\{\delta\tilde{o}_k\}_{k=1}^N$ be iid zero-mean Gaussian with standard deviation σ_D. Define $\psi_\eta = \frac{\sigma_D}{\eta\sigma_R}$ as a parameter relating the measurement quality of Doppler and range measurements. To obtain a similar level of error performance between Doppler and ranging we need:

$$\frac{\sigma_D}{\eta}DDOP(\eta) = RDOP\ \sigma_R \Rightarrow \psi_\eta = \frac{RDOP}{DDOP(\eta)}.$$

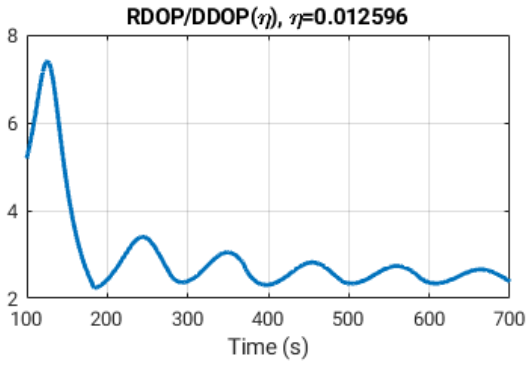

FIGURE 51: RATIO OF RDOP AND DDOP(H) AS A FUNCTION OF TIME. WHEN Ψ_H EQUALS THIS RATIO THE ERROR PERFORMANCE OF RANGE AND DOPPLER MEASUREMENTS IS THE SAME.

Figure 51 shows $\frac{RDOP}{DDOP(\eta)}$ as a function of time. Thus, if range measurements have accuracy of σ_R=1[m], Doppler measurement must have accuracy $\sigma_D = \frac{RDOP}{DDOP(\eta)}\eta$ ≈[0.03, 0.04][m/s], which is equivalent to ≈[0.2, 0.27] Hz at 2GHz, in order to provide equivalent 1[m] positioning accuracy (RMS). Thus, we see that Doppler measurements demand high accuracy in measurements.[5]

Next, looking at combining Doppler and range measurements, we can write the basic linearization equations as

$$\begin{bmatrix} \delta\tilde{\boldsymbol{o}}_R \\ \frac{1}{\eta}\delta\tilde{\boldsymbol{o}}_D \end{bmatrix} = \begin{bmatrix} G_R \\ G_{D,\eta} \end{bmatrix}\delta\boldsymbol{x}.$$

Assuming the same measurement statistics for range and Doppler as before, we can write the covariance of $\delta\boldsymbol{x}$ as

$$\Sigma_{C,\delta\boldsymbol{x}} = \sigma_R^2(G_R^T G_R + G_{D,\eta}^T G_{D,\eta})^{-1}(G_R^T G_R + \frac{\sigma_D^2}{\eta^2\sigma_R^2}G_{D,\eta}^T G_{D,\eta})(G_R^T G_R + G_{D,\eta}^T G_{D,\eta})^{-1}.$$

The combined DOP (CDOP) can then be defined as:

$$CDOP(\psi_\eta, \eta) = (Tr((G_R^T G_R + G_{D,\eta}^T G_{D,\eta})^{-1}(G_R^T G_R + \psi_\eta^2 G_{D,\eta}^T G_{D,\eta})(G_R^T G_R + G_{D,\eta}^T G_{D,\eta})^{-1}))^{\frac{1}{2}},$$

where the metric has been parameterized on relative quality of Doppler and ranging measurements (ψ_n and η). Note here that $CDOP(\psi_\eta, \eta)$ has been implicity referred to the ranging variance σ_R^2 to facilitate the comparison with ranging.

[5] Longer observation with filtering and smoothing improves Doppler estimation over time. The study of associated time-convergence characteristics, while being interesting and important, is outside the scope of the current document.

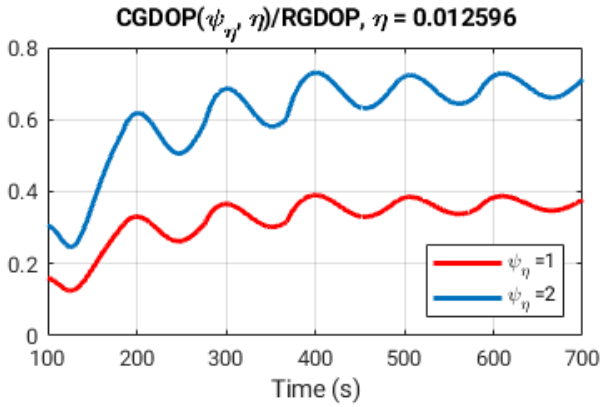

FIGURE 52: RATIO OF COMBINED DOP TO THAT OF RANGE DOP. ITS VALUE BEING LESS THAN ONE SHOWS THE BENEFITS OF COMBINING DOPPLER WITH RANGING METHODS.

Figure 50 also shows $CDOP(\psi_\eta, \eta)$ for two different values of ψ_n. Figure 52 shows the ratio $\frac{CDOP(\psi_\eta,\eta)}{RDOP}$ as a function of time for $\psi_n = 1$ and $\psi_n = 2$. We observe that the ratio is less than 1 indicating that the RDOP can be improved by combining with Doppler measurements. Further, both Figure 50 and Figure 52 indicate that Doppler combining is much more effective when fewer measurements have been made (earlier in time) since RDOP is much worse early on and eventually becomes better.

5.2 SUMMARY AND CONCLUSIONS

We motivated the exploration of Doppler-positioning for LEO by noting that Doppler measurements are much better suited for positioning with LEOs than MEOs. We studied Doppler-based positioning in the context of LEO constellations that offer (i) single satellite in visibility and (ii) two satellites in visibility. In the former case, the problem is complicated by the presence of unknown, time-varying XO-error that arises because of the poor quality XOs used in mobile phones. Even under very good measurement conditions and long observation durations, it is hard to achieve better than 40-50 [m] positioning accuracy in this case. The situation vastly improves in the case when two-satellites are always visible, where differencing between satellites can be beneficial to eliminate XO-error. In the scenarios of 3 or more simultaneous satellites being measured, the error performance is expected to be greatly improved due to improved DDOP and CDOP. In fact, with a constellation that can ensure at least 4 satellites in view at the same time, snapshot-based 3D positioning is possible, where the UE can instantaneously obtain positioning-fix upon measurement from each satellite; this may also benefit UE's battery-life, especially in the cases of navigation and tracking.

Doppler-observables provide independent set of equations for solving the positioning problem. The error performance of Doppler-positioning is quite sensitive to measurement errors. If Doppler can be measured accurately, the Doppler and ranging measurements can potentially be effectively combined to get much further improvement in positioning-error.

6 HYBRID TN-NTN POSITIONING [TH-SIX]

At least for the regulatory constraints, other potential techniques can be based on network-verified UE location using TN gNB where available. The general hypothesis for this part considers that NTN UE has both TN and NTN capabilities; TN communication is using TDD mode, while NTN communication may use FDD or TDD modes. Moreover, TN and NTN share the same 5G Core Network (or at least same Location Management Function or LMF functionalities) as seen in Figure 53.

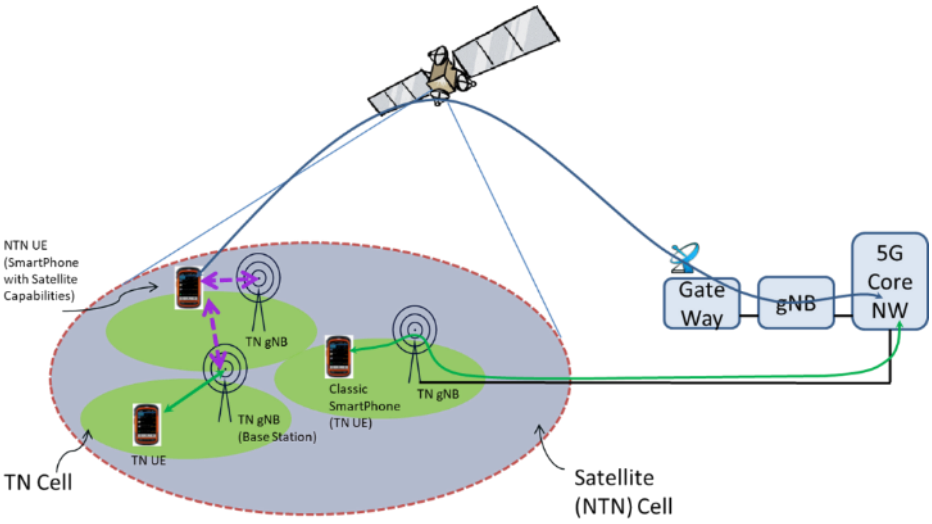

FIGURE 53: ILLUSTRATION OF NTN/TN SYSTEM

6.1 DESCRIPTION OF THE SOLUTION

The general principle is to reuse information with respect to the channel measurement CH_i at both UE side and TN gNB_i side due to the reciprocity of the TDD channel. As a first step, as represented in the Figure 54 below, while UE reports GNSS position (or potentially the position obtained through PRS signaling and SIB19 satellite data) through the NTN link to the 6GC. At the same time, both UE and gNB_i perform channel measurement/estimation on TN $link_i$. Due to the reciprocity of the TDD TN channel, the channel estimates on both UE and gNB_i should have relatively similar values.

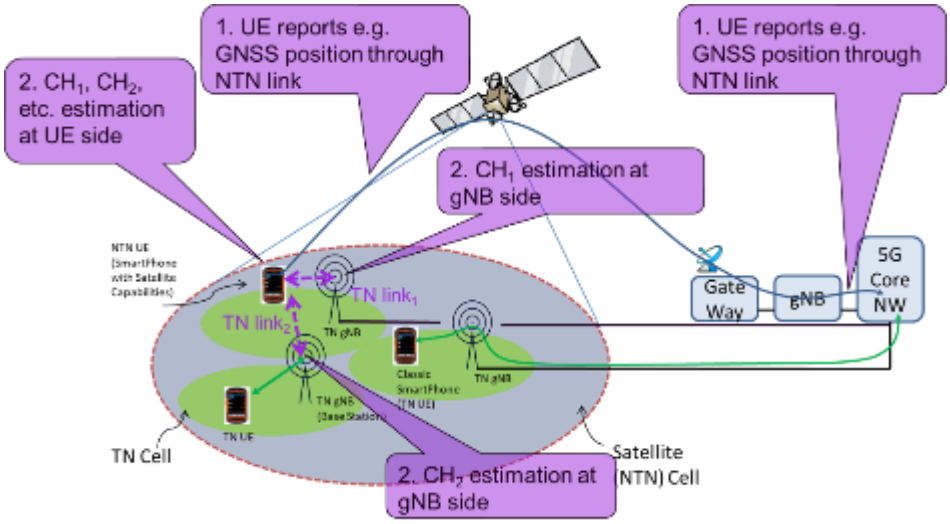

FIGURE 54: ILLUSTRATION OF CHANNEL ESTIMATION

Further, as represented in Figure 55, UE and gNB_i report at the same time CH_i channel measurement to the LMF. At the next step, LMF compares UE and gNB_i channel estimates for a match. As a result, if there is a match, the reported UE GNSS location (or potentially the location obtained through PRS signaling and SIB19 satellite data) is then compared against know location of gNB_i. Therefore, this mechanism assures that the UE reported position is correlated to the gNB_i positions known in advance by the 5G Core Network.

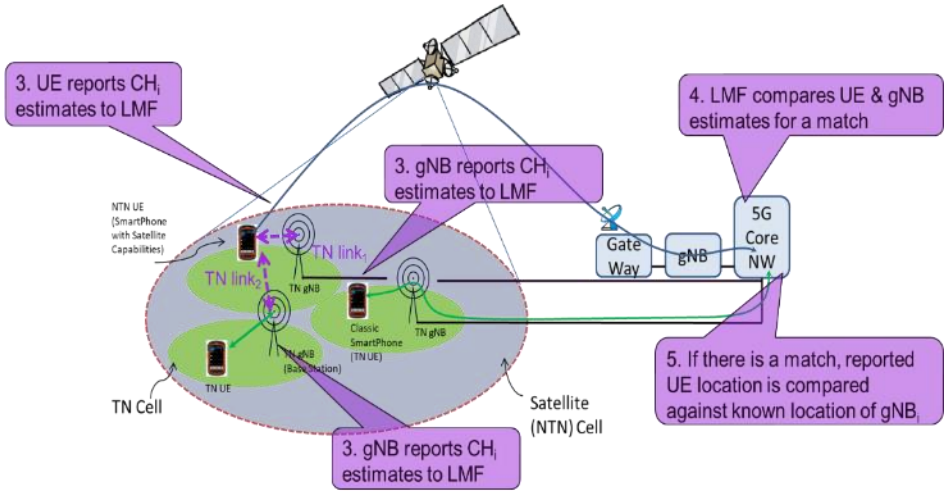

FIGURE 55: ILLUSTRATION OF REPORTING MECHANISMS AND NETWORK NTN UE VERIFIED LOCATION USING TN

6.1.1 SYSTEM ARCHITECTURE

6.1.1.1 OFDM SIGNAL

Figure 56 describes a simple baseband OFDM signal generation and reception with two numerologies. The transmitter uses an inverse fast Fourier transform (IFFT) operation to generate OFDM symbols in the time domain from the input subcarriers (transmitted in the frequency domain), where each of the subcarriers contains pilot or useful data information modulated using $\pi/2$ BPSK, QPSK, or QAM with different modulation orders. A CP is added to the useful OFDM symbol transporting I/Q samples and transmitted to the Digital to Analog Converter (DAC) towards the Tx antenna. On the receiver side, after the Rx antenna, the signal is transformed using the Analog to Digital Converter (ADC) into digital samples. The CP is removed and the received useful OFDM signal goes through an FFT operation in order to recover the information transmitted on each of the subcarriers (i.e., pilot or useful data information modulated using π /2 BPSK, QPSK, or QAM with different modulation orders).

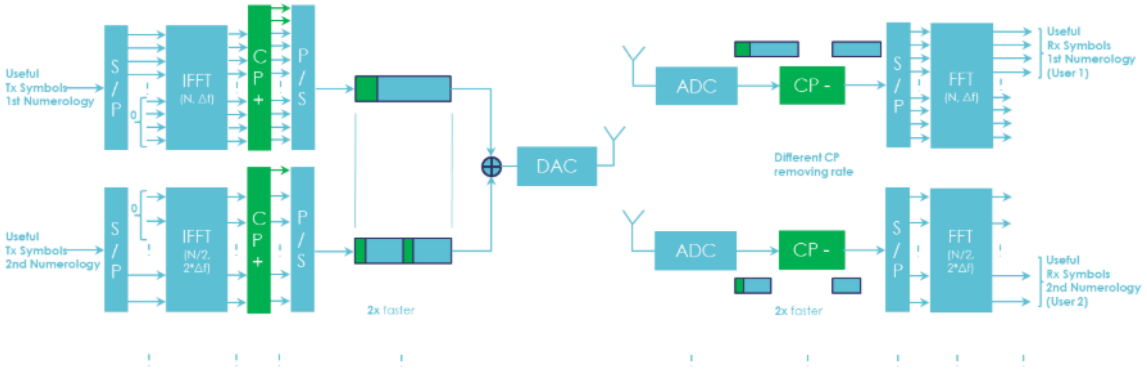

FIGURE 56: EXAMPLE OF OFDM TRANSMITTER (TX) AND RECEIVER (RX)

Due to the radio channel impact, each of the subcarriers from the transmitted OFDM waveform can be attenuated by a channel coefficient as represented in Figure 57. In a legacy implementation, the received OFDM signal is first equalized (i.e., all received carriers are multiplied with the inverse of the channel coefficient in order to correctly recover the signal as transmitted before the radio channel), this process being essential before the received signal is decoded.

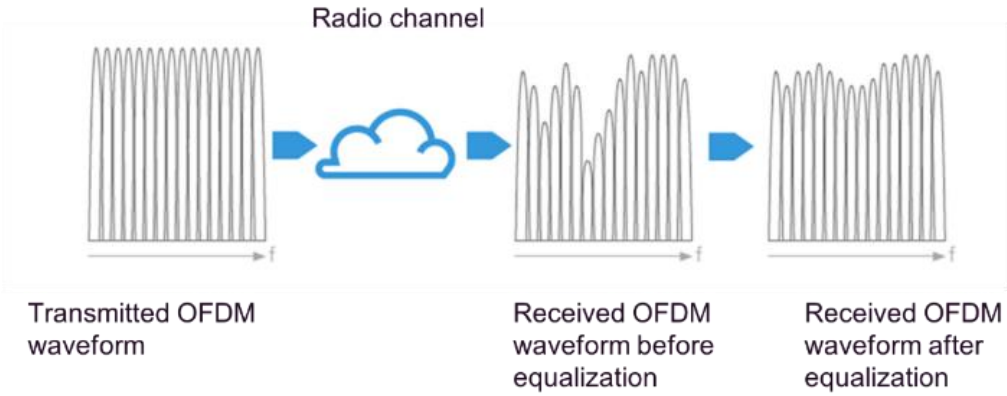

FIGURE 57: REPRESENTATION OF RADIO CHANNEL IMPACT ON RECEIVED OFDM SIGNAL

However, if the channel information is recovered directly after the IFFT, before the equalization process, this information could be used to derive channel information potentially on each of the subcarriers. Therefore, in the case when a satellite UE can measure a terrestrial base station for a limited period of time (and at the same time the base station can measure the same satellite UE), this very precise measurement can be used to determine that the UE was (during a period of time) in the proximity of the terrestrial base station. This process is unique and very precise. As a matter of fact, due to the channel reciprocity between TDD transmission-reception pairs (UE to base station, or base station to UE) the channel estimation is unique per each UE-gNB configuration with respect to a given position, channel multipath, and UE movement. Moreover, since the IFFT/FFT size can be up to 4096 in 5G NR and up to 2048 in 4G LTE, it can be shown that the number of subcarriers can provide sufficient data to derive unique channel estimations for each of the UE-BS pairs, with an excellent level of randomness between different consecutive measurements at different times and different locations. This performance can be achieved in a very short time and even if one single OFDM symbol is used, thanks to the wide-band nature of the signals and the number of subcarriers. Thanks to this approach, even in the case of GEO networks with beam sizes up to 300 km, the reciprocal UE-BS channel measurement can serve as sufficient information in order to validate the position of a UE by the satellite network when the UE is or was under the coverage of the terrestrial base stations.

6.1.2 5G NR EXISTENT PROTOCOLS

There are several TS of interests describing the following information see Figure 58:

- Non-roaming reference architecture for Location Services in reference point representation (see TS 23.273);

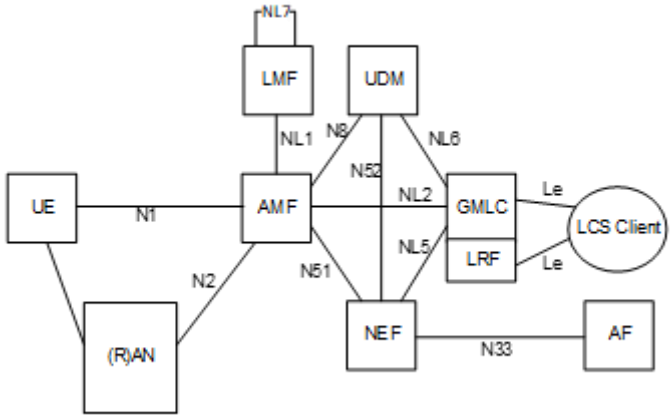

FIGURE 58: E POSITIONING OVERALL ARCHITECTURE APPLICABLE TO NG-RAN (TS 38.305)

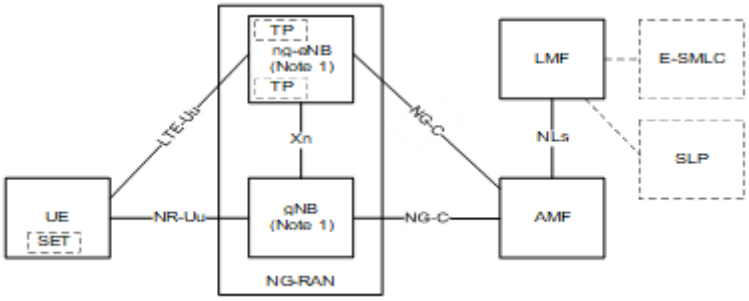

FIGURE 59: LPP CONFIGURATION FOR CONTROL- AND USER-PLANE POSITIONING IN E-UTRAN OR NG-RAN (TS 37.355)

Where e-SMLC is the enhanced Serving Mobile Location Centre, GMLC is the Gateway Mobile Location Centre, SLP is the SUPL Location Platform Subscriber potentially using an SUPL for Secure User Plane Location, with some other know entities such as AMF for Access and Mobility Management Function and LMF for Location Management Function. We do not intend to enter again in those details as already presented in previous chapters/sections. However, it deserves being mentioned that the there is a specific mapping for the location protocols based on:

- NG-RAN implementation where the NG-RAN estimates the position and transmits it toward NRPPa protocol (as per TS 38.455) to the LMF;
- UE implementation where the UE estimates the position and transmits it toward LPP protocol (as per TS 37.355) to the LMF;
- This mapping is further represented in the figure below from Location Service Support by NG-RAN (TS 38.305)

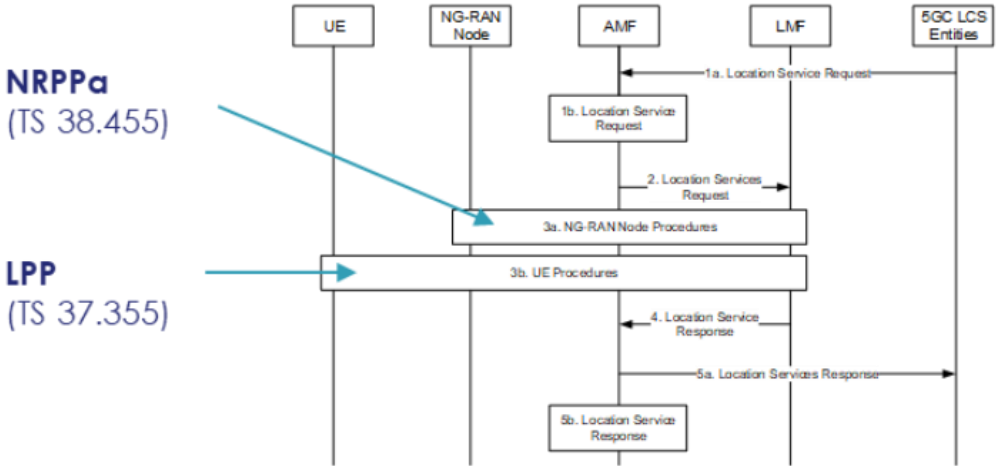

6.1.2.1 LTE EXISTENT PROTOCOLS

There are several TS of interests describing the following information:

- UE positioning overall architecture applicable to E-UTRAN and system architecture underlying positioning (TS 36.305) where SLP is the Service Location Protocol and E-SMLC;
- Positioning interfaces in E-UTRAN and protocol layering for LCS-AP (TS 29.171)

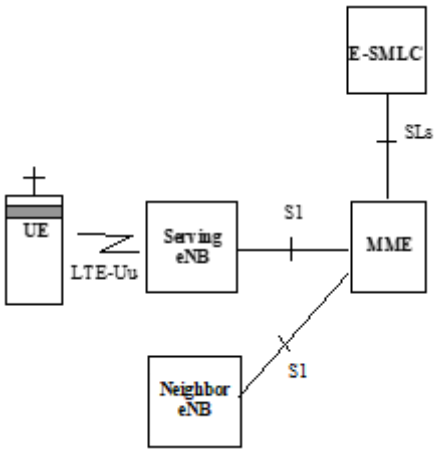

Method	UE-based	UE-assisted, E-SMLC-based	eNB-assisted	LMU-assisted/ E-SMLC-based	SUPL Note 3
A-GNSS	Yes	Yes	No	No	Yes (UE-based and UE-assisted)
Downlink Note1	No	Yes	No	No	Yes (UE-assisted)
E-CID	No	Yes	Yes	No	Yes (UE-assisted)
Uplink	No	No	No	Yes	No
Sensor	Yes	Yes	No	No	No
WLAN	Yes	Yes	No	No	Yes
Bluetooth	No	Yes	No	No	No
TBS Note 2	Yes	Yes	No	No	Yes (MBS)
NOTE 1: This includes TBS positioning based on PRS signals. NOTE 2: In this version of the specification only for TBS positioning based on MBS signals. NOTE 3: This shows whether the positioning method is supported by SUPL ULP [22].					

6.2 PROTOCOL CHALLENGES OF THE SOLUTION

5G NR protocol stacks and potential implementation with transparent payloads are further described below.

Figure 60 represents the UE reporting GNSS positioning (or position acquired through other means, e.g. PRS) to the LMF. At the same time, UE also reports CH_i channel estimates from measured gNB_i. As further seen, this information will serve to validate the UE position report to the LMF. The CH_i channel estimate report can contain values for each of the gNB_i measured sub-carriers.

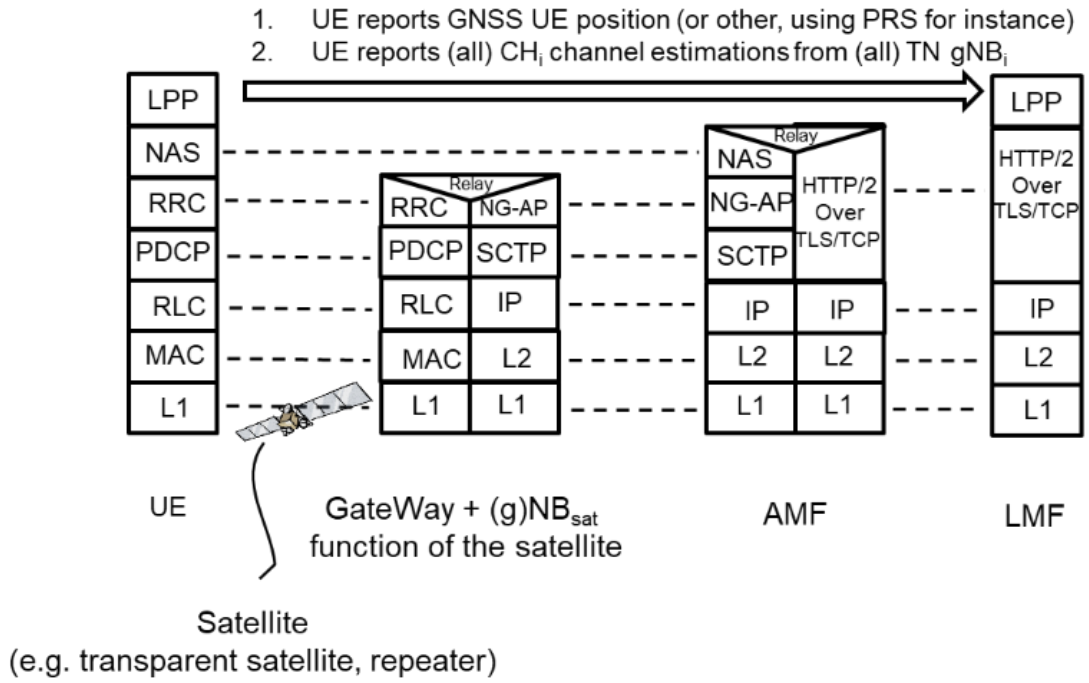

FIGURE 60: REPRESENTATION OF UE REPORTING MECHANISM OVER SATELLITE CONNECTIVITY

Similarly, in Figure 61 the CH_i channel estimate report of the gNB_i measuring the UE is represented. The CH_i channel estimate report can contain values for each of the UE measured sub-carriers.

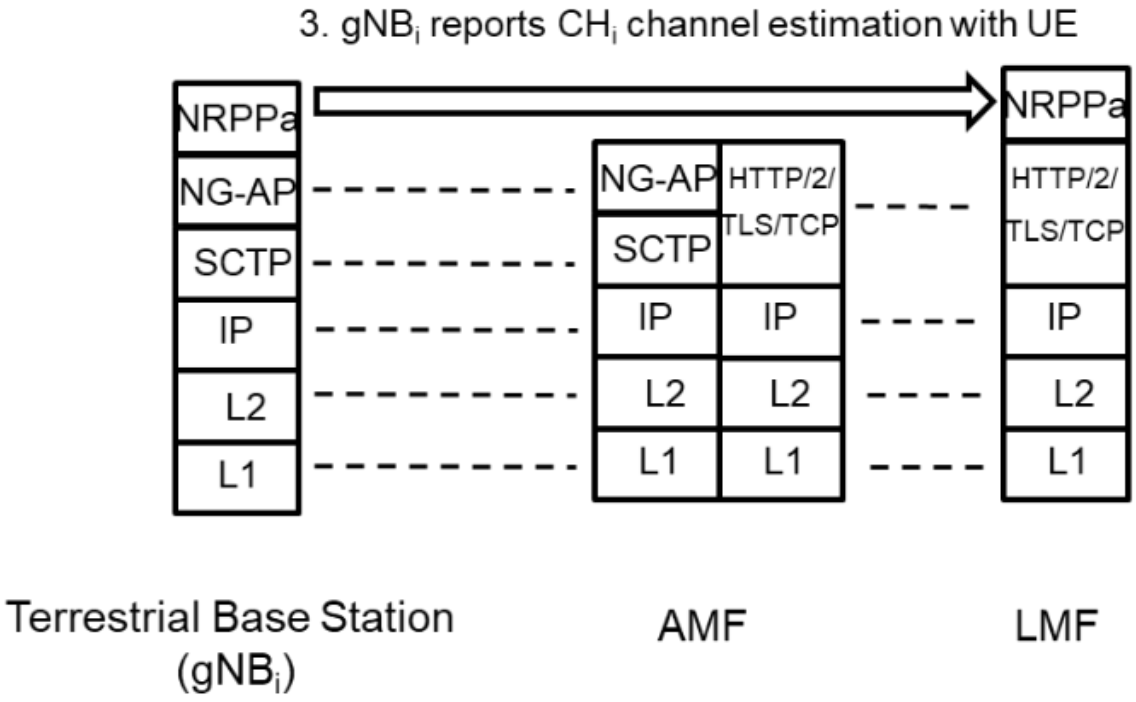

FIGURE 61: REPRESENTATION OF GNB REPORTING MECHANISM

Once the LMF receives all information from the UE measurements and gNB_i measurements together with the (GNSS or PRS-based) UE location, the LMF compared the UE and gNB estimates for a match. If the channel estimates match, the GNSS or PRS-based UE position is compared against known location of gNB_i and if the two values correspond (UE located next to terrestrial gNB during a certain amount of time in present or past with a certain granularity/accuracy) then it can be claimed that the GNSS or PRS-based UE reported position is valid. Therefore, the GNSS or PRS-based UE position can be further used in the future since validated by the NTN network side as an accurate and reliable position.

Finally yet importantly, a similar implementation over LTE can be represented below:

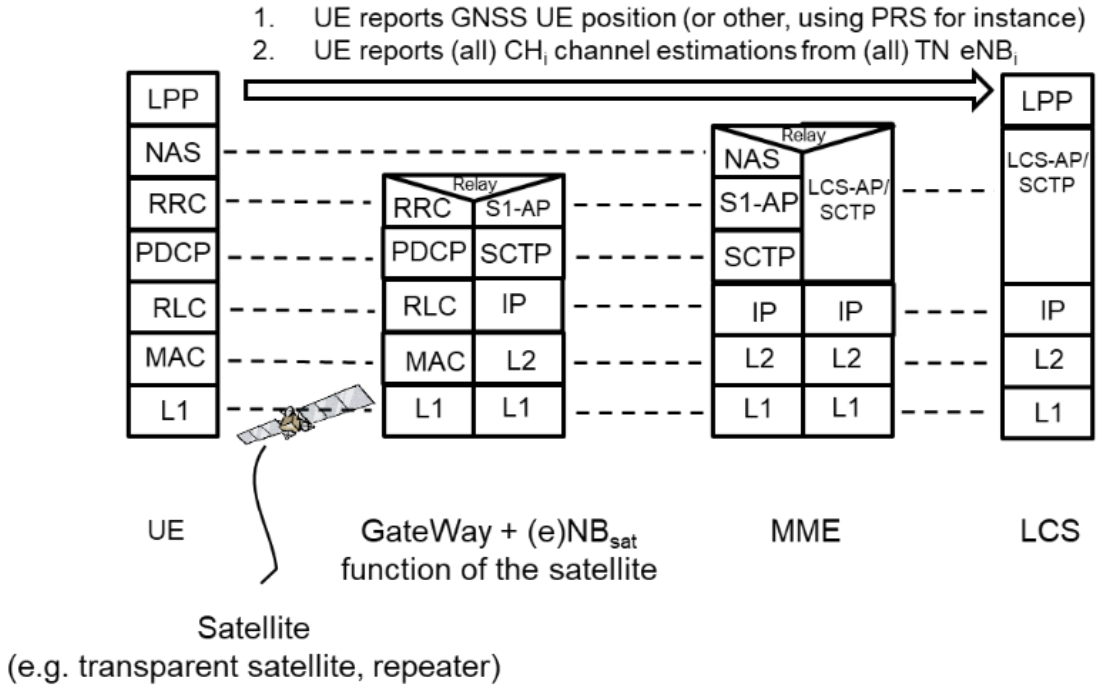

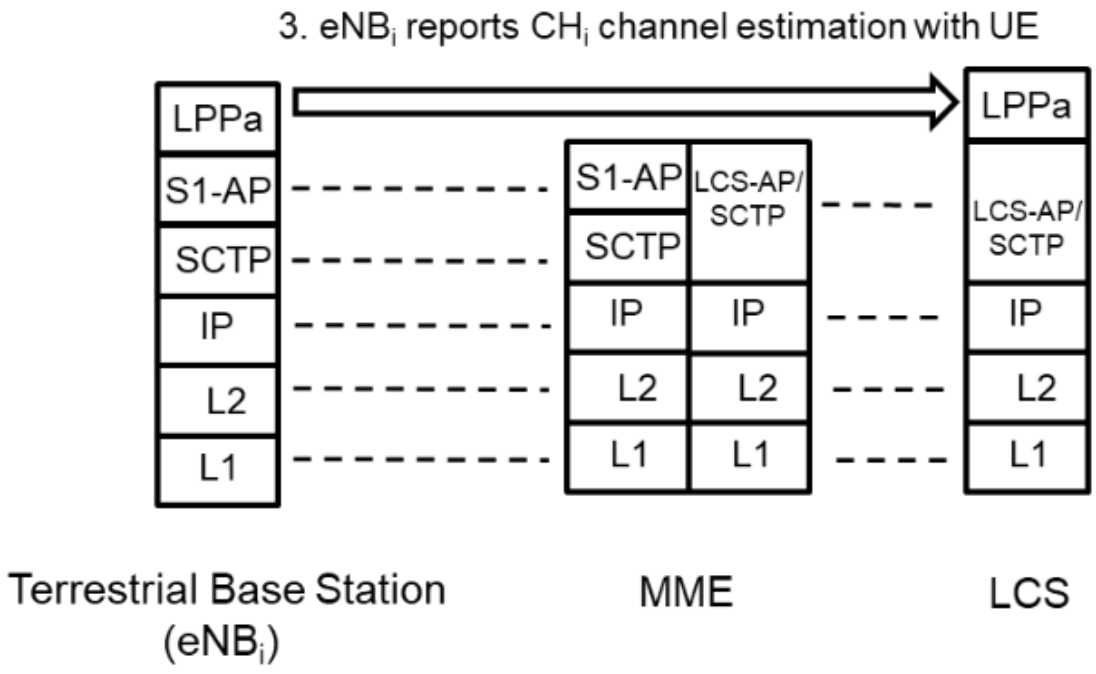

However, even if this solution is sufficient in some cases, for instance to guarantee location verification at the border between two countries, it will obviously not guarantee location verification in situations where no TNs are or were not available in the near past.

7 COMPARISON OF DIFFERENT SOLUTIONS FOR POSITIONING

The methods and solutions presented in this document are complementary and are jointly intended to meet the required positioning accuracy.

Ranging-based positioning methods rely on distance measurements, which can be either absolute or differential. Absolute distance measurements directly represent the distance between the transmitter (ground base station or satellite) and the target device. In this case, the target device is located on the surface of a sphere centered at the transmitter, with a radius equal to the measured distance. When multiple absolute distance measurements are available, the intersection of the corresponding spheres determines the position of the target device.

Differential distance measurements represent the difference in propagation distances from multiple transmitters to the same target device. Under this approach, the target device lies on a hyperboloid with the transmitters as foci and the distance difference as the real semi-axis. The intersection of multiple such hyperboloids enables estimation of the target device position.

In this work, the analysis focuses on a ranging-based solution using PRS and a TDOA algorithm to estimate user position. The study includes theoretical ranging accuracy analysis in the C and Q/V bands, as well as PRS-based simulations in a 6G NTN context using multi-satellite LEO positioning. This forms the basis of the proposed ranging method.

In addition, a Doppler-based positioning method is considered as a complementary approach, particularly to compensate for scenarios with limited satellite visibility (one or two satellites). This method can be combined with the PRS-based ranging solution after appropriate PRS signal design for localization. However, Doppler-based positioning is primarily intended for limited-visibility scenarios and is not applied in cases with multiple satellites in view. Hybrid TN-NTN Positioning, it might be related to systems or techniques that combine Traditional Network (ground-based) positioning with NTN positioning systems. This could be relevant in fields like GNSS 5G/6G communication (where hybrid positioning methods are being developed to improve accuracy and coverage) or IoT applications where ground and satellite data are integrated for enhanced geolocation.

Co-funded by the European Union

8 CONCLUSION AND FUTURE WORK

In this task, we studied the satellite positioning technology based on the 6G NTN system. This work proposed several solutions suitable for satellites positioning, analyzed the factors influencing positioning performance, and performed a simulation evaluation of positioning performance.

The simulation results show that NTN multi-satellite positioning offers higher positioning accuracy and faster positioning speed compared to NTN single-satellite positioning. It is foreseeable that, with the continuous increase in the number of satellites in low Earth orbit constellations, multi-satellite positioning will become an important technological direction for the development of NTN positioning. Furthermore, with the growing popularity of mobile phones directly connected to satellites, NTN-based multi-satellite positioning technology for mobile phones will deeply integrate with communication systems, forming an integrated service system for communication and navigation, and promoting the integrated development of communication and navigation in the satellite-ground fusion field. Positioning accuracy without relying on GNSS is often referred to as GNSS-independent or GNSS-denied positioning, and it is especially important in environments where satellite signals are blocked or jammed.

Achieving 10 cm level of performances with GNSS independent positioning solution is challenging but possible with the right combination of technologies:

- Using Multi-LEOs satellites ranging, ensuring feasibility within the beam management strategy of the NTN system(s),
- Providing system corrections based on a network of reference stations (similar to Galileo HAS for MEO systems),
- Implementing tailored processing in the user receiver, PPP-like techniques in FR1 (mostly to solve ionosphere delay) and ultra-tight coupling techniques in FR2.

These techniques theoretically allow to reach cm accuracy level, but they are quite advanced solutions and they would require in-orbit demonstration. The ESA Celeste IOD project is covering this need for FR1, but the context for testing in FR2 is to be refined.

Finally, these solutions can be either implemented in a LEO-only context, or in a LEO + GNSS context, in which the LEO measurements will mostly be used to reduce the convergence duration of MEO PPP technologies from 10-20 minutes to 20s-40s. The main difference is that the number of needed LEO satellites to achieve such improvement is lower in a LEO + GNSS context than in a LEO standalone context, which may be easier to support for a more limited NTN constellation and/or with less constraints on its beam management.

- PRS signal and LEO PNT hybridization aim to achieve a positioning accuracy of 10 cm level, using a configuration of four LEO satellites at an altitude of 600 km.

The network architecture to support NTN positioning is expected to be developed based on the legacy TN positioning architecture by involving the location management function (LMF). However, it is expected that there will be some enhancements through adding new features functions and in the signaling mechanism between network nodes.

Although TN and NTN positioning have operated independently and have been used for different purposes in 5G, we envision that 6G TN and NTN will be co-designed from the start. This will facilitate a common signal design and network architecture, enabling a smooth integration of TN and NTN.

In the 6G period, NTN positioning is expected to have tighter requirements to support more use cases. The legacy positioning measurements in TN positioning, such as angle-based measurement and timing-based measurement, can be extended to NTN positioning.

For NTN positioning, it is essential to consider deployment scenarios where the user may have visibility of either a single satellite or multiple satellites, as this directly affects how positioning measurements are carried out. Additionally, with the advent of 6G, there is an opportunity to explore new reference signals or waveforms for positioning, known as PRS. These signals could provide enhanced capabilities for accurate positioning in NTN environments

9 REFERENCES

[1] "URL," [Online]. Available: https://data.gsmaintelligence.com/research/research/research-2023/radar-satellites-and-telcos.

[2] "3GPP. Study on requirements and use cases for network verified UE location for Non-Terrestrial-Networks (NTN) in NR (Release 18): TR 38.882[S]. 2022".

[3] "3GPP TS 38.821, Solutions for NR to support non-terrestrial networks (NTN) (Release 16). Technical Specification Group Radio Access Network; 38.821. Version 16.0.0. 3rd Generation Partnership Project (3GPP), Dec. 2019.".

[4] C. S. H. S. D. a. R. M. B. H. K. Dureppagari, "NTN-Based 6G Localization: Vision, Role of LEOs, and Open Problems," *IEEE Wireless Communications,* vol. 30, no. 6, pp. 44-51, December 2023.

[5] "Report on road user needs and requirements," EUSPA, Sep. 2021.

[6] R. R. J. A. L.-S. a. G. S. G. A. del Peral-Rosado, "Survey of cellular mobile radio localization methods: From 1G to 5G," *IEEE Comm.*

[7] "EUSPA, “Power-efficient positioning for the internet of things,” June 2020,".

[8] "3GPP TS 38.305. NG Radio Access Network (NG-RAN); Stage 2 functional specifications of User Equipment (UE) positioning in NG-RAN (Release 16). Technical Specification Group Radio Access Network; 38.305. Version 16.0.0. 3GPP," Mar, 2020.

[9] "Qualcomm - 5G: Bringing precise positioning to the connected intelligent edge," [Online]. Available: https://www.qualcomm.com/news/onq/2021/12/5g-bringing-precise-positioning-connected-intelligent-edge?li_fat_id=196ebcbb-85fa-4b85-93c0-a2b42ecdd481.

[10] "L. Pan et al., “Satellite availability and point positioning accuracy evaluation on a global scale for integration of GPS, GLONASS, BeiDou and Galileo,” in Advances in Space Research, vol. 63, no. 9, pp. 2696–2710, May 2019.".

[11] "B. W. Parkinson, “Global Positioning System Theory and Applications,” The American Institute of Aeronautics and Astronautics, Vol. 1, 199.".

[12] "Z. Bodnaar, Z. Herczku, J. Bearces, I. Papp, F. Som, B. G. Molnaar,and I. Frigyes, ``A detailed experimental study of the LEO satellite to indoor channel characteristics,'' Int. J. Wireless Inf. Netw., vol. 6, no. 2,pp. 7991, 1999.".

[13] "A. Tkac and V. Wieser, ``Channel estimation using measurement of channel impulse response,'' in Proc. ELEKTRO, May 2014, pp. 113 117.".

[14] "Technical Specification Group Services and System Aspects; Location Services (LCS); Service description; Stage 1,” 3GPP TS 22.071, version 17.0.0.".

[15] "Samsung, Ericsson, “Support for Multiple QoS Class in deferred location requests,” 3GPP SA2 144e CR, S2-2103085".

[16] "URL NTN overview," [Online]. Available: https://www.3gpp.org/technologies/ntn-overview.

[17] "URL Starlink," [Online]. Available: https://www.starlink.com/publicfiles/Starlink_Approach_to_Satellite_Demisability.pdf.

[18] "Unveiling Starlink for PNT, Sharbel Kozhaya Joe Saroufim, and Zaher (Zak) M. Kassas, NAVIGATION: Journal of the Institute of Navigation Mar 2025 , 72 (1) navi.685; DOI: 10.33012/navi.685.".

[19] "Orbit Determination for Continuously Maneuvering Starlink Satellites Based on an Unscented Batch Filtering Method, Anqi Lang & Yu Jiang, Sensors 2025, 25(13), 4079; https://doi.org/10.3390/s25134079.".

[20] "T.E. Humphreys, P. A. Iannucci, Z. Komodromos and A. M. Graff, “Signal Structure of the Starlink Ku-Band Downlink”, IEEE Transactions on Aerospace and Electronic Systems, vol 59, pp. 6016-6030, Oct. 2023, doi: 10.1109/TAES.2023.3268610".

[21] "M. Asad Ullah, G. Pasolini, K. Mikhaylov, and H. Alves, “Understanding the limits of LoRa Direct-to-Satellite: The Doppler perspectives,” IEEE Open Journal of the Communications Society, vol. 5, pp. 51–63, 2024.".

[22] "SpaceX, “Revised SpaceX Gen2 non-geostationary satellite system,” Tech. Attachment SAT-AMD-20210818-00105, Aug.2021. [Online]. Available:https://licensing.fcc.gov/myibfs/download.do".

[23] "Bader, Qamar, et al. "Doppler-Based Positioning with LEO Satellites: A Survey of Techniques, Challenges, and Opportunities." 948627272053c03834635d702cfa0112.pdf".

[24] "Neinavaie, Mohammad, Khalife, Joe, Kassas, Zaher M., "Exploiting Starlink Signals for Navigation: First Results," Proceedings of the 34th International Technical Meeting of the Satellite Division of The Institute of Navigation (ION GNSS+ 2021), St. Louis,".

[25] "URL Kuiper," [Online]. Available: https://www.aboutamazon.com/news/innovation-at-amazon/what-is-amazon-project-kuiper.

[26] "Kuiper URL 2," [Online]. Available: Kuiper mission updates: Kuiper constellation grows to more than 100 satellites.

[27] "Oneweb url," [Online]. Available: https://oneweb.net/our-network.

[28] "M. L. Psiaki, “Navigation using carrier Doppler shift from a LEO constellation: TRANSIT on steroids”, NAVIGATION: Journal of the Institute of Navigation Sep 2021, 68 (3) 621-641; DOI: 10.1002/navi.438.".

[29] "S. Kozhaya and Z. M. Kassas, "A First Look at the OneWeb LEO Constellation: Beacons, Beams, and Positioning," in IEEE Transactions on Aerospace and Electronic Systems, vol. 60, no. 5, pp. 7528-7534, Oct. 2024, doi: 10.1109/TAES.2024.3410252".

[30] "Komodromos, Zacharias M., Morgan, Samuel C., Clements, Zachary L., Qin, Wenkai, Morrison, W. Jeremy, Humphreys, Todd E., "Network-Aided Pseudorange-Based LEO PNT from OneWeb," 2025 IEEE/ION Position, Location and Navigation Symposium (PLANS), Salt Lake Ci".

[31] “W. Qin, Z. M. Komodromos, and T. E. Humphreys, “An analysis of the short-term time stability of the Starlink Ku-band downlink frame clock,” in Proceedings of the IEEE International Conference on Wireless for Space and Extreme Environments (WISEE 2024), 20”.

[32] ". Qin, A. M. Graff, Z. L. Clements, Z. M. Komodromos, and T. E. Humphreys, “Timing properties of the Starlink Ku-band downlink,” IEEE Transactions on Aerospace and Electronic Systems, 2025, submitted for review.".

[33] "Z. M. Komodromos, Z. L. Clements, and T. E. Humphreys, “Signal parameter estimation and demodulation of the OneWeb Ku-Band downlink,” IEEE Transactions on Aerospace and Electronic Systems, 2025, in preparation.".

[34] "S. Zhou, R. Yang, Y. Li, X. Zhan and H. Qin, "Iridium TOA Estimation and Positioning Based on Carrier Tracking and Beam Decoding," in IEEE Transactions on Instrumentation and Measurement, vol. 74, pp. 1-23, 2025, Art no. 8503523, doi: 10.1109/TIM.202".

[35] "Z. Tan, H. Qin, L. Cong and C. Zhao, "New Method for Positioning Using IRIDIUM Satellite Signals of Opportunity," in IEEE Access, vol. 7, pp. 83412-83423, 2019, doi: 10.1109/ACCESS.2019.2924470.".

[36] "Z. Tan, H. Qin, L. Cong, and C. Zhao, “Positioning using IRIDIUM satellite signals of opportunity in weak signal environment,” Electronics, vol. 9, no. 1, p. 37, Dec. 2019.".

[37] "URL 5G PRS mapping," [Online]. Available: https://fr.mathworks.com/help/5g/ug/5g-new-radio-prs.html .

[38] "Shi, C. Z. (2023). Revisiting Doppler positioning performance with LEO satellites. GPS Solut 27, 126.".

[39] Seeber, G. (2003). Satellite Geodesy. Berlin, New York: De Gruyter..

[40] "Kassas, Z. M. (2019). New-age satellite-based navigation STAN: Simultaneous Tracking and Navigation with LEO satellite signals. Inside GNSS, 14(4), 56-65.".

[41] "H. Benzerrouk, Q. N. (2019). Alternative PNT based on Iridium Next LEO Satellites Doppler/INS Integrated Navigation System. International Conference on Integrated Navigation Systems (ICINS), (pp. 1-10)".

[42] "URL 3gpp," [Online]. Available: https://www.qualcomm.com/content/dam/qcomm-martech/dm-assets/documents/otdoa_positioning_in_3gpp_lte_v1.pdf.

10 APPENDIX

A satellite positioning system consists of a constellation of satellites that transmit signals, which are used to determine the position of a receiver. The general term for such a system is GNSS (Global Navigation Satellite System). GNSS refers to a network of satellites that offer global or regional coverage, and is used for navigation as well as other applications such as geology and geophysics. There are several types of GNSS, including the Global Positioning System (GPS), Galileo, Global Navigation Satellite System (GLONASS), and BeiDou Each system has its own satellite constellation, coverage area, and accuracy levels. GPS, being the oldest and most widely used GNSS, provides global coverage and is available in most countries.

In this section, a description of the existing satellite positioning solutions and terrestrials positioning solutions will be given.

10.1 GNSS FOR POSITIONING (GPS) AND RANGING MEASUREMENT

GPS consists of three segments: control segment, space segment and user segment. The control segment consists of a group station that controls, monitors and tracks the satellites. The space segment is composed of a satellite constellation that rotates around the Earth at a very high altitude. The user segment is the user equipment; it can be military or civilian equipment that receive the GNSS signals. As shown in FIGURE TBD, the GPS constellation consists of 24 operational satellites in six different orbital planes, covering the whole Earth. GPS satellites are MEO satellites, which orbit around the Earth in circular orbits at an altitude of approximately 20 200 km. It is designed in such a way that users at any place on Earth [4] see at least four satellites simultaneously.

FIGURE: GPS CONSTELLATION SEGMENT

A GPS signal consists of two carrier signals, transmitted at frequencies of 1575.42 MHz (L1) and 1227.60 MHz (L2). Each carrier signal is modulated with a combination of a navigation message and a unique satellite-specific code.

The L1 carrier is modulated with two codes: the coarse/acquisition (C/A) code and the precise (P) code, while the L2 carrier is modulated only by the P code. The C/A code has a frequency rate that corresponds to a wavelength of approximately 300 meters, while the P code has a frequency rate 10 times higher, at 10.23 MHz, with a wavelength of about 30 meters and a 7-day repeat cycle. As a result, the P code is significantly more precise than the C/A code, making it suitable for military use, whereas the C/A code is employed for civilian applications. The navigation message itself contains information on satellite position, velocity, and time parameters. This message has a duration of 12.5 minutes and a data rate of 50 bits per second [11].

GPS satellites transmit signals to GPS receivers, which include information about the satellite's three-dimensional position and the time the signal was sent. The time provided by the GPS satellites is highly accurate, as their atomic clocks are more stable than the clocks in the receivers. Upon receiving the signal, the receiver calculates the time difference between when the signal was sent and when it was received.

By using this time difference and the constant speed of radio waves (the speed of light), the receiver determines the distance or range between the satellite and itself. This allows the receiver to calculate the four unknowns: the three position coordinates and the time. To achieve this, the receiver must receive signals from at least four satellites. The atomic clocks of the satellites and the clock of the satellites and the clock of the receiver are not precise. As a result, the calculated range includes clock errors and additional delays caused by the radio signals traveling through the ionosphere and troposphere layers of the Earth's atmosphere. Therefore, the distance between the satellite and the receiver denoted as $R_i$where i represent the $i-th$ satellite can be determined using two methods. The first method is as follows

$$R_i = \Delta t_i \times \mathrm{C} \qquad (5.1)$$

$$\Delta t_i = T_{rec} - T_{sent_i} + T_{bias} - T_{err_i} + T_{atm_i} \qquad (5.2)$$

Where $\Delta t_i$is the path delay between the satellite and the UE, C is the speed of light, T_{rec} is the receiver clock time when the signal is received, T_{sent_i} is the transmitter clock time when the signal is transmitted,

Where Δt is the path delay between the satellite and the UE, C is the speed of light,

T_{rec} when the signal is transmitted, T_{biais} is the unknown receiver clock error,

T_{err_i} is the satellite clock error and T_{atm_i} is the extra delay resulting from the Earth's atmosphere change.

The second method to compute

$$R_{i=\sqrt{(X-X_i)+((Y-Y_i)^2+(Z-Z_i)^2)}} \qquad (5.3)$$

Where X, Y, Z, are the user's coordinate andX_i,Y_i, Z_i are the satellite's coordinate Combining the two equations, R_i We are left with four unknown parameters, which are the UE longitude, latitude and altitude and the receiver clock bias. However, the equation set is nonlinear. Accordingly, one method to solve the equations is by linearizing the equations and using an iterative approach. In this method, initial assumed values for the user location and the user clock error are used and they are called nominal values. Moreover, delta terms are

added to the nominal values to produce the actual values of the user location and the user clock error as follows [14]

,

$$X = X_n + \nabla X \quad (5.4)$$

$$Y = Y_n + \nabla Y \quad (5.5)$$

$$Z = Z_n + \nabla Z \quad (5.5)$$

$$T_{biais=T_{bn}} + \Delta T_b \quad (5.6)$$

Were the X_n, Y_n ,Z_n the user's nominal position are, Tb_n is the nominal clock error and $\Delta X, \Delta Y, \Delta Z, \Delta Tb$ are the difference between the actual and the assumed values of three user position coordinates and the receiver clock error respectively.

Using an iterative method, the delta terms are calculated. If these deltas are zero or sufficiently small, the nominal values can be considered accurate approximations of the actual values. However, if the deltas are large, they are added to the current nominal values to generate updated nominal values. This process is repeated until the delta terms become small enough to indicate convergence [14].

The Pseudo-Range (PR_i)

for each satellite can be calculated using equation (5.7). Pseudo-Range is the biased range between the satellite and the UE. In addition, the nominal Pseudo-Range (PR_n) is computed using equation

$$PR_i = \sqrt{(X - X_i)^2 + (Y - Y_i)^2 + (Z - Z_i)^2} + T_{bias} \times C \quad (5.7)$$

$$PR_{ni} = \sqrt{(X_n - X_n)^2 + (Y_n - Y_i)^2 + (Z_n - Z_i)^2} + Tb_n \times C \quad (5.8)$$

Using the calculated nominal Pseudo-Range, the actual Pseudo-Range can be to calculated as the sum of the assumed Pseudo-Range of delta term

$$PR_i = PR_{ni} + \Delta PR_i \quad (5.9)$$

Where PR_i the difference between the actual and the estimated Pseudo-Range is can be calculated as the sum of assumed Pseudo-Range and the delta term. Combining equations

Using the measured path delay, the ∇PR_i can be calculated as:$\Delta PR_i = \alpha_{i1}\nabla X + \alpha_{i2}\nabla Y + \alpha_{i3}\nabla Z + C + \nabla Tb$ (5.10)

$$\alpha_{i1} = \frac{[X_n - X_i]}{PR_{ni} - T_{bn} \times C} \quad (5.11)$$

$$\alpha_{i2} = \frac{[Y_n - Y_i]}{PR_{ni} - T_{bn} \times C} \quad (5.12)$$

$$\alpha_{i3} = \frac{[Z_n - Z_i]}{PR_{ni} - T_{bn} \times C} \quad (5.13)$$

Finally, the measured delta terms (ΔX, ΔY, ΔZ, ΔTb) must be examined. If they are small, then we can calculate the user position and receiver clock bias; else, we have to repeat the process until we reach acceptable small values for the delta terms [14].

10.2 STANDARIZATION POSITIONING

10.2.1 NTN POSITIONING IN RELEASE 19/20

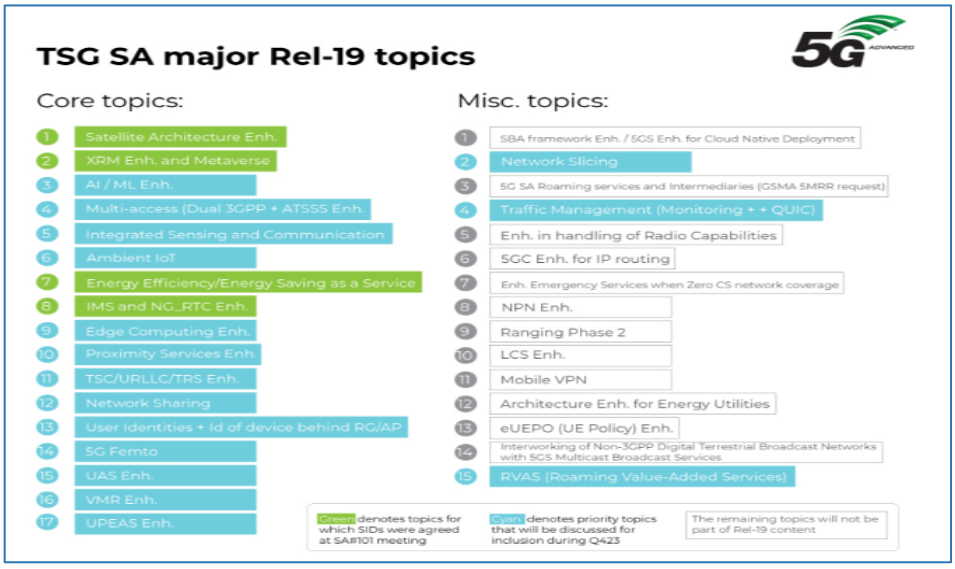

FIGURE 7: KEY TOPICS FOR RELEASE 19 (SATELLITE ARCHITECTURE IS ITEM 1)

10.2.1.1.1 POSITIONING IN RELEASE 19/20 (5G ADVANCED, 6G)

- The schedule of R.19 is already quite challenging
- The specific question of positioning in NTN is more directly addressed in R.20

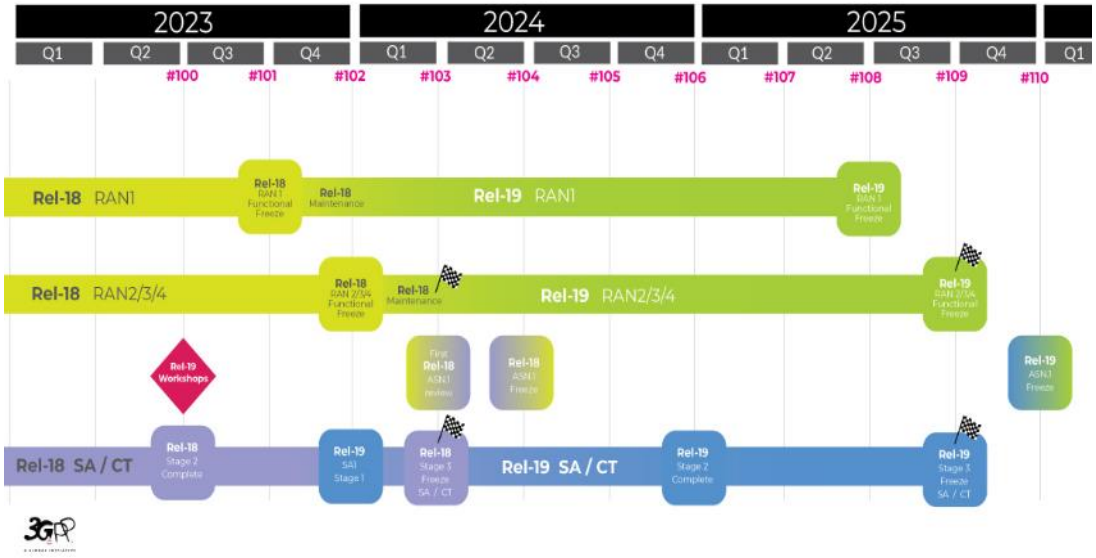

FIGURE 8 : 3GPP RELEASE 19 TIMELINE

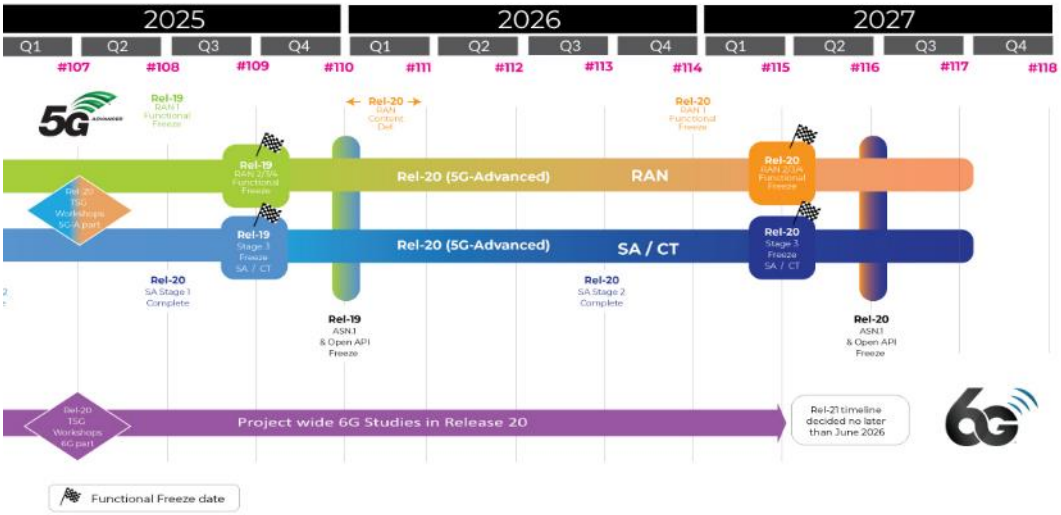

FIGURE 9 : 3GPP RELEASE 20 TIMELINE

The specific topic of NTN positioning is in particular very well shown by Section 6.4.10 of document TS 22.261 (Service requirements for the 5G system; Stage 1, Release 20).

The RAN WG in Rel-20 of 3GPP will cover the 6G study item from Q3/2025 until Q4/2027.